Sponsored by

Agilent

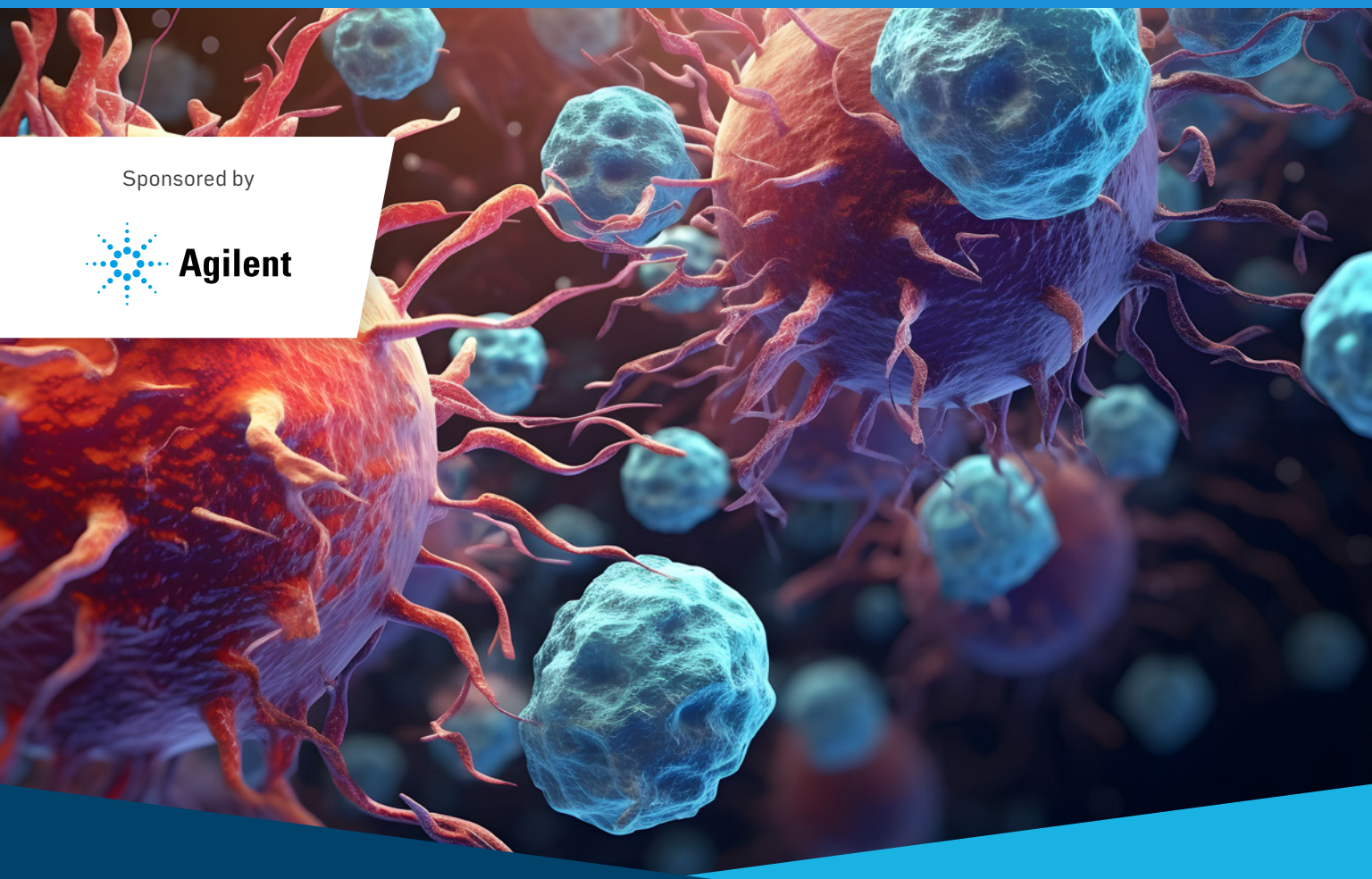

What's Next: Future Trends in Immune Cell Therapy

Innovative approaches to improve in vivo efficacy

LabX

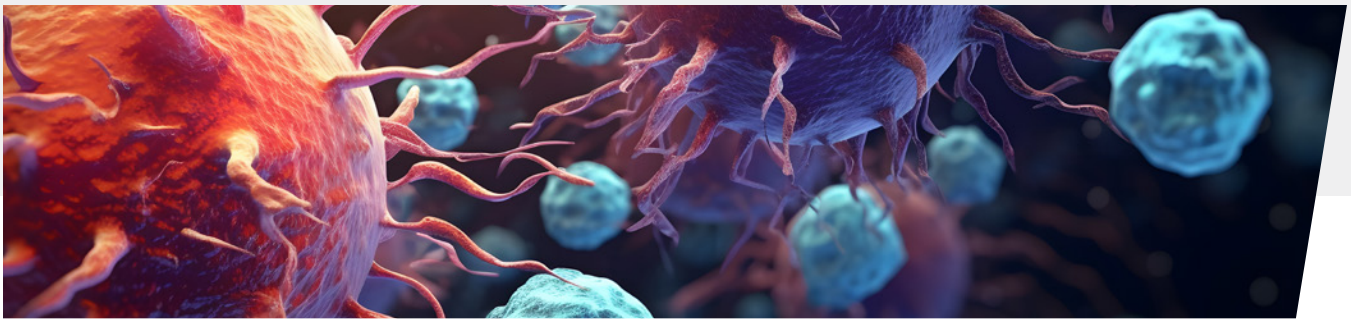

Table of Contents

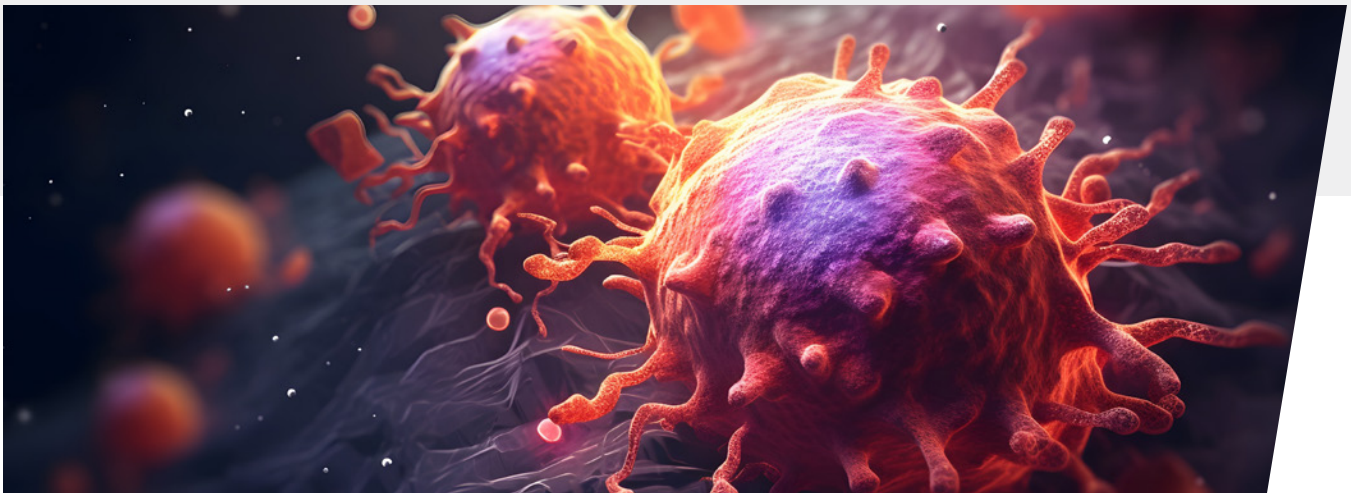

Chapter 1: The Current Landscape of Immune Cell Therapies

A review of current strategies for genetically modified immune cells and CAR-T cell therapies

Genetically modified immune cell therapies use cells that have been engineered to improve their abilities to fight cancer, infectious disease, and other applications. This approach involves engineering immune cells such as T cells, B cells, natural killer (NK) cells, dendritic cells (DCs), and macrophages in the following ways:

- **Modifying antigen receptors by engineering transgenic T cell receptors (TCRs) and synthetic antigen receptors, termed chimeric antigen receptors (CARs)**
- **Modifying intracellular pathways that modulate natural properties such as metabolism, survival, and proliferation**
- **Introducing accessory genes that provide new functions to immune cells**

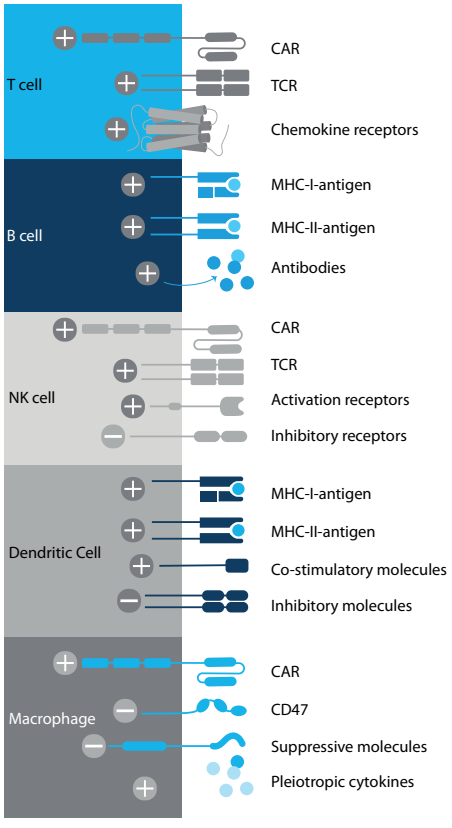

Figure 1. Strategies for generation of genetically modified immune cells to enhance tumor-specific immunogenicity, migration, longevity, cytokine secretion, or a combination of these properties. Platforms include antigen-specific CARs, antigen-specific TCRs, antigen over-representation, blockade of inhibitory molecules, and activation of costimulatory molecules. Plus or minus symbols indicate activation/up-regulation or inhibition/down-regulation, respectively.

Chapter 1:
The Current Landscape of Immune Cell Therapies

T Cells

In recent years, several chimeric antigen receptor (CAR)-T cell therapies for hematological cancers have been approved. CAR-T cell therapies are customized for each patient by collecting individual T cells and reengineering them to produce surface CAR proteins. The T cells are scaled up ex vivo and then reinfused into the patient. Once inside the body, they latch onto specific antigens and selectively kill tumor cells.

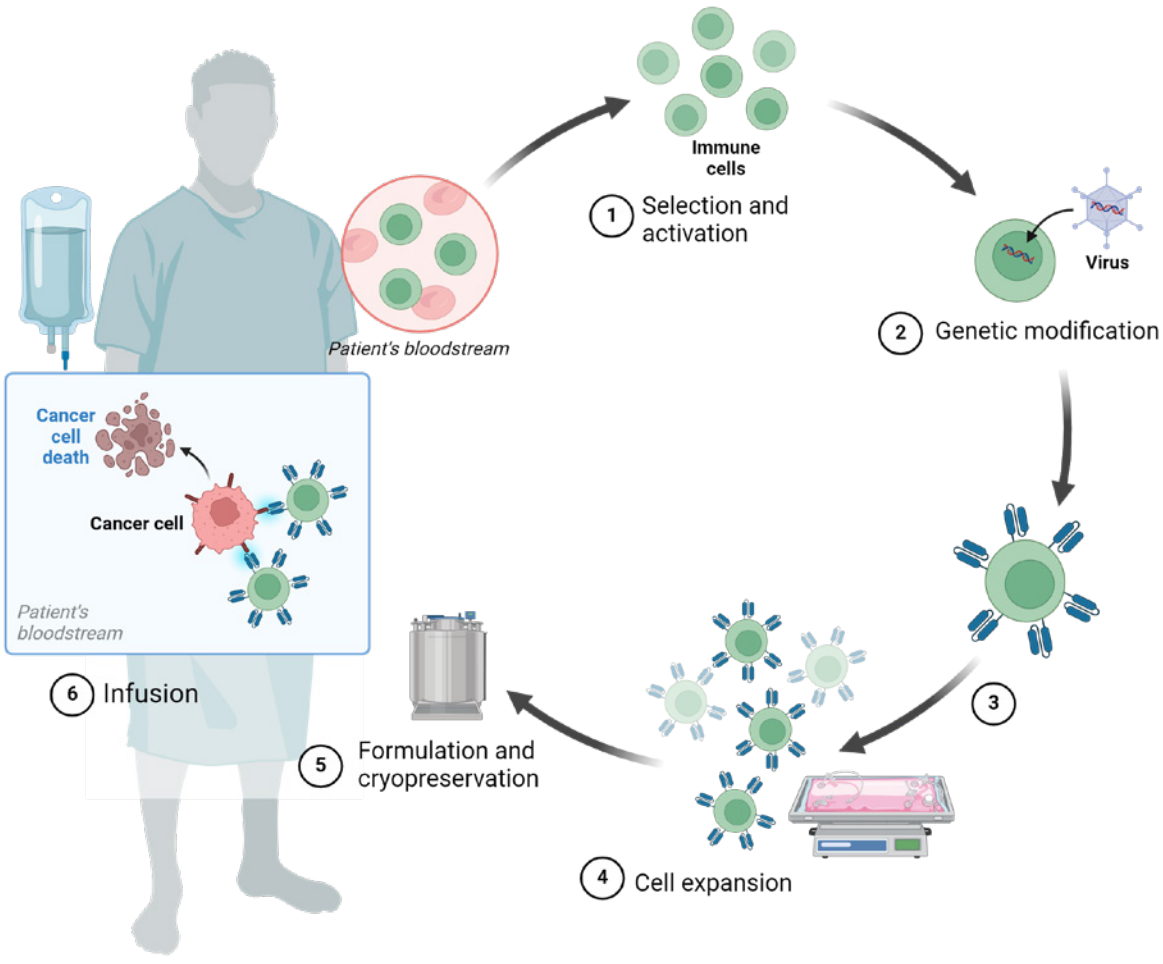

Figure 2. CAR-T cell therapy uses patient T cells which have been engineered in the laboratory to target cancer cells when introduced back into the patient. T cells are initially obtained from patient blood, after which CAR-T cells are produced by introduction of a CAR transgene. These engineered cells produce antigen-specific CAR proteins on the surface and can be expanded to produce millions of replicate cells for infusion back into the patient. Upon re-introduction, the CAR-T cells specifically bind to and kill cancer cells.

Created with BioRender.com

Chapter 1:
The Current Landscape of Immune Cell Therapies

CAR-T cell therapy is an emerging technology with many early successes[1]. The approach, however, faces several challenges in mass production, including complicated manufacturing processes with stringent regulatory requirements and a long production cycle of days to weeks[2]. Eliminating complications in CAR-T cell production—for instance, using gene-editing or in vitro induced pluripotent stem cell (iPS) approaches—may facilitate manufacturing scale-up while decreasing production costs[2].

T cell receptor (TCR)-T cell therapy represents an alternative that offers several advantages for solid tumors. In contrast to CAR-T, TCR-T cells can recognize peptides derived from mutated or overexpressed intracellular proteins, thereby expanding the search space for potential antigen targets. TCR-T cells appear less prone to systemic toxicity, for example, cytokine release syndrome[3]. Moreover, TCRs also have remarkable sensitivity, with the capacity to recognize a single ligand on a target cell[4]. TCRs are, however, restricted because they require a specific major histocompatibility complex (MHC) molecule that must match the patient's MHC repertoire. This limits the number of patients that can be treated with any individual TCR product.

Natural killer (NK) cells

NK cells have several advantages over CAR-T cells in cancer immunotherapy[5,6,7]. NK cells are a type of innate immune cell that can rapidly kill multiple adjacent cancer cells through non-MHC-restrictive effects. They can be extracted from peripheral blood, cord blood, induced pluripotent stem cells, and NK cell lines. In vitro activation, expansion, and genetic modification of NK cells can greatly enhance their antitumor activity and give them the ability to overcome drug resistance. CAR-NK cells, generated through genetic engineering, have demonstrated significant clinical responses and lower adverse effects compared with CAR-T cell therapy. The benefits of NK cells over CAR-T cells include their lower risk of cytokine release syndrome, absence of graft-versus-host disease (GvHD), multiple mechanisms of inducing cytotoxicity, and off-the-shelf feasibility.

Macrophages

Macrophages can efficiently infiltrate tumors, are major immune regulators, and are abundantly present in the tumor microenvironment (TME). CAR-macrophages have certain potential advantages over CAR-T, including high intra-tumoral migration capacity, antigen-dependent/independent phagocytosis, enhanced antigen-presenting capacity, and remodeling the immunosuppressive microenvironment.

Chapter 1:
The Current Landscape of Immune Cell Therapies

Autologous vs allogeneic cell therapies

With autologous cell therapies, each batch is specific and originates from an individual patient. In contrast, "off the shelf" allogeneic cell therapies involve batches of cells that come from a donor and can be used to treat multiple patients. The uniform starting material for allogeneic therapeutic cells creates more predictable and reproducible manufacturing. In addition, moving away from patient-specific manufacturing reduces labor time and costs, as there is less of a requirement for assay redesign and repetition. The drawback, however, is that donor cells can induce an immune response creating immune-mediated rejection and graft-versus-host disease.

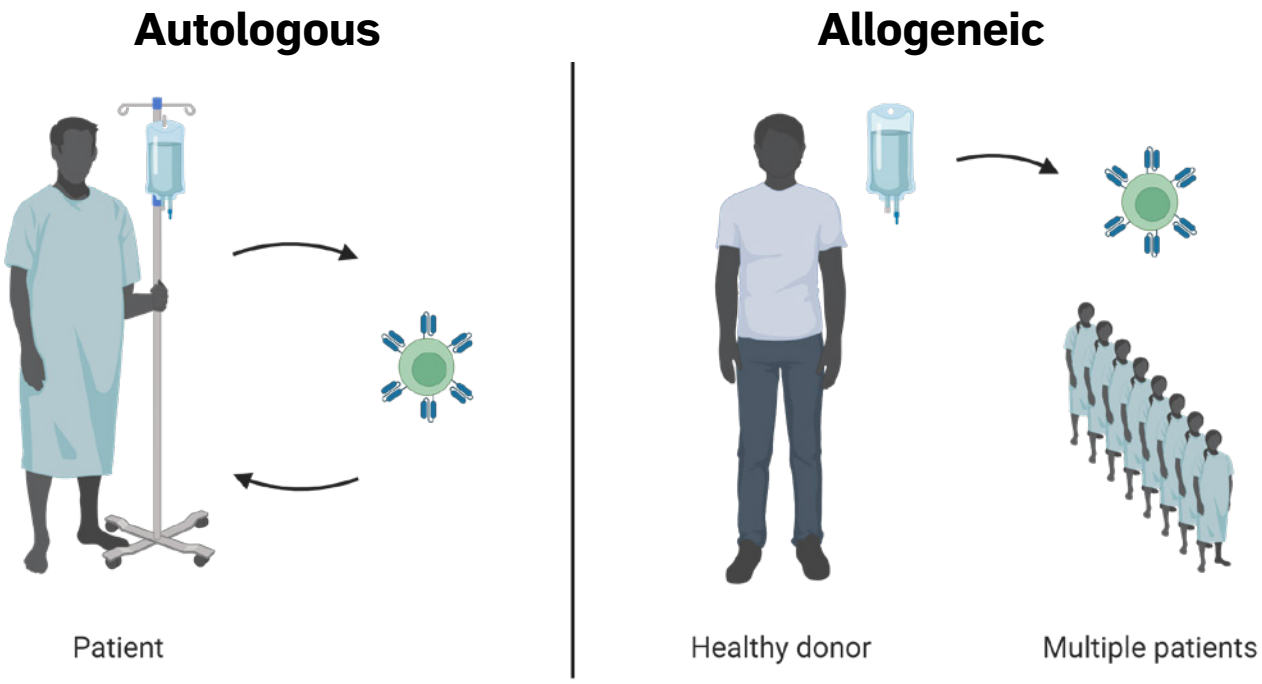

Figure 3. The source of cells is the main difference between autologous and allogeneic cell therapies. While autologous therapies use patient-specific cells, allogeneic therapies offer increased scalability by using cells that have been isolated from healthy donors and expanded to treat multiple patients.

Created with BioRender.com

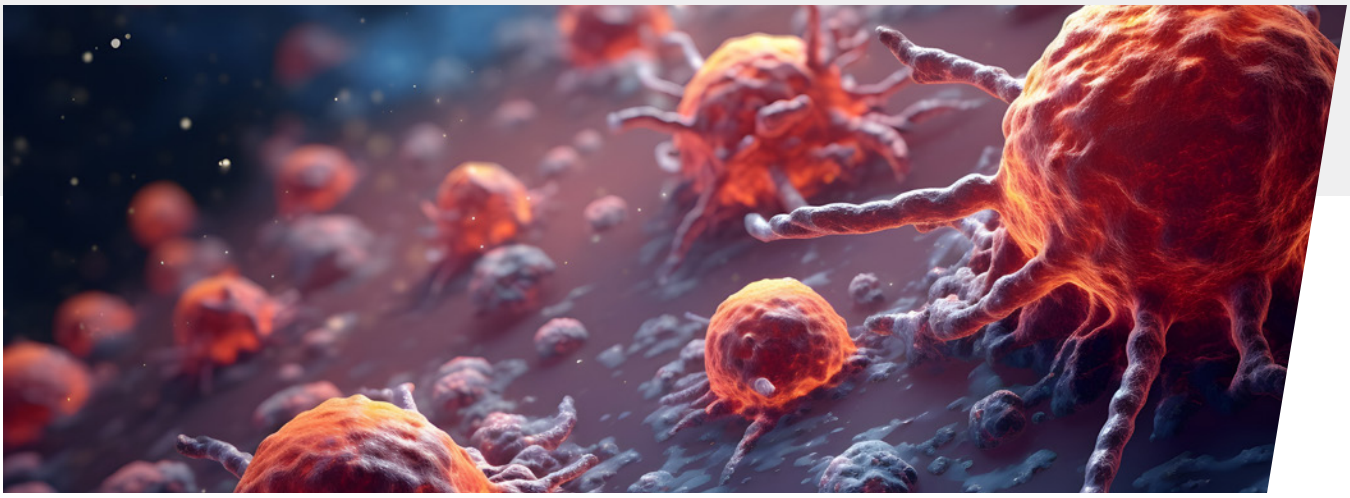

Chapter 2: Challenges to Cell Therapy Development

The cell therapy field has grown dramatically and there are now many companies developing novel types of engineered immune cells. Significant biologic challenges remain, including:

- **In leukemias and lymphomas initially susceptible to CAR-T cell treatment, loss or downregulation of antigens targeted by the CAR-T cells can lead to relapse.**
- **Although small clinical studies have reported striking responses in patients with carcinomas[8] or brain cancers[3] treated with TCR- or CAR-engineered T cells, responses to autologous cell therapy in common solid tumors have been poor.**
- **The immunosuppressive tumor microenvironment (TME) reduces immune cell activity due to restricted nutrient availability, acidosis, and local hypoxia, resulting in inefficient tumor infiltration, and poor functional persistence or exhaustion of cells[9,10].**

Determining the efficacy of cell therapies

As opposed to conventional pharmaceuticals, Advanced Therapy Medicinal Products (ATMPs) are required to meet a standard of "potency" as part of the final release criteria during manufacturing. Cell therapy products have no standardized potency assay for measuring biological activity and efficacy[11]. Such assays help confirm a product's specifications, as well as the biological functions of active ingredients related to the product's clinical mode of action (MOA).

Despite the lack of standardization, regulators require cell therapeutic developers to measure potency to ensure that a consistent product is delivered to all patients[11]. The measurements must be sensitive, quantitative, and convenient. Selecting meaningful potency assays can be difficult due to the varied, multifaceted, and sometimes ill-defined MOAs of cell therapies. To address this, regulators have suggested using a matrix of assays in combination with each other. Ideally, there should be a connection between product efficacy or clinical response and its characteristics, which can only be achieved by closely coordinating product characterization and clinical translation activities. An ideal potency assay should represent the product's relevant biological properties to assess the MOA and efficacy of cancer cell killing.

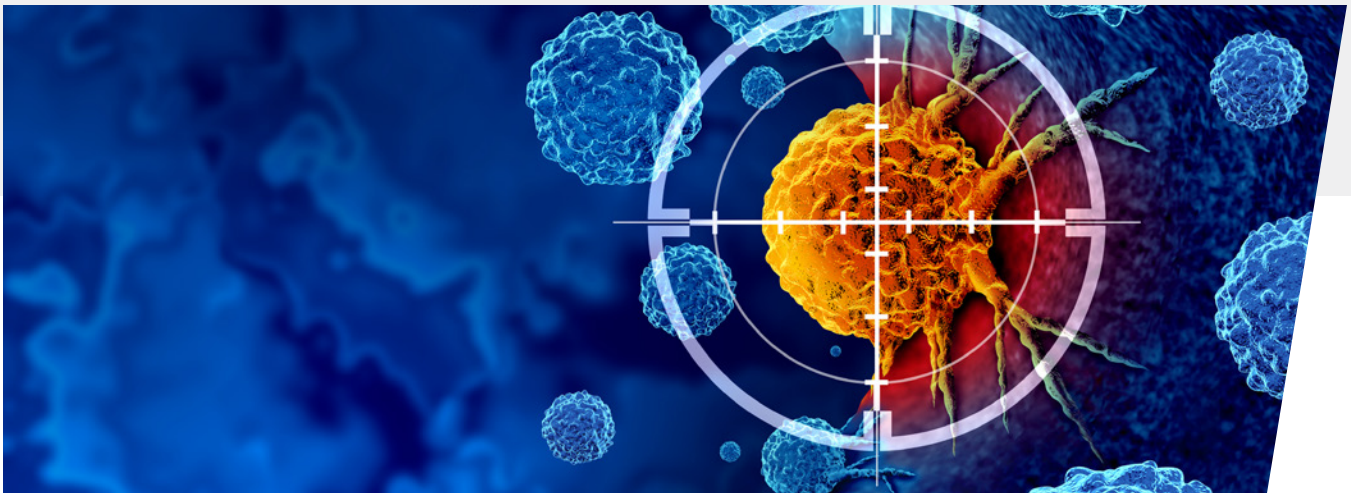

Chapter 3: Potency Assays

A detailed look at current assays for determining cell therapy efficacy

Common types of potency assays:

- Cytokine release assay
- Real-time impedance cytotoxicity assay
- LDH release assay

Cytokine release assay

When CAR-T cells are activated by the corresponding target cells, they release large amounts of cytokines that are important for T cell cytolytic activity and immune cell activation. CAR-T adoptive transfer in vivo is marked by rapid elevation of several cytokines in serum, including tumor necrosis factor-alpha (TNF-α), interferon-γ (IFN-γ), interleukin-6 (IL-6), and interleukin-10 (IL-10). Most CD19-targeting CAR-T cell therapies in clinical trials measure cytokine production for potency testing before product release. Common methods to measure cytokines include ELISA (enzyme-linked immunosorbent assay) or enzyme-linked immunospot (ELISpot) assays. Flow cytometry-based assays can also accurately measure cytokine release, in addition to cell activation and cell death[10].

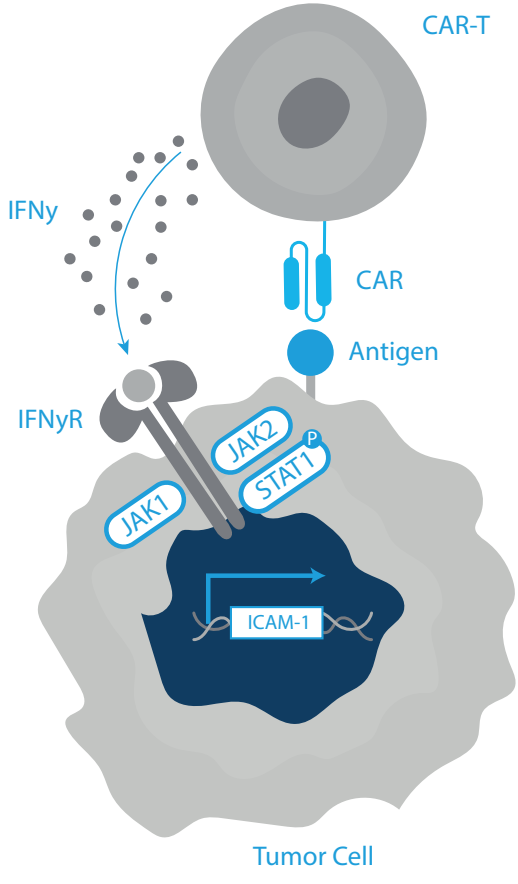

Chapter 3: Potency Assays

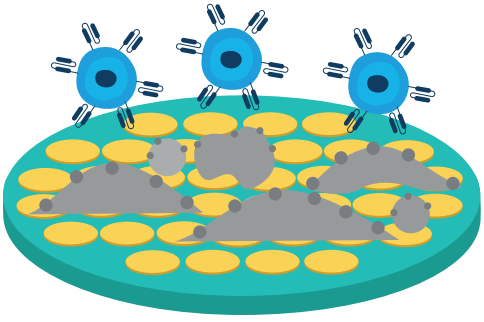

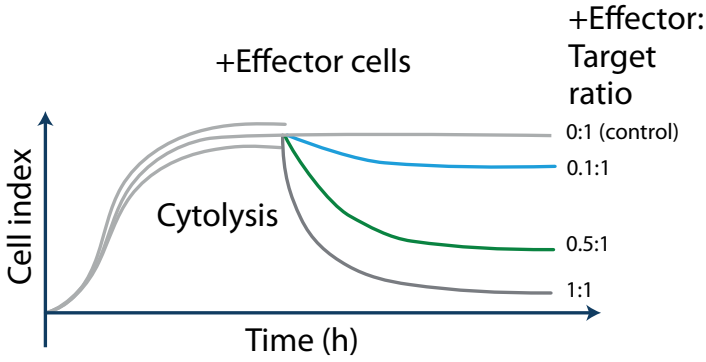

Cell index decreases as target cells are killed

Real-time impedance cytotoxicity assay

The impedance-based assay allows for label-free, real-time monitoring of cytolysis (measured as target cell detachment) over an interval of time[10]. Dynamic monitoring of treatment efficacy can be used to compare the cytotoxicity kinetics of different cells and varied constructs at multiple Effector versus Target (E:T) ratios over a period of several days. This is a major advantage when compared with other assays. Very low E:T ratios (in the range of 0.05:1 to 10:1) are feasible due to the nature of the assay, allowing it to be conducted over the course of several days. In addition, actual percentages for cytolysis data can be shown for further insight into assay results. The assay is suitable for 21 CFR Part 11 compliance requirements.

LDH release cytotoxicity assay

Cytotoxicity is often assessed by measuring the integrity of the cell membrane and detecting the release of markers that leak from the cytoplasm into the culture medium. Lactate dehydrogenase (LDH) is a commonly used marker for this type of assay[10]. When the plasma membrane is damaged, LDH is released into the surrounding cell culture medium. In the LDH assay, an excess amount of lactate and NAD+ drives LDH to generate pyruvate and NADH. The NADH is used to convert a substrate (resazurin) into a fluorogenic product (resorufin), which can be measured using a microplate reader. The amount of fluorescence is directly proportional to the number of damaged cells.

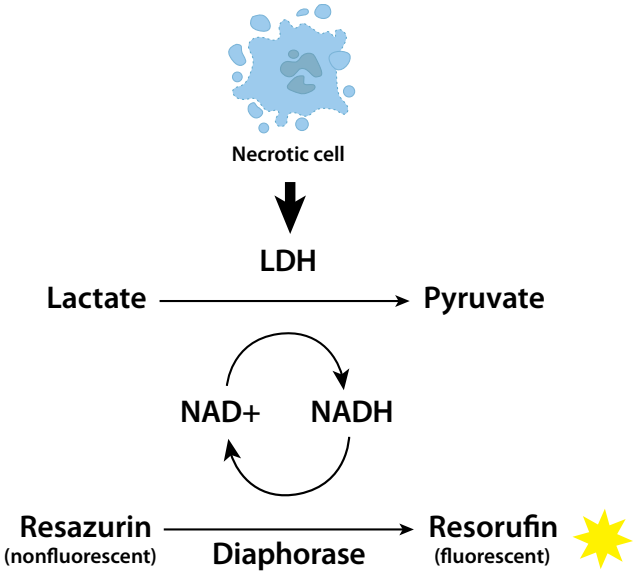

Chapter 3: Potency Assays

Related Solutions

Real-time Impedance Solutions
Monitor immune cell killing kinetics using **Agilent xCELLigence RTCA** technology. Easily analyze cytolysis data using the FDA 21 CFR Part 11 compliant **Agilent xCELLigence RTCA Software Pro** immunotherapy module.

Flow Cytometry Solutions
Measure immune cell activation, differentiation and exhaustion markers using the **Agilent NovoCyte Flow Cytometers**. Integrate the **Agilent NovoSampler Q** into different laboratory automation platforms and efficiently process FACS tubes and 24-, 48-, 96-, and 384-well plates. The intuitive FDA 21 CFR Part 11 compliant the **Agilent NovoExpress software** provides an exceptional user experience in data acquisition, analysis and reporting.

Imaging, Automation & Detection Solutions
Agilent provides a full range of solutions for conducting ELISpot assays across all commonly used formats. The **Agilent BioTek Cytation cell imaging multimode readers** can be used in conjunction with the FDA 21 CFR Part 11 Compliant **Agilent BioTek Gen5 software for imaging and microscopy** to quantitate changes in cytokine secretion. Automate the most labor-intensive aspect of the ELISpot workflow with Agilent BioTek washers and process up to 50 plates per run with **Agilent BioTek BioStack microplate stacker**.

Plate reader-based cytotoxicity assays are easy to perform using the **Agilent BioTek Synergy Multimode Readers**, which offer flexibility and ease of use over a broad range of applications.

xCELLigence Functional Potency Assay

Label-free, real-time, sensitive, robust, reproducible, 21CFR Part 11 compliant

Pharmaceutical companies need to develop reliable methods for product quality inspection to shorten the period of product release. To evaluate the efficacy of cell therapies, various *in vitro* methods have been developed, such as luciferase, lactic dehydrogenase (LDH), cytokine detection, and flow cytometry. However, all these methods require cell labeling, are labor-intensive, and only provide information about the cytotoxic effect of products at a selected time point. Agilent xCELLigence technology offers a label-free, real-time measurement of the immune-cell-mediated killing of cancer cells that is accurate and reproducible, and which satisfies the needs of analytical development in cell therapy manufacturing.

xCELLigence: a robust potency assay you can trust from discovery, process development to manufacturing QC release

- Small footprint
- 21CFR Part 11 compliance
- 16, 96, and 384-well format and HT options
- Convenient and simple workflow
- Automated data output and analysis
- Simple maintenance and calibration
- IQ/OQ/PQ and CSV service
- Over 4,800 peer-reviewed publications
- Highly cited by thought leaders in cell therapy
- Recommended by top cell therapy CRO/CDMO
- Adopted by leading cell therapy companies
- For both adherent and liquid tumor types

Evaluation of cytolytic activity of CART19 with xCELLigence

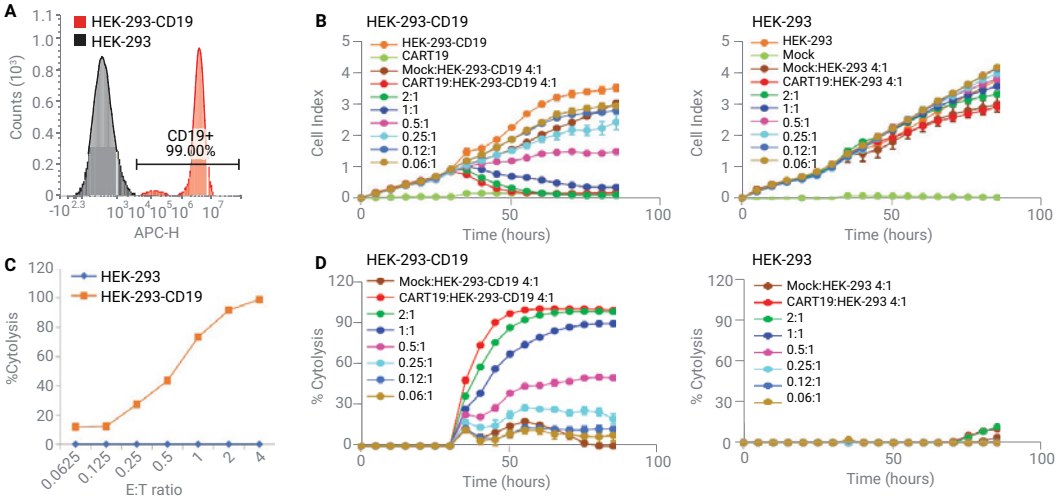

xCELLigence potency assay validation

Specificity

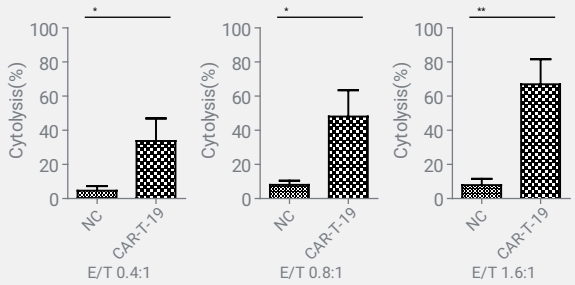

Only transduced T cells with CAR expression show high cytotoxicity potency to target cells.

Robustness

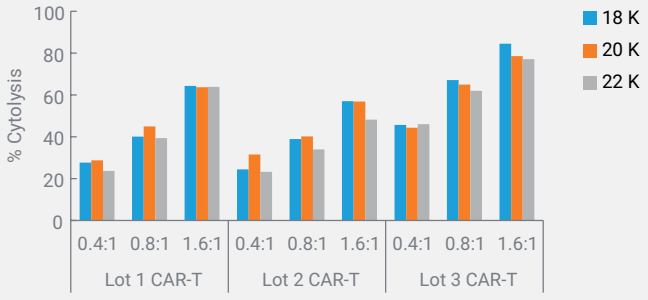

Slight changes in seeding density do not change the % cytolysis results.

Repeatability

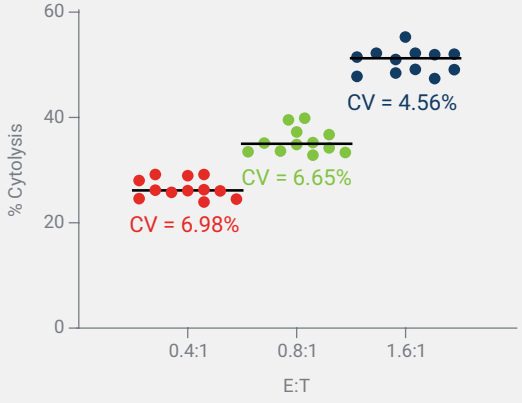

The same results were obtained when two analysts measured for six times with three replicates in each measurement.

Selected testimonials

"As a CRO, the xCELLigence RTCA MP (multi-plate) version is the workhorse of the over 80 to 90 CAR T and CAR-NK projects already completed. The real-time kinetic readout has accelerated the patent and IP positions of many of our clients. The ease-of-use is also wonderful. Plate cells, 24 hours later add compound or CAR T, and walk away for the next 80 hours, leaving our scientists to continue all their other experiments. I can attest to the fact that xCELLigence MP data have been very predictive in animal models and have led to clinical study initiation in just 9 months from the first experiment."

John Wu, PhD, CEO, ProMab Biotechnologies

"Bio-gene used Agilent's xCELLigence Real-Time Cell Analysis (RTCA) label-free platform for real-time release testing (RTRT). This technology can automatically detect cells in the whole process without labeling cells, which can greatly reduce the manual operation steps, and ensure the objectivity, accuracy, and integrity of experimental data. This scheme can more accurately evaluate the biological characteristics, efficacy, or potency of the product. More importantly, it can continuously detect the dynamic changes of cells in several hours or even dozens of days in real time."

Ding Wen, Director of Clinical Production Department, Bio-gene

RA45061.5984375

Published in the USA, May 24, 2023
5994-6161EN

Agilent
Trusted Answers

Application Note

Immunotherapy Research

Agilent

Trusted Answers

Ex Vivo Phenotyping and Potency Monitoring of CD19 CAR T Cells

Using a combined flow cytometry and impedance-based real-time cell analysis workflow

Authors

Lauren Jachimowicz, Ming Lei, Peifang Ye, Yan Lu, Xiaoping Ji, Yu Yan, Garret Guenther, and Nan Li

Agilent Technologies, Inc.

Abstract

The development of cell-mediated immunotherapies has revolutionized cancer research as well as the study of the immune system. One of the most promising types of cell therapy involves the genetic engineering of novel chimeric antigen receptor (CAR) T cells to target cancer cells. To efficiently determine optimal CAR construction, researchers must develop a robust screening protocol to identify the ideal parent T cell populations and evaluate their cell killing potency. Here, we describe a workflow using a combination of the Agilent xCELLigence RTCA analyzer and Agilent NovoCyte Quanteon flow cytometer to thoroughly evaluate and characterize CAR T cells.

Introduction

Advancements in immunotherapy have altered the available treatments for cancer, using the specific ability of the immune system to recognize and kill cancer cells. A novel class of immunotherapy, CAR T cells, involves genetically engineering T cells to target a tumor antigen. Currently, adoptive T cell therapies are used for the treatment of B cell malignancies. However, significant challenges remain in the application to many cancers, including the treatment of solid tumors, side effects such as cytokine release syndrome, and long development timelines. The ideal universal receptor structure for highly potent CAR T cells is undergoing continuous improvements, with new generations of CAR structures being developed to maximize T cell longevity and cytotoxicity. More recent versions of CAR structures include costimulatory molecules and signaling molecules that help with better T cell function and persistence *in vivo*. The development of novel CAR T cells requires fast and in-depth evaluation of their potency to ensure efficacy and the identification of any nonspecific effects such as antigen-independent signaling.

Unlike other cytolytic endpoint assays, the Agilent xCELLigence RTCA continuously monitors CAR T cell cytolytic activity in real time over multiple days. To determine the quality of the CAR T cells under investigation, orthogonal Agilent NovoCyte flow cytometry assays can be performed to evaluate T cell activation, differentiation, and exhaustion. Here, we combined impedance-based real time cell analysis (RTCA) and flow cytometry workflow for *ex vivo* cytolytic potency monitoring of CD19-specific CAR T cells (CART19). We also examined phenotypic and functional responses to antigen exposure over time. The potency evaluation and characterization of CAR T cells were performed in several ways:

- CAR expression and T cell phenotyping
- Cytolytic potency by an RTCA cytotoxicity assay
- Cytokine production in response to antigen with a flow cytometry multiplex cytokine detection assay
- Characterization of CAR T cell state following antigen-specific activation.

This powerful workflow can be used to easily measure the cytolytic capacity of CAR T cells in conjunction with an in-depth analysis of T cell cytokine production, cell differentiation, and activation state.

Experimental

Effector and target cell culture and characterization

HEK-293 cells were maintained at 37 °C/5% CO_2 in MEM/EBSS (HyClone, catalog number SH30024.01) supplemented with 10% FBS (Gibco, catalog number 16050-122). These cells were engineered to express CD19 using lentiviral transduction. Expression of CD19 on the surface of HEK-293 cells was verified by flow cytometry with an Agilent anti-CD19 PE antibody (part number 8920007).

CD19-specific CAR T cells were constructed using PBMCs from a healthy donor and cultured for nine days with anti-CD3/anti-CD28 beads with the addition of 200 IU/mL of IL-2 in the same growth media as target cells.

CAR expression on T cells

CAR expression was analyzed in T cell populations using Agilent anti-CD3 FITC (part number 8931016), anti-CD4 PE-Cy5 (Biolegend 300510), Agilent anti-CD8 PE-Cy7 (part number 8931024), Agilent anti-CD19 APC (part number 8930007), anti-CD16 APC-Cy7 (BD, 561726), and anti-CD56 BV605 (Biolegend 318334) antibodies, and a CARTEST-19 kit provided from the CAR T manufacturer. The CAR T kit consisted of a CD19 antigen fused to a Fc tag, followed by a secondary anti-FC PE antibody. 1×10^6 CAR T cells were stained with live/dead AViD stain followed by incubation of cells with Fc block buffer (D-PBS containing 10% heat-inactivated human serum, 0.5% BSA, and 0.5% heat-inactivated FBS). Following this, cells were stained with the primary CAR T antibody for one hour on ice, then excess antibody was removed with the addition of 4% bovine serum albumin followed by centrifugation. Cells were then resuspended in antibody cocktail with anti-CD3, anti-CD4, anti-CD8, and secondary CAR T cell antibody for 30 minutes at 4 °C. Following incubation, cells were washed with the addition of 1% BSA and resuspended for flow cytometry acquisition. All analyses were performed on an Agilent NovoCyte Quanteon.

Characterization of CAR T cells and cytokine production

CAR T cells were analyzed before addition into the T cell cytolytic assay and at 40 and 88 hours after addition. Cells were stained with live/dead AViD stain followed by incubation of cells with Fc block buffer (D-PBS containing 10% heat-inactivated human serum, 0.5% BSA, and 0.5% heat-inactivated FBS). Excess stain was removed with the addition of PBS and the solution was centrifuged for five minutes at 300 g. The antibodies used are specified in Table 1, which provides information on antibody clone and fluorophore used. Cells were stained with the antibody cocktail for 30 minutes on ice. Following antibody incubation, cells were washed with the addition of 1% BSA and resuspended for flow cytometric analysis. FMO controls

were made by staining a sample with all antibodies except the one in which background was to be assessed.

Cytokine production bead-based multiplex assay

50 µL of cell supernatant was collected 24 hours after addition of T cells into the T cell cytolytic assay. IL-2, 4, 6, 10, 17A, IFN-γ, TNF-α, soluble Fas, soluble FasL, Granzyme A, Granzyme B, Perforin, and Granulysin in the cell supernatant were detected following the kit manufacturer's instructions, Human CD8/NK Panel, Biolegend, catalog number 740267.

CAR T cell cytolytic assay

The CAR T cell cytolytic assay was monitored on the Agilent xCELLigence MP, impedance measurements were taken every 15 minutes. The same growth medium and conditions were used as described for the target cells. After measuring background impedance using 50 µL of media/well, 10,000 target cells, in 100 µL of media, were added to each well. Proliferation was monitored for 23 hours, then 50 µL of media was removed and replaced with 50 µL of CD19 CAR T cells. Total numbers of T cells added differed to achieve E:T ratios of 0.06, 0.12, 0.25, 0.5, 1, 2, or 4. When using the impedance data, % cytolysis = [1 – Normalized $CI_{treatment}$/Normalized CI_{target} only] × 100

Results and discussion

Determination of T cell CAR expression and T cell state

Assessment of CAR expression and CAR T-cell phenotype is essential during CAR T discovery and for quality control during manufacturing. A CAR construct that targets CD19, a receptor expressed on B cell lymphoma cells was generated and used to transduce peripheral blood mononuclear cells (PBMCs). After generation, cells were expanded *ex vivo* and examined for the expression of CAR (Figure 1). *Ex vivo* expansion of PBMCs with anti-CD3 and anti-CD28 antibodies activates the T cell receptor and exclusively expands T cell populations. After nine days of culture, over 99% of live cells were CD3+ demonstrating that T cells were specifically expanded, and only small numbers of other cells were present. Approximately 50% of the total cells expressed chimeric antigen receptor (CAR), specifically 50% of CD4+ T cells and 46% of CD8 T cells, demonstrating successful stable transduction of the CAR construct.

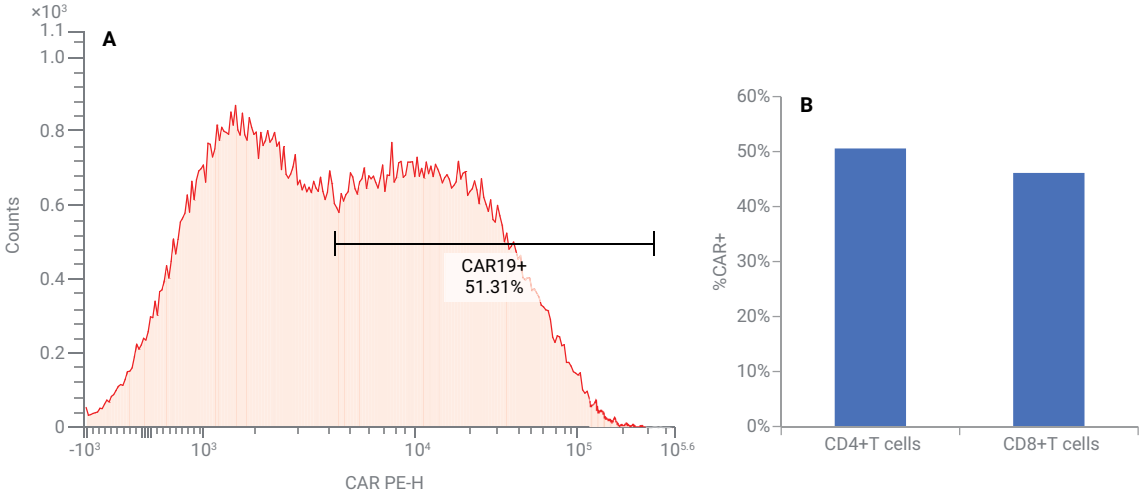

Figure 1. CAR expression and T cell phenotype of CART19 cells. CART19 cells were prepared by a collaborator for commercial use. Human PBMCs were transduced with a CD19 CAR construct or a mock vector and CAR19 expression was evaluated on T cell populations by flow cytometry. CAR T cells were stained with live/dead AViD stain, anti-CD3 FITC, anti-CD4 PE-Cy5, anti-CD8 PE-Cy7, anti-CD19 APC, anti-CD16 APC-Cy7, and anti-CD56 BV605 antibodies. The final CAR expression in total live cells was evaluated by staining with CD19 antigen with a FC tag and anti-FC PE antibody (A). Expression of CART19 in CD4+ and CD8+ subpopulations (B).

To further characterize the CART19 cells, a 12-color immunophenotyping flow cytometry panel was devised (Table 1) to examine T cell differentiation, activation, and exhaustion markers and provide insight into the status of CAR T cells. In this immunotherapy panel, after removal of dead cells and debris, T cells are identified by CD3 and divided into CD4 and CD8 T cell subsets (Figure 2A). The following differentiation states of T cells were identified using the expression patterns of CD45RA and CCR7; naïve-like (CCR7+CD45RA+), effector (CCR7-CD45RA+), effector memory (CCR7-CD45RA–), and central memory (CCR7+CD45RA–) T population. The naïve-like T cell population can be

Table 1. A 12-color flow cytometry panel was developed for analysis of differentiation, activation, and exhaustion of CART19 cells.

	Fluorochrome	Clone	Description
Dead cells	Aqua	AViD	Dead cells
CD3	BV570	UCHT1	T lineage
CD4	BV785	OKT4	
CD8	FITC	SK1	
CD45RA	BV650	HI100	Differentiation
CCR7	PE-Cy7	G043H7	
CD95	PE-Dazzle594	DX2	
CD25	BV421	M-A251	Activation
CD127	PE-Cy5	A019D5	
PD-1	APC	EH12.2H7	Exhaustion
TIM-3	PE	F38-2E2	
LAG-3	BV605	11C3C65	

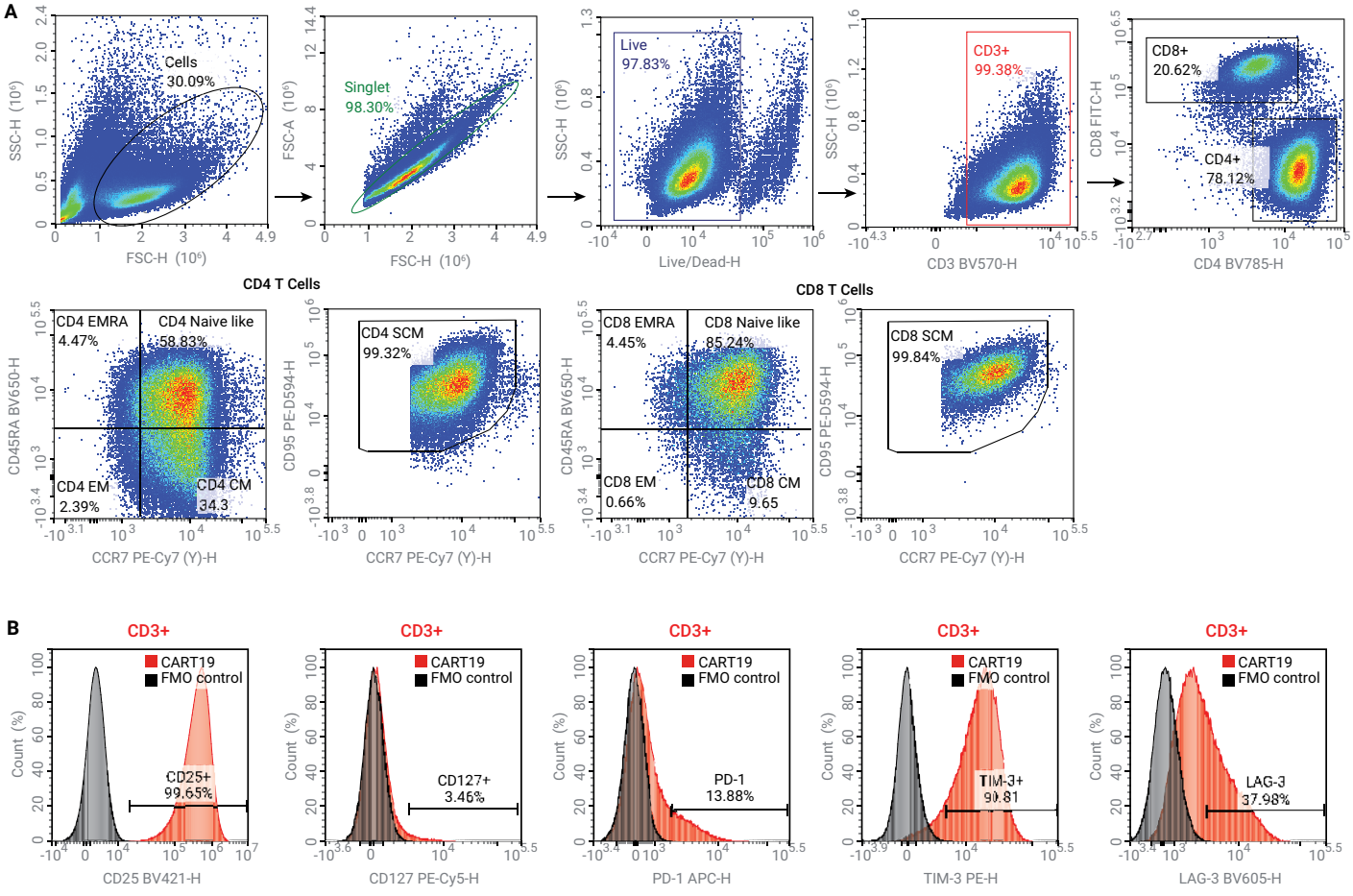

Figure 2. CART19 cell immunophenotyping before T cell cytolytic assay. CART19 cells stained with the 12-color immunophenotyping panel described in Table 1 (A). FMO controls are shown for CD25 BV421, CD127 PE-Cy5, PD-1 APC, TIM-3 PE, and LAG-3 BV605 (B).

further separated into stem cell-like memory T cells (CD95+) and true naïve T cells (CD95–). CAR T cells before addition to the cytolytic assay consisted of ~20% CD8 T cells and ~80% CD4 T cells. A substantial proportion of the cells were CCR7+CD45RA– central memory T cells (34% CD4+ cells, 9.38% CD8+ cells) and CCR7+CD45RA+CD95+ stem cell-like T cells (58% CD4+ cells and 85% CD8+ cells), demonstrating that most CAR T cells derived from PBMCs develop a memory-like phenotype in response to CD3/CD28 stimulation *in vitro*. Development of a memory like phenotype after *in vitro* expression has been demonstrated previously to be beneficial for CAR T cell persistence *in vivo*. Expression of T cell activation markers CD25 and CD127 as well as presence of co-inhibitory receptors PD-1, TIM-3, and LAG-3 provides an in-depth analysis of T cell status. After T cell activation and expansion, the CART19 cells express high levels of CD25 and express co-inhibitory receptors (exhaustion markers) PD-1, TIM-3, and LAG-3. While normally upregulated after T cell activation, sustained high expression of these co-inhibitory receptors can inhibit T cell cytolytic function. For efficient cancer immunotherapy, it is important to prevent CAR T cell exhaustion. Therefore, monitoring the expression of activation and exhaustion markers on novel CAR T candidates is essential for the development of new adoptive cell therapies. An in-depth investigation of CAR T cell candidates can be achieved, through the assessment of T cell phenotype and activation status, combined with functional assays, such as T cell cytolytic activity and cytokine production.

CD19 CAR T cell cytolytic activity measured by xCELLigence RTCA

The xCELLigence RTCA system uses a microplate with biosensors in the base of the wells to monitor cellular interaction with the plate surface. This cellular interaction is used as a measurement of cell concentration, adhesion, and morphology. The cell signal is recorded continuously throughout the assay at set intervals and represented as Cell Index, providing real-time analysis of the cells. Lymphocytes do not adhere to the bottom of the well and do not generate signal, therefore, in this assay, the Cell Index measurement is exclusively from the target cancer cells. As CAR T cells lyse target cancer cells, a decrease in the cell index is observed.

The cytolytic capacity of CART19 cells was measured using a T cell cytolytic assay. CART19 cells were cultured with CD19 expressing HEK-293 cells while real time measurements of T cell mediated cytolysis were taken with the xCELLigence instrument. One day before the addition of CART19 cells, HEK293 cells that ectopically expressed CD19 or controls were seeded. After the addition of CART19 cells, rapid cytolysis of HEK-293-CD19 cells occurs (Figures 3B to 3D) reaching more than 95% cytolysis within 24 hours post-CART19 addition (Figure 3C). There was almost no cytolysis from nonspecific CAR T cells, and it was only observed at very late time points of the coculture of effector and target cells (Figure 3D). The CART19 response was also dose-dependent, increased E:T ratios resulted in more rapid and a higher total percentage of cytolysis of target cells than lower E:T ratios. T cell cytolysis assays performed using xCELLigence RTCA allow rapid real-time assessment of CAR T function.

Upregulation of CD19 CAR T cell cytokine and cytolytic protein production

When CAR T cells are activated by the corresponding target cells, they release large amounts of cytokines important for T cell cytolytic activity and immune cell activation. CAR T adoptive transfer *in vivo* is marked by rapid elevation of several cytokines in serum including tumor necrosis factor-alpha (TNF-α), interferon γ (IFN-γ), interleukin 6 (IL-6), and interleukin-10 (IL-10). In addition to aiding in the immune cell response, an overabundance of cytokines can lead to cytokine release syndrome. It may be beneficial to monitor cytokine production in an *in vitro* model to better predict T cell efficacy and screen for an overexuberant cytokine response. Further characterization was performed by quantifying the amount of cytokine produced by CART19 while killing target cells. Cytokine levels were measured in the supernatant of CART19-HEK-293-CD19 cultures using a bead-based multiplex flow cytometric assay that measures multiple cytokines simultaneously. Higher E:T ratios of CART19 cells resulted in increased expression of cytokines IFNγ, TNFα, IL-2, and IL-10 as well as cytolytic proteins granzyme A, granzyme B, granulysin, perforin, and sFasL. Almost no cytokine production was observed from CART19 cultured with HEK-293 demonstrating that increased secretion of cytokines and cytolytic proteins was induced by CAR-dependent signaling.

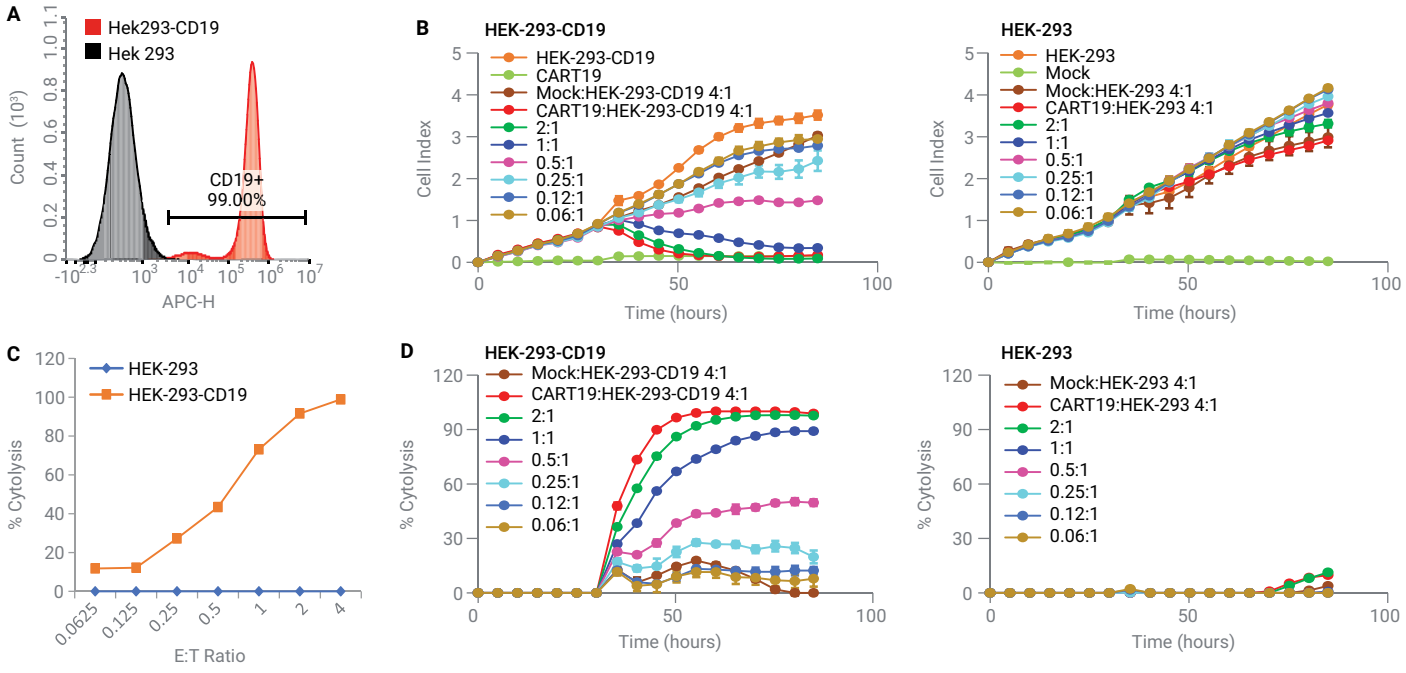

Figure 3. Evaluation of cytolytic activity of CART19 by the Agilent xCELLigence RTCA system. CD19 expression was evaluated on HEK-293 and HEK-293-CD19 cell lines by surface stain with anti-CD19 APC antibody (A). 10,000 HEK-293-CD19 and HEK293 cell were seeded in a 96-well E-Plate, and Cell Index (CI) measurements were taken every 15 minutes using an xCELLigence MP system. (B) After 24 hours, CART19 effector cells (left plot) or mock CAR T (right plot) were added at various E:T ratios ranging from 2:1 to 0.06:1. (D) The Cell Index plots are converted to % cytolysis by the xCELLigence Immunotherapy software. % Cytolysis was measured at 24 hours after CART19 addition with HEK-293 or HEK293-CD19 target cells (C).

Characterization of CD19 CAR T cell activation upon antigen stimulation

CAR T cells were also assessed at the end of the T cell cytolytic assay using the same 12-color immunophenotyping panel used to assess the CAR T cells before the cytolytic assay. This enabled the detection of any changes in the expression of T cell activation and exhaustion markers. Effector CART19 cells displayed a more activated T cell state at both 40 and 88 hours after T cell addition compared to control cocultures. CART19 cells that were cultured with CD19-HEK-293 cells showed increased FSC, higher expression of CD25, PD-1, TIM-3, and LAG-3 and downregulation of CD127. Combining CART 19 cytolysis measurements with flow cytometric assessment of T cell status and cytokine production may provide a comprehensive understanding of underlying mechanistic aspects of CAR T cell mediated killing.

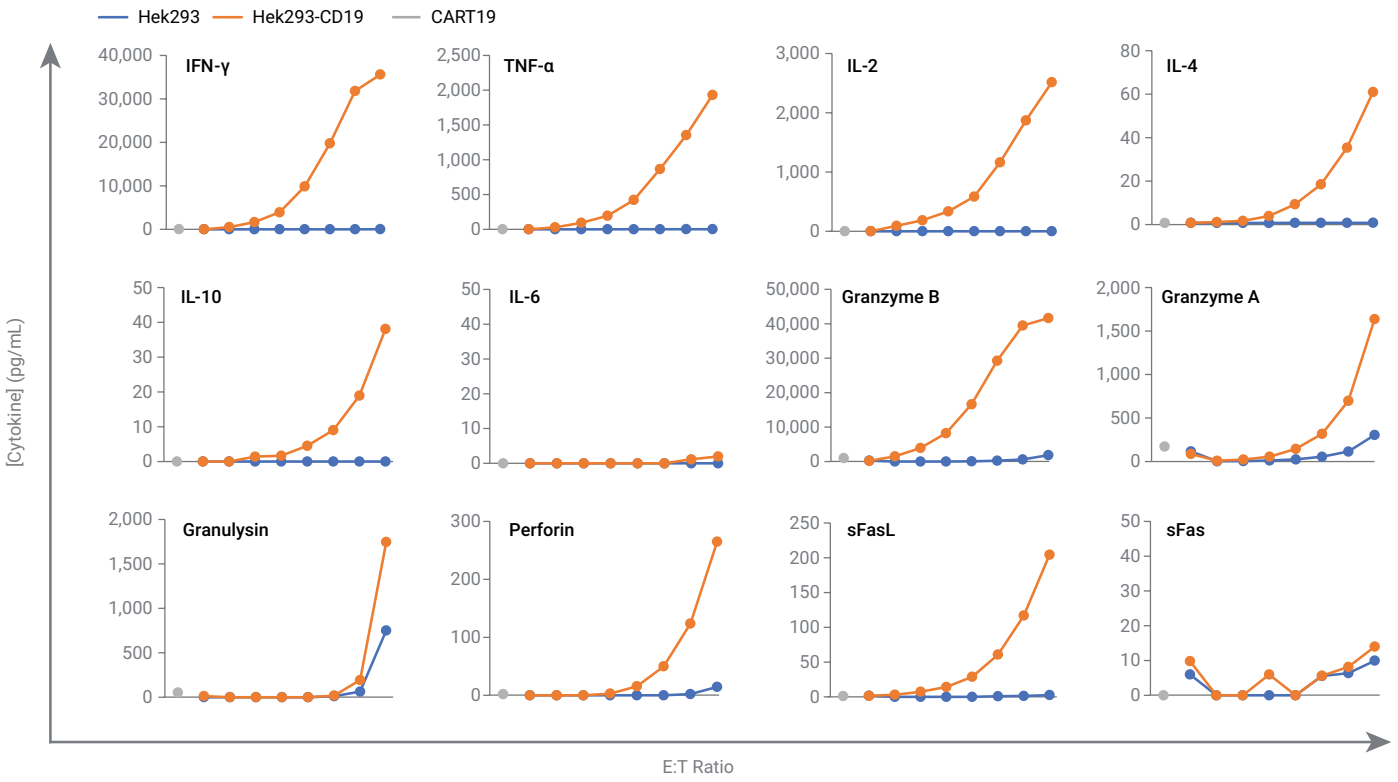

Figure 4. Cytokine production by CART19 after cocultured with HEK-293-CD19. CART19 cells were added at different E:T ratios 24 hours after HEK-293-CD19 or HEK-293 cells seeding. Supernatant was collected 18 hours later and the cytokine concentration was measured on the Agilent NovoCyte Quanteon flow cytometer using BioLegend LEGENDplex Human CD8/NK panel.

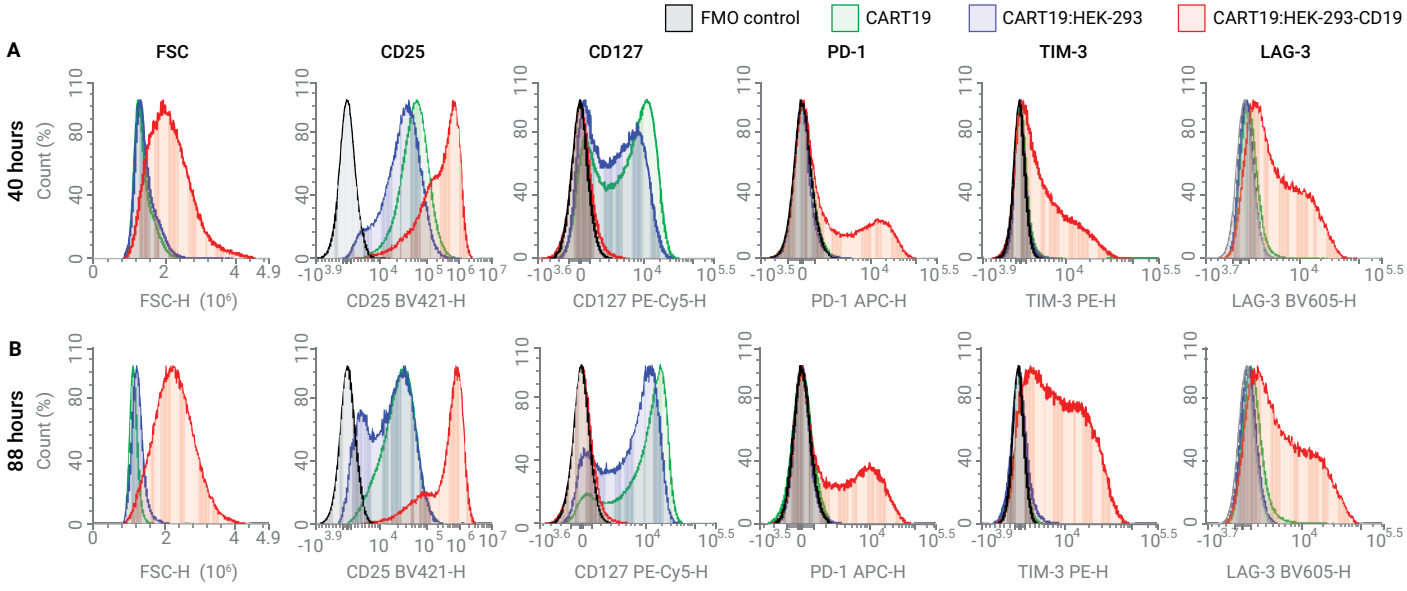

Figure 5. Characterization of CART19 cells after coculture with HEK-293-CD19. Cells were collected from CART and HEK-293 or HEK-293-CD19 cocultures after 40 hours (A) and 88 hours (B) at a 1:1 Effector:Target ratio. Cells were stained with the 12-color immunophenotyping panel described in Table 1. Expression of activation and exhaustion markers were compared.

Conclusion

The therapeutic potential of CAR T cell therapies has driven the development of these treatments, requiring rapid analysis of novel CAR T cell candidates. The combined Agilent xCELLigence RTCA and NovoCyte Quanteon flow cytometer cell analysis workflow provides researchers comprehensive and convenient results of cytolytic potency, cytokine secretion, CAR T characterization, and impurity analysis.

References

1. Gattinoni, L. *et al.* T Memory Stem Cells in Health and Disease. *Nat. Med*. **2017**, *23(1)*, 18–27.
2. McLellan, A. D.; Ali Hosseini Rad, S. M. Chimeric Antigen Receptor T Cell Persistence and Memory Cell Formation. *Immunol. Cell Biol.* **2019**, *97*, 664–674.
3. Schmueck-Henneresse, M. *et al.* Comprehensive Approach for Identifying the T Cell Subset Origin of CD3 and CD28 Antibody-Activated Chimeric Antigen Receptor-Modified T Cells. J Immunol. 2017;199(1):348–362.
4. Yu, S. *et al.* Next Generation Chimeric Antigen Receptor T cells: Safety Strategies to Overcome Toxicity. *Mol. Cancer*. **2019**,*18(1)*, 125. Published 2019 Aug 20. doi:10.1186/s12943-019-1057-4
5. Lee, D. W. *et al.* Current Concepts in the Diagnosis and Management of Cytokine Release Syndrome [published correction appears in *Blood*. **2015** Aug 20, *126(8)*, 1048. Dosage error in article text] [published correction appears in *Blood* **2016** Sep 15, *128(11)*, 1533]. *Blood* **2014**, *124(2)*, 188–195. doi:10.1182/blood-2014-05-552729

www.agilent.com/chem

RA.6848263889

Printed in the USA, October 27, 2020
5994-2377EN

Agilent
Trusted Answers

Application Note

Immuno-Oncology

Agilent

Trusted Answers

Stimulation of Human Peripheral Blood Mononuclear Cells

Using the Agilent BioTek Cytation 7 cell imaging multimode reader to image and analyze ELISpot assays

Author

Paul Held, PhD
Agilent Technologies, Inc.

Abstract

Human peripheral blood mononuclear cells (PBMCs) are routinely isolated from blood samples, then used in several fields of research including autoimmune disorders, infectious diseases, vaccine development, and cancers. The ELISpot assay monitors *ex vivo* cellular immune responses to antigenic stimuli. This application note uses the Agilent BioTek Cytation 7 cell imaging multimode reader in conjunction with Agilent BioTek Gen5 microplate reader and imager software to quantitate changes in cytokine secretion in PBMCs using the colorimetric ELISpot assay format.

Introduction

PBMCs are differentially stimulated to secrete a number of cytokines as a result of a receptor-mediated cascade based on the cell type and the stimuli. The response of this diverse group of cells to different stimuli offers insights into their role in disease and the development of treatment modalities.

PBMCs are peripheral blood cells that have a round nucleus.[1] These cells consist of lymphocytes (T-, B-, and NK-cells) as well as monocytes. Other peripheral blood cells either have no nuclei (erythrocytes and platelets) or have multilobed nuclei (neutrophils, basophils, and eosinophils). In humans, lymphocytes make up the majority of the PBMC population, followed by monocytes, and only a small percentage of dendritic cells.[2]

Cytokines are small molecular weight proteins or peptides secreted by many cell types (particularly immune system cells) that regulate the duration and intensity of the immune response. The cytokine interleukin 2 (IL-2) is a pleiotropic cellular regulatory molecule that is produced by lymphoid cells in response to several stimuli. It plays a role in preventing autoimmune diseases by promoting differentiation of immature T cells into regulatory T cells.[3] In addition, IL-2 causes the differentiation of T cells into effector T cells and memory T cells when the original T cell was stimulated by an antigen.[4] Interferon gamma (IFN-γ), is a cytokine critical for innate and adaptive immunity against infections. IFN-γ is produced predominantly by natural killer (NK) and natural killer T (NKT) cells as part of the innate immune response, and by cytotoxic T lymphocyte (CTL) effector T cells once antigen-specific immunity develops.[5] The importance of IFN-γ in the immune system stems in part from its ability to inhibit viral replication directly, and from its immune-stimulatory and immunomodulatory effects. Aberrant IFN-γ expression is associated with a number of auto-inflammatory and autoimmune diseases.

T cell activation is normally initiated by the interaction of a cell surface receptor to its specific ligand molecule along with a co-stimulatory molecule.[6] This binding event triggers the rapid hydrolysis of inositol phospholipids to diacylglycerol and inositol phosphates by phospholipase C (PLC).

Diacylglycerol is an allosteric activator of protein kinase C (PKC). PKC activation and inositol phosphates, which trigger Ca^{2+} release and mobilization, result in a cascade of additional cellular responses mediating T cell activation (Figure 1). Two of these cellular responses are the production and secretion of IL-2 and INF-γ. Triptolide is a diterpene triepoxide that is a potent immunosuppressant and anti-inflammatory (Figure 2). Triptolide has been shown to inhibit the expression of IL-2 in activated T cells at the level of purine-box/nuclear factor and NF-κB mediated transcription activation.[7]

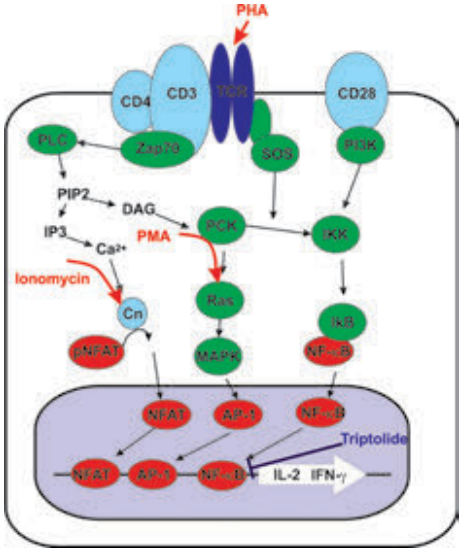

Figure 1. Schematic of signal cascade for stimulation of IL-2 and INF-γ secretion.

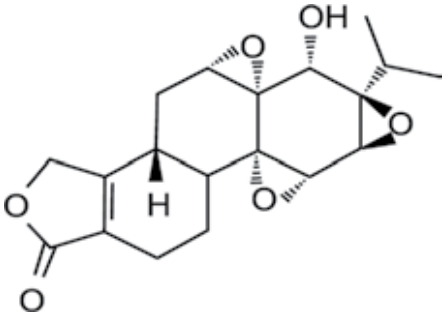

Figure 2. Structure of triptolide.

While some PBMCs are known to produce IL-2 and INF-γ, under normal growth conditions little is produced. Only after stimulation will substantial amounts of the cytokines be expressed.[8] Phytohemagglutinin (PHA) is a lectin that binds to the sugars on glycosylated surface proteins, including the T cell receptor (TCR), and nonspecifically binds them. The result is the low level stimulation of the signal cascade required for IL-2 or INF-γ secretion.[9] Likewise, phorbol myristate acetate (PMA) is a small organic compound, which has a structure analogous to diacylglycerol, that diffuses through the cell membrane into the cytoplasm where it directly activates protein kinase C (PKC). When used in combination with ionomycin, a calcium ionophore, which triggers calcium release, it results in a moderate level of cytokine release. However, when PMA and a co-stimulator, such as PHA, stimulate PBMC cells concurrently, cytokine production is strongly enhanced.[10]

The ELISpot assay procedure is very similar to that of a conventional ELISA. The plates are first coated with the appropriate capture antibody. Cultured secreting cells are added to the wells along with any interested experimental mitogen or antigen. Cells are maintained for a period of time after which they are removed. The secreted analyte remains bound to the capture antibodies in close proximity to the location on the plate where the cell that produced the analyte was situated. After removal of the cells and any unbound materials, a detection antibody (usually biotinylated) is added followed by an enzyme conjugate with an incubation to allow binding and a wash to remove unbound materials after each step. As the substrate is converted by the conjugate enzyme to colored compounds, spots on the plate membrane bottom at the locations of the original analyte capture are formed. The resultant spots are then analyzed/counted using image analysis (Figure 3).

Materials and methods

Human IL-2 ELISpot colorimetric kit was obtained from U-CyTech biosciences (Utrecht, The Netherlands) and a two color human IFN-γ/IL-2 ELISpot kit was from Cellular Technology Limited (Cleveland, OH). Phorbol 12-myristate (PMA), and Triptolide (part number T3652) were purchased from MilliporeSigma (Burlington, MA). Ionomycin (part number 407952) was from EMD Millipore (Chicago, IL). Human PBMCs were obtained from Astarte Biologicals (Bothell, WA). White PVDP membrane 96-well (part number MSIP4W10) were from MilliporeSigma.

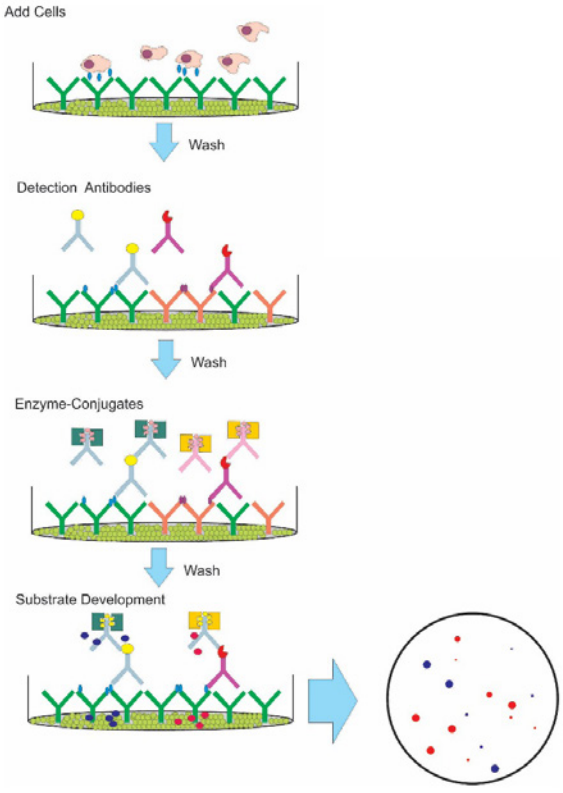

Figure 3. ELISpot stain procedure.

Cell culture

Purified human PBMCs were received and maintained frozen until needed. After rapid thawing cells were immediately diluted 1:10 in RPMI-1640 plus 10% FBS supplemented with 2 mM glutamine, penicillin, and streptomycin. Cells were centrifuged at 300 × g for 10 minutes and the supernatant removed. Cells were resuspended in 10 mL of fresh RPMI media, counted, and diluted as needed to provide a density of 5×10^4 cells/well.

Plate coating

Either a human IL-2 ELISpot kit from U-CyTech Biosciences or a 2-color human INF-γ/IL-2 kit from CTL were used for these experiments. PVDF membrane plates are first coated with the appropriate concentration of capture antibody (anti-IL-2 or anti-FTN-γ) and allowed to absorb overnight at 4 °C. The unbound antibody is aspirated and the plate is manually washed 3x with PBS. The wells are then filled with a blocking solution (200 µL) and allowed to incubate for at least 1 hour at room temperature. Blocking buffer is aspirated without washing immediately before the addition of cells.

Cell seeding

Unless otherwise indicated, cells were plated in 96-well membrane plates previously coated with antibody at a density of 5 × 10^4/well. PBMCs were stimulated to secrete IL-2 with a PMA (50 ng/mL), ionomycin (1 µg/mL) mixture. Typical experiments used a volume of 100 µL for cells followed by the addition of 100 µL of stimulant mixture at a 2x concentration.

Triptolide inhibition

PBMCs were plated at 5 × 10^4/well in 50 µL volume of complete RPMI media. After allowing cells to recover for 1 hour at 37 °C, in a humidified 5% CO_2 environment, triptolide treatment was added in complete RPMI media at 4x of final concentration to each well in 50 µL. IL-2 stimuli mixture (2x) was then added in 100 µL for a final volume of 200 µL.

One-color ELISpot assay

The assays were performed according to the U-Cytech BioSciences kit instructions. After seeding, cells were incubated for 24 hours, at 37 °C in a humidified 5% CO_2 environment plates and then assayed using an ELISpot kit. Briefly, cells were removed by washing 5x with 250 µL of PBS-Tween 0.05% using an Agilent BioTek MultiFlo FX multimode dispenser. A biotinylated detection antibody (100 µL) was added to the well and allowed to incubate for 60 minutes at 37 °C or overnight at 5 °C, after which unbound detection antibody was removed by washing. A streptavidin-HRP conjugate was then added (100 µL) and incubated at 37 °C for 60 minutes. Again, unbound conjugate is removed by washing. Next a two-part AEC substrate was added that deposits dye onto the well membrane bottom. Reactions were halted after 30 minutes at RT by washing with deionized water (250 µL) 3x using the MultiFlo FX and allowed to dry in the dark. Entire wells were then imaged.

Two-color ELISpot development

The assays were performed according to the C.T. L. Immunospot 2-color ELISpot kit instructions. After seeding, cells were incubated for 24 hours at 37 °C in a humidified 5% CO_2 environment plates were then assayed using an ELISpot kit. Briefly, cells removed by washing 5x with 250 µL PBS-Tween 0.05% using a MultiFlo FX. A detection antibody solution (80 µL/well) was added to the well and allowed to incubate at room temperature (RT) for 120 minutes, after which unbound detection antibody is removed by washing. Tertiary solution (80 µL/well) was added and allowed to incubate for 60 minutes at RT. Unreacted reagents were removed by washing 2x with PBS-Tween, followed by 2 washes with dH_2O, then allowed to air dry in the dark. Blue developer solution was then added (80 µL/well) and incubated for 15 minutes at RT. The reaction was stopped by washing 3x with dH_2O. Red developer solution was then added (80 µL/well) and incubated at RT for 7 minutes. The plate was then washed 3x with dH_2O. The plate was air-dried in the dark for at least 2 hours prior to imaging.

Plate washing

Plates were washed according to the assay kit instructions using a MultiFlo FX. Wash buffer consisted of PBS (NaCl 137 mM, KCl 2.7 mM, Na_2HPO_4 10 mM, KH_2PO_4 7.4 mM) supplemented with 0.05% Tween 20. Unless specifically indicated, plates were washed five times with 250 µL buffer per well.

Plate imaging

Prepared microplates were imaged using a Cytation 7 configured with an upright color camera. The imager uses a white LED light source in conjunction with a color digital camera. A series of images were taken with the 2x lens to image the entire well in a single frame. Once the focal plane and camera exposure were determined manually, images were captured automatically using a fixed focal height routine using reflected light in Gen5.

Table 1. Image capture and preprocessing parameters.

Imaging	
Channel	Upright camera
Light Source	Reflected light
Objectives	2x
Focus	Fixed focus
Crop Image	Yes
Preprocessing	
Image Set	Red+Green+Blue
Background	Light
Background Flattening	
Rolling Ball	470 µm 136 pixels
Priority	Fast speed
Image Smoothing	0

Analysis

Table 2. Image analysis parameters.

Object Selection	
Channel	TSF[Green]
Threshold	
Value	7,000
Background	Light
Split Touching Objects	Yes
Fill Holes in Mask	Yes
Advanced Options	
Smoothing	0
Background	20
Object Size Selection	
Minimum	25
Maximum	500
Include Edge Objects	Yes
Entire Image	Yes
Object Analysis	
Cell Count	Count
Calculated Metrics	
Channel	Blue: Mean[TSF[Blue]] Red: Mean[TSF[Red]]
Red-Blue Ratio Custom Metric	
Metric	**Name**
M1	Mean[TSF[Blue]]
M2	Mean[TSF[Red]]
Equation	M1/M2
Subpopulation Analysis	
Subpopulation	**Metric Value**
Red Spot	Blue-Red ratio <0.85
Blue Spot	Blue-Red ratio >1.00
Red and Blue Spot	0.85 >Red-Blue ratio <1.00

Results and discussion

Initial experiments demonstrate the specificity of the ELISpot reaction. PBMCs that have been stimulated with a combination of PMA/ionomycin produce numerous spots, while unstimulated cells produce few if any. Treatment alone without PBMCs does not produce any spots.

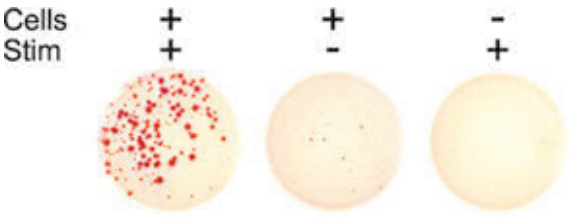

Figure 4. Specificity of IL-2 ELISpot reaction. Images of ELISpot wells containing PBMCs treated with or without PMA (1 ng/mL), ionomycin (1 µg/mL). Negative control that lacks cells, but received stimulant.

Correct sizing of the identified objects is necessary for accurate determinations. The intent of the ELIPOT assay is to identify and quantitate the number of cells responding to specific stimuli. The antibody-coated plate captures its specific target rather than the actual secretory cell. While most of the secreted analyte will be captured in the area immediately surrounding the position of the cell, some of the analyte will diffuse into the media and be captured elsewhere. The high concentration of analyte near the cell will result in a spot as large, or larger, than the physical size of the cell, while dispersed analyte will result in very small intense deposits. Figure 5 demonstrates the number of spots present in a typical ELISpot well. Only those spots exceeding 25 µm in size are designated as true spots.

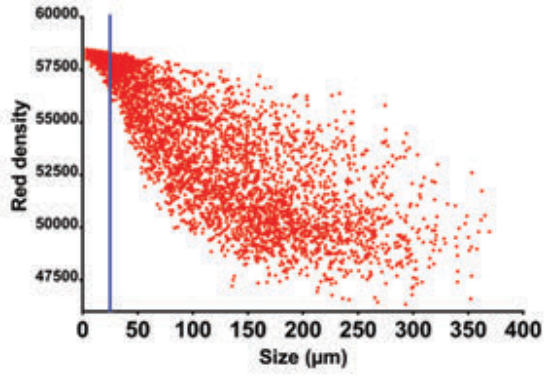

Figure 5. Scatterplot of object size vs red density. All spots achieving a green threshold of 7,000 greater than were plotted against their designation number. The size threshold of 25 µm is indicated with a blue vertical line.

The number of recorded spots produced from stimulated cells is proportional to the number of secreting cells. When a titration of PBMCs are exposed to a fixed concentration of stimulant the number of counted spots is proportional to the cell number. As demonstrated in Figure 6, increasing cell number in a well results in an increase in spots counted. Cell counts above 50,000 per well resulted in the spots coalescing together. Subsequent experiments used 5,000 cells per well.

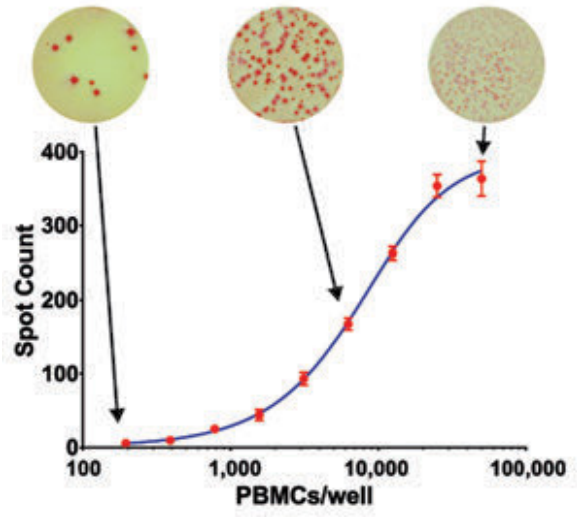

Figure 6. Cell titration. PBMC were seeded at various concentration into an ELISpot plate and stimulated with 50 ng/mL PMA, 1 µg/mL ionomycin for 24 hours. The ELISpot plate was then assayed for IL-2 secretion. Data points represent the mean of 8 determinations.

Stimulation of IL-2 secretion by a mixture of PMA and ionomycin is dose dependent. As observed in Figure 7, increasing concentration of PMA produces more spots.

Pretreating PBMCs with triptolide for 1 hour prior to stimulation reduces IL-2 secretion in a dose-dependent manner. Increasing concentrations of triptolide result in fewer spots indicative of an IL-2 secreting cell (Figure 8). In these experiments, a stimulatory dose that was 80% of maximal was employed. The IC_{50} under these conditions was determined to be 40 nM, which is similar to reports in the literature.[8]

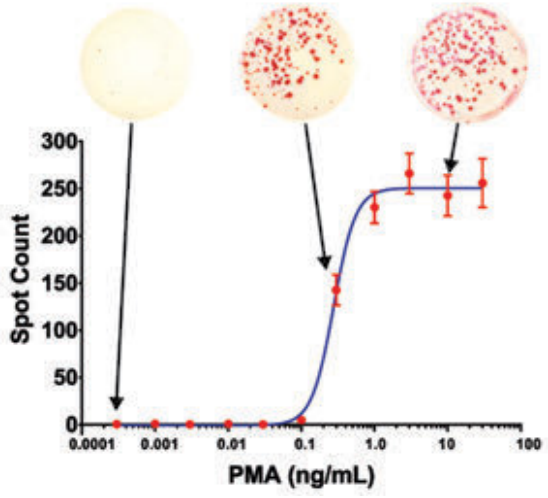

Figure 7. Titration of PMA stimulate. PBMCs (5,000 cells/well) were stimulated with various dilutions of PMA and 1 µg/mL ionomycin for 24 hours in an ELISpot plate coated with IL-2 antibody. After stimulation IL-2 secretion was assessed and spots counted. Data points represent the mean of 7 determinations.

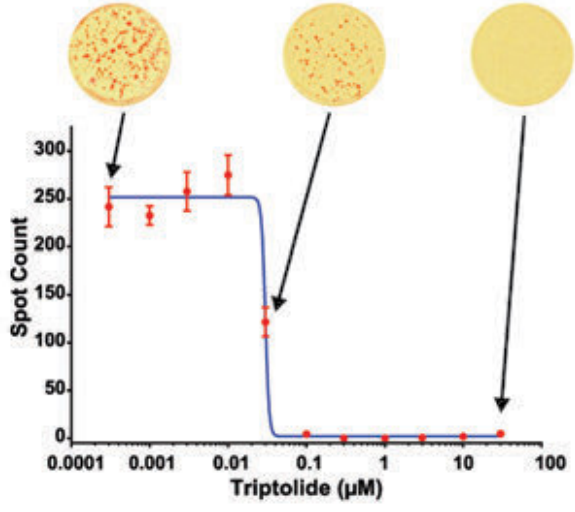

Figure 8. Inhibition of IL-2 secretion by triptolide. PBMCs (5,000 cells/well) were pre-incubated for 60 minutes with various concentrations of triptolide were stimulated with 6 ng/mL PMA, 1 µg/mL ionomycin, to secrete IL-2. After 24-hours ELISpot plate was assayed for IL-2 secretion. Data represent the mean of 7 data points.

Multiplex ELISpot assays are available to quantitate a number of different analytes simultaneously. While there are several fluorescence-based assays that provide information for up to 4 analytes in a single well, colorimetric ELISpot assays are limited to two analytes per well. Initial experiments using a two-color ELISpot specific to human IL-2 and IFN-γ demonstrated the specificity of the assay to specifically identify IL-2 or IFN-γ secreting cells. In this assay, cells secreting IL-2 can be visualized by the formation of blue spots, while those secreting IFN-γ form red spots. As observed in the control experiment (Figure 9), wells coated with anti-IL-2 antibodies only form blue spots, while wells coated with only anti-IFN-γ antibodies only form red spots. Wells receiving both coating antibodies formed both red and blue spots, while cells lacking PBMCs or PMA stimulation failed to form any spots.

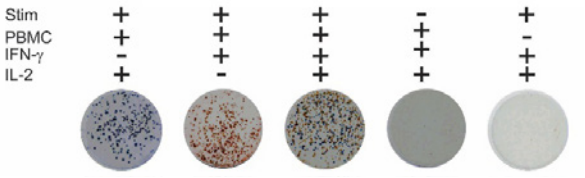

Figure 9. Specificity of two-analyte ELISpot detection. Images of ELISpot wells that have PBMC that have been treated with or without PMA (10 ng/mL). Well membranes were coated with both IL-2 and IFN-γ specific antibodies and color developed for either IL-2 or IFN-γ or both. Negative control that lacks cells, but received stimulant.

Discrimination between red and blue colored spots can be achieved using the differences in red and blue densities of the spots. The histogram plots in Figure 10 demonstrate differences in the calculated red/blue density ratio between red-only and blue-only control wells. The mean of the red/blue ratio plus two times its standard deviation can be used as the upper limit for red-only spots. Likewise, the mean minus two standard deviations of the blue spot controls defines the lower limit of the red/blue ratio for blue spots. Spots with ratio values between these two thresholds are considered to be both blue and red.

These threshold values can be used to quantitate single-color reactions where only IL-2 or IFN-γ reactions are developed. As shown in Figure 11, both IL-2 and IFN-γ cytokines are secreted when PBMCs are stimulated with PMA. The stimulation occurs in a concentration-dependent fashion with the EC_{50} values being very similar (EC_{50} = 0.05 ng/mL). Interestingly, twice as many PBMCs, as measured by the spot count, are likely to secrete IFN-γ as compared to IL-2.

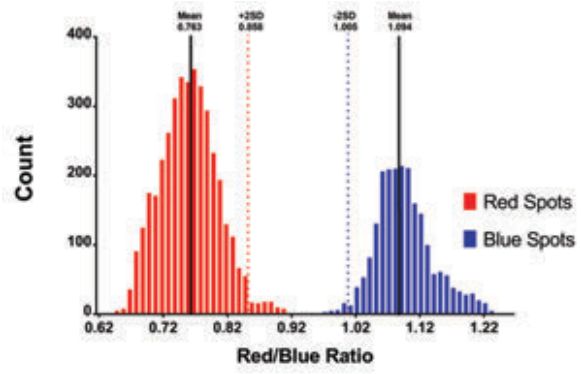

Figure 10. Frequency histogram analysis of red-blue ELISpot intensity ratio values. The frequency of red-blue ratio values from 8 red only and blue only control wells. The mean and the mean plus or minus 2 times the standard deviation of the population are indicated.

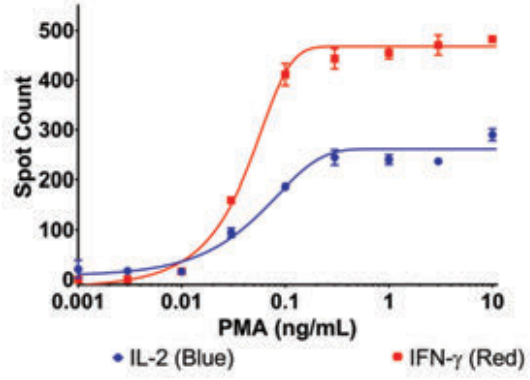

Figure 11. Comparison of IL-2 and IFN-γ secretion by PBMCs after stimulation with PMA. PBMCs were stimulated with PMA in a PVDF membrane ELISpot plate coated with both IL-2 and IFN-γ capture antibodies. After 24 hours plates were processed and colors were developed in parallel wells. Spots (red and blue) were quantitated and plotted as a function of PMA concentration. Data represent the mean and standard deviation of duplicate wells.

Multiplex, two-color analysis in the same well can be performed when both colors are developed using the same criteria. A frequency histogram of the data from several separate wells where both colors were developed in the wells is depicted in Figure 12. When the images are examined by eye, most wells have spots that are visibly either red or blue, with a smaller percentage that appear appear as a mixture. These observations are corroborated by the frequency histogram depicted in Figure 12 that demonstrates that the identified spots have a spectrum of red/blue ratio values. There are two obvious peaks based on the red/blue ratio that correspond to the red and blue spots observed when only one color has been developed. Between their respective cutoff values is a significant number of spots that have an intermediate red/blue ratio.

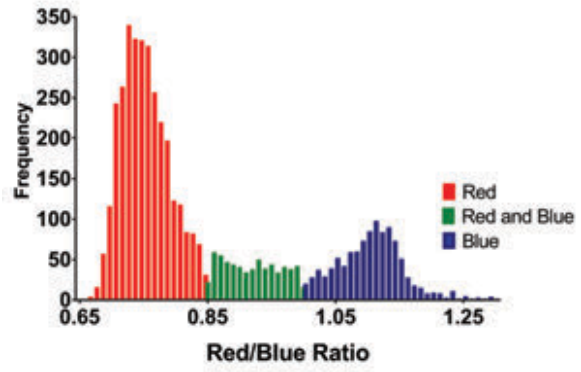

Figure 12. Frequency histogram of ELISpot red-blue ratio values. The red-blue ratio of ELISpot spots from 8 wells of a two-color ELISpot assay plate were plotted as a function of frequency. Subpopulations analysis based on cut off values for red, blue or red and blue spots are indicated by color.

These visibly correspond to spots that appear purple (i.e. a mixture of red and blue). The relative number of spots identified as red or blue is similar to the numbers identified when a single color was developed. When one analyzes the data with a scatter plot that compared the red/blue ratio to spot size, two loose clusters of spots that correspond to red or blue spots are observed along with a number of intermediate ratio spots (Figure 13). While all three subpopulations of spots have the same range in size, red spots tend to be more numerous and smaller in size than spots identified as blue.

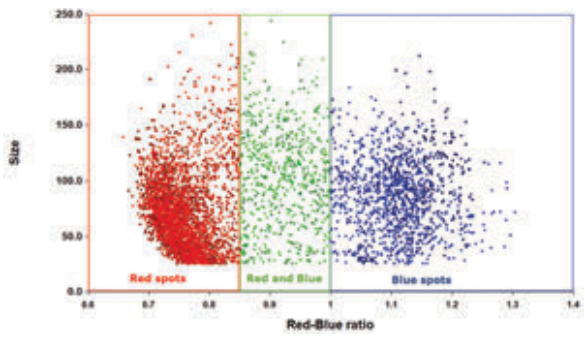

Figure 13. Scatter plot of ELISpot red/blue ratio values. The red/blue ratio of ELISpot spots from 8 wells of a two-color ELISpot assay plate were plotted as a function of size. Subpopulations analysis based on cut off values for red, blue or red and blue spots are indicated.

This multiplex analysis can be used on individual wells with different experimental conditions. Figure 14 demonstrates the response of PBMCs to PMA stimulation where both blue (IL-2) and red (IFN-γ) colors are developed in the same well. As with separate color development, PMA stimulated cytokine secretion on PBMCs in a concentration-dependent manner. Also, more PBMCs secreted IFN-γ than IL-2, with equivalent EC_{50} values. If one compares the total number of cells that secrete IFN-γ (red-only spots plus red and blue spots) or the total number of cells that secrete IL-2 (blue-only spots plus red and blue spots), the numbers are consistent with wells where only one color was developed.

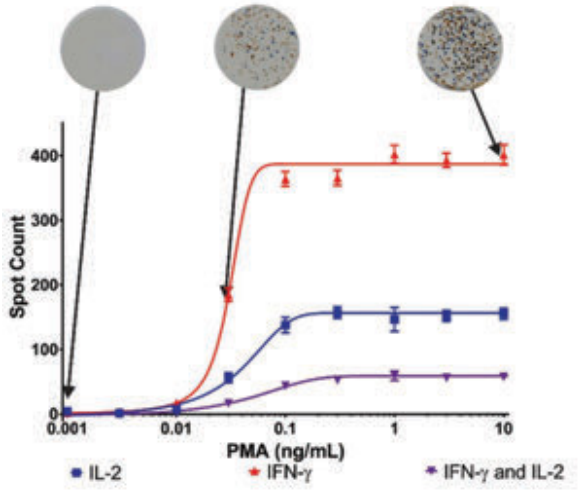

Figure 14. Comparison of IL-2 and IFN-γ secretion in stimulated PBMCs. PBMCs were stimulated with various concentrations of PMA using a PVDF membrane 96-well plate that was pre-coated with both anti-IL-2 and anti-IFN-γ antibodies. After ELISpot processing, the plate wells were imaged and the images analyzed using the Agilent BioTek Gen5 microplate reader and imager software. Subpopulation analysis defined spots that were either red, blue or a mix of red and blue. The number of each spot subpopulation was plotted against PMA concentration. Data represent the mean and standard deviation of 4 determinations.

Conclusion

These data demonstrate the utility of the Agilent BioTek Cytation 7 cell imaging multimode reader in conjunction with the Agilent BioTek Gen5 microplate reader and imager software to image and analyze colorimetric PVDF ELISpot assay plates. The combination of a PMA/ionomycin has been shown to markedly stimulate IL-2 secretion in PBMCs. Without stimulation, IL-2 is virtually absent. The ability of triptolide, a known transcription inhibitor, to prevent IL-2 secretion suggests that new protein synthesis is required after stimulation.[11]

ELISpot is a sensitive assay to monitor the *ex vivo* cellular immune response at the single cell level by detecting secreted proteins released by cells. This technique has been derived from the sandwich enzyme-linked immunosorbent assay (ELISA) to accommodate the use of whole cells to identify the frequency of the secreting cells. As such, there are a number of critical parameters that need to be optimized in order for experiments to be successful. Depending on the degree of cellular secretion, developed spots can be quite large. The expected number of positive cells is of greater importance than the total number of cells used initially. The presence of too many secreting cells results in the individual spots coalescing making a numerical determination difficult. For example, an investigation of a relatively rare secreting event would require a greater number of cells to be seeded as compared to a more common event. Timing of the response relative to the stimulation and/or the inhibition is important. Receptor mediated events often will take longer to elicit a response than a stimulatory molecule that can interact within the cell directly. It is important that appropriate interval between stimulation and measurement be used. The testing of inhibitors still requires a stimulating agent to be present. In these experiments, it is important that a less than maximal concentration of the stimulatory agent be used, lest it mask any inhibitory affects.

The Cytation 7 is an ideal platform to interpret colorimetric PVDF membrane ELISpot assays. The imager supports digital top-down color imaging with 2x, 4x, and 8x microscope objectives that are factory installed. The 2x objective can capture the entire well in a single image, making it ideal for 96-well ELISpot determination. If desired, higher resolution can be obtained by using a higher magnification objective and a montage of the well. Using this camera both reflected or transmitted light can be used for optimal imaging. While this research only used the upright top-down camera with PVDF membrane plates, the imager also supports brightfield imaging using an inverted camera for silver stain ELISpot assays. In addition, the inverted microscope supports fluorescence-based microscopy with LED and filter cubes. Gen5 microplate reader and imager software, besides controlling reader function, can be used to automatically perform stitch of separate montage image tiles, perform background subtraction and mask off regions outside the well prior to analysis.

References

1. Delves, P. *et al.* Roitt's Essential Immunology, 11th Ed. ISBN 978-1-4051-3603-7
2. Eds. Verhoeckx, K. *et al.* The Impact of Food Bioactives on Gut Health: *in vitro* and *ex vivo* models., European Cooperation in the Field of Scientific and Technical Research (Organization), 2105. Cham. ISBN-13: 978-3-319-15791-7ISBN-13: 978-3-319-16104-4.
3. Liao, W.; Lin, J. X.; Leonard, W. J. IL-2 Family Cytokines: New Insights into the Complex Roles of IL-2 as a Broad Regulator of T Helper Cell Differentiation. *Curr. Opin. Immunol.* October **2011**, *23(5)*, 598–604. doi:10.1016/j.coi. 2011.08.003.
4. Carter, L. L.; Swain, S. L. Single Cell Analysis of Cytokine Production, *Curr. Opin. Immunol.* **1997**, *9(2)*, 177–182.
5. Schoenborn, J. R.; Wilson, C. B. Regulation of Interferon-γ During Innate and Adaptive Immune Responses. Regulation of Interferon-Gamma During Innate and Adaptive Immune Responses. *Advances in Immunology* **2007**, *96*, 41–101. doi:10.1016/S0065-2776(07)96002-2. ISBN 978-0-12-373709-0. PMID 17981204.
6. Williams, M. A.; Bevan, M. J. Effector and Memory CTL Differentiation. *Annual Review of Immunology* **2007**, *25(1)*, 171–192. . PMID 17129182. doi:10.1146/annurev.immunol.25.022106.141548
7. Qiu, D. *et al.* Immunosuppressant PG490 (Triptolide) Inhibits T-cell Interleukin-2 Expression at the Level of Purine-box/Nuclear Factor of Activated T-cells and NF-kB Transcriptional Activation, *J. Biol. Chem*. **1999**, *274(19)*, 13443-13450 PMID:10224109
8. Weiss, A.; Wiskocil, R. L.; Stobo, J. D. The Role of T3 Surface Receptors in the Activation of Human T Cells: a Two Stimulus Requirement for IL-2 Production Reflects Events Occurring at a Pre-translational Level, *J. Immunology* **1984**, *133*, 123–128. PMID:6327821
9. Chen, L.; Flies, D. B. Molecular Mechanisms of T Cell Co-Stimulation and Co-Inhibition, *Nat. Rev. Immunology* **2013**, *13(4)*, 227–242. doi: 10.1038/nri3405.
10. Manger, B. *et al.* Differential effect of Cyclosporine A on Activation Signaling in Human T Cell Lines. **1986**.
11. McCallum, C. *et al. In Vitro* Versus *In Vivo* Effects of Triptolide: The Role of Transcriptional Inhibition, *Therapy* **2005**, *2(2)*, 261–273. ISSN 2044-9038.

www.agilent.com/lifesciences/biotek

Printed in the USA, February 1, 2021
5994-2398EN
AN031820_02

Agilent
Trusted Answers

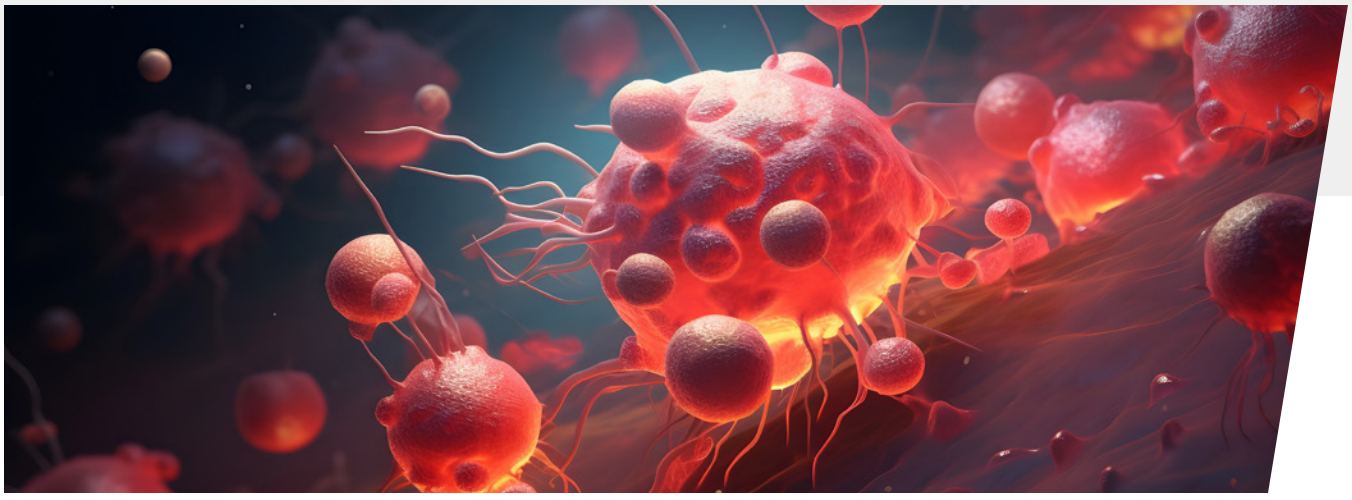

Chapter 4 : Solid Tumors and 3D Tumor Models

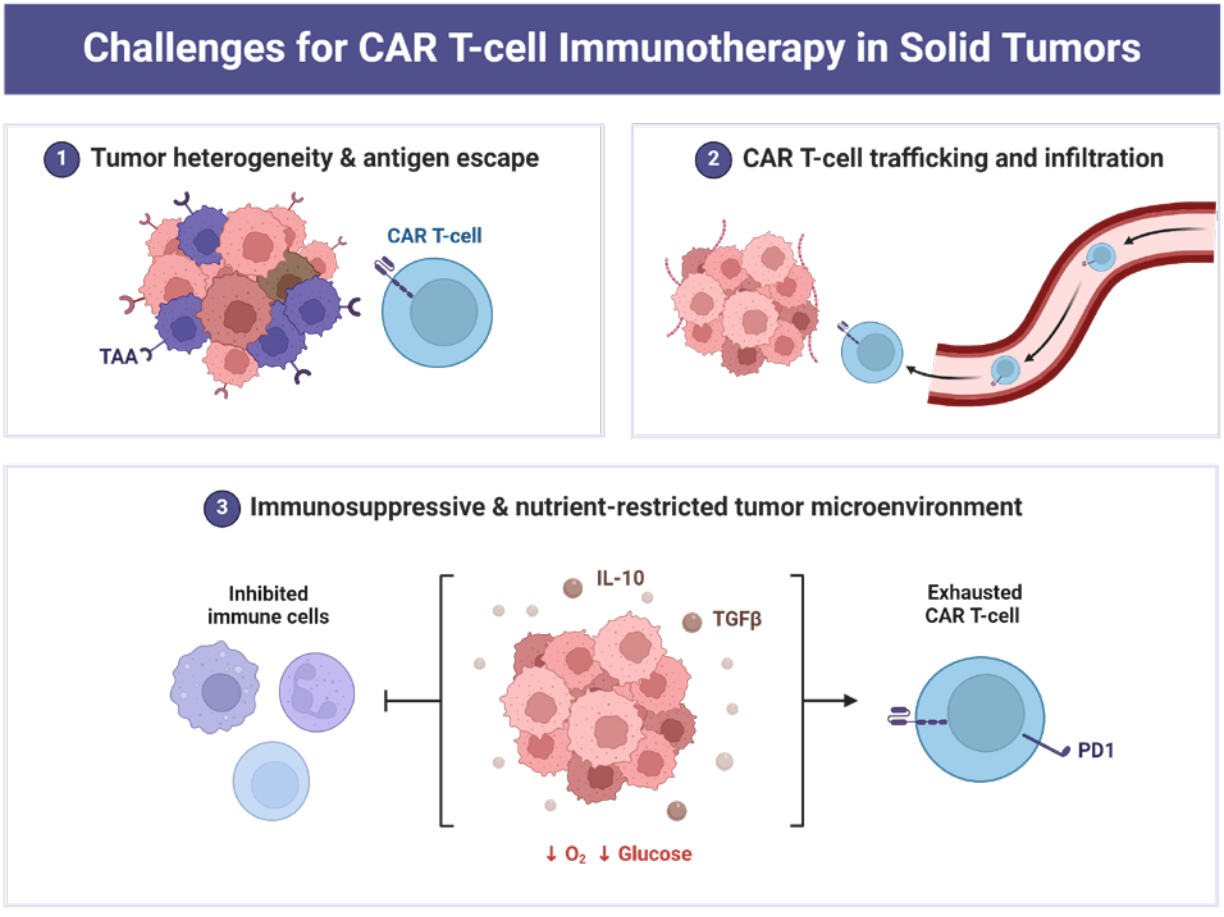

Created with BioRender.com

Chapter 4 :
Solid Tumors and 3D Tumor Models

Solid tumors account for approximately 90 percent of adult cancers. However, all six currently approved CAR-T cell therapies target CD19 and BCMA-positive liquid hematologic tumors[12]. For liquid tumor cancers, specific target antigens are homogenously expressed at higher levels compared to healthy cells. In contrast, solid tumors have greater heterogeneity in their antigen profiles, with overall inconsistent expression, making identification of targets for specific solid tumor cells challenging.

In liquid tumor cancers, CAR-T cells have fewer obstacles when traveling to tumors in the lymph nodes or bone marrow due to this medium being the native trafficking environment. In contrast, T cell trafficking and infiltration into solid tumors are more of a challenge, as the effector T cells must move effectively from the bloodstream to the lumen of the solid tumor. If the T cells can reach the tumor interior, the immunosuppressive tumor microenvironment can prevent further attacks due to restricted nutrient availability. Many tumor-associated myeloid cells also produce immunosuppressive cytokines (for example, IL-10 and TGF-β), which prevent effector T cells from killing. In addition, T cells can become dysfunctional or exhausted because of persistent antigen and inflammatory signal exposure. Combined with nutrient restriction, these persistent exposures can lead to significant challenges within the T cell metabolic exhaustion (TME) state.[13]

3D Cell Models

Cell therapy development for solid tumors remains challenging, partially due to a lack of reproducible, cost-effective, in vitro three-dimensional (3D) models and effective quantitative tools to measure them. However, recent advances in 3D cell culture systems, including matrix-embedded cocultured tumoroids—which are more predictive of the heterogeneous and complex tumor microenvironment—in combination with advanced quantitative imaging techniques, can provide new insights into growth, differentiation, and cell-cell interactions to confront these challenges. Such technologies may ultimately help with the development of effective cell therapy treatments for solid tumors.

The latest cell analysis instrumentation and application solutions provide robust, quantitative methods for monitoring 3D tumor growth and invasion.

Related Solutions

Imaging and Automation Solutions
The **Agilent BioTek Cytation C10 confocal imaging reader** performs microplate reading, widefield imaging as well as confocal imaging on a single instrument. The **Agilent BioTek BioSpa 8 automated incubator** links Agilent BioTek readers or imagers together with Agilent BioTek washers and dispensers for full workflow automation of up to eight microplates. The **Agilent BioTek Gen5 microplate reader and imager software** enables highthroughput, quantitative analysis of 3D cell models.

Real-Time Impedance and Imaging Solutions
Monitor immune cell invasion and cytotoxicity using **Agilent xCELLigence RTCA eSight**, which combines real-time impedance with imaging capabilities in one instrument. The **RTCA eSight software** provides capability for flexible experimental setups, real time imaging acquisition, and powerful data analysis functions.

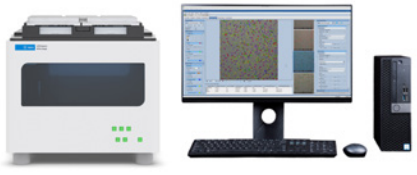

Application Note

Cancer Biology

Agilent

Trusted Answers

3D Spheroid-Based Tumor Invasion Assay

Author

Brad Larson
Agilent Technologies, Inc.
Winooski, VT, USA

Jan Seldin
Greiner Bio-One
North America, Inc.
Monroe, NC, USA

Abstract

Establishment of *in vitro* models that mimic tumor invasion as part of the metastatic process are a critical part of oncology research. The need to incorporate multiple cell types, long-term kinetic analysis, methods to allow 3D invasion into the surrounding matrix, and appropriate detection and analysis, has made it difficult to create new models. The procedure described in this application note meets these needs through inclusion of advanced imaging capabilities allowing for capture of multiple images throughout a range of z-heights, using brightfield and fluorescence channels in a kinetic fashion. Final processed images, following stitching and z-projection, enable accurate cellular analysis to discern the invasive capabilities of 3D cellular structures over time.

Introduction

Oncology drug discovery has been met with multiple challenges over the years. As cancers develop multiple mutations during carcinogenesis, targeted approaches to individual gene mutations common to many drug discovery campaigns have mostly limited efficacy. Conversely, the advancement of novel methods that focus on the inhibition of the invasive phenotype of metastasis offers greater potential for meaningful intervention, particularly due to the fact that most cancer patients die only after metastasis has occurred. For this approach to work, *in vitro* cell models used in early drug discovery should mimic as close as possible the complex metastatic process. Tumors *in vivo* exist as a three-dimensional (3D) mass of multiple cell types, including cancer and stromal cells. Therefore, incorporating a 3D spheroid-type cellular structure that includes co-cultured cell types forming a tumoroid provides a more predictive model than the use of individual cancer cells seeded in microplates. A further constraint is the need for long-term kinetic experiments to capture the invasion process which typically require multiple days. Thus, environment control of the assay is needed such that the cell viability of the spheroid is maintained over this long period and putative drug effects properly assessed. Finally, the only suitable readout for monitoring tumor invasion is microscopy due to the small size of the spheroid. To be effective in drug discovery, the microscope must have automated image capture, processing, and analysis to be able to cope with the multiple assay conditions, compounds tested, and kinetic images taken. This work will demonstrate a procedure for the generation of 3D spheroidal tumoroid structures, creation of a suitable invasion matrix, automated kinetic image-based monitoring, and cellular analysis of captured z-stacked images of tumor invasion.

U-87 and LN-229 glioblastoma multiforme (GBM) cell lines were used in this study as they have demonstrated phenotypic differences and metastatic ability.[1] Notably, the growth suppressing PTEN gene is mutated in U-87 cells, yet functions normally in LN-229 cells. Additionally, the human cytomegalovirus phosphotransferase protein UL-97 inhibits DNA elongation and replication and is absent from U-87 cells, but present in LN-229 cells.[2] This supports a more aggressive growth and invasion pattern for U-87 cells. Both cell types were co-cultured with fibroblasts to create 3D tumoroids more closely representing *in vivo* tumor conditions and allowed to invade through a protein matrix.

17-allylamino-17-demethoxygeldanamycin (17-AAG), known to inhibit the function of heat shock protein 90 (Hsp90), a chaperone protein that stabilizes proteins required for tumor growth, was used here to inhibit potential tumor invasion.[3] Quantification of kinetic captured images was used to characterize the invading potential of inhibited and uninhibited tumoroid cultures.

Materials and methods

Materials

Cells

U-87 GBM cells expressing GFP were generously donated by Dr. Sachin Katyal (University of Manitoba, Winnipeg, Manitoba, Canada). LN-229 GBM cells (part number CRL-2611) were obtained from ATCC (Manassas, VA). Human neonatal dermal fibroblasts expressing RFP (part number cAP-0008RFP) were purchased from Angio-Proteomie (Boston, MA).

Experimental components

Matrigel basement membrane matrix, phenol red-free (part number 356237) was purchased from Corning Life Sciences (Corning, NY). The selective Hsp90 inhibitor 17-AAG (part number 1515) was sourced from Tocris Bioscience (Avonmouth, Bristol, UK). CellTracker Deep Red dye (part number C34565) was purchased from Thermo Fisher Scientific (Waltham, MA). 96-well, cell-repellent, polystyrene, round bottom, clear, sterile, microplates with lid (part number 650979) were generously donated by Greiner Bio-One North America, Inc. (Monroe, NC).

Agilent BioTek Cytation 5 cell imaging multimode reader

Cytation 5 is a modular multimode microplate reader combined with an automated digital microscope. Filter- and monochromator-based microplate reading are available, and the microscopy module provides up to 60x magnification in fluorescence, brightfield, color brightfield, and phase contrast. The instrument can perform fluorescence imaging in up to four channels in a single step. With special emphasis on live cell assays, Cytation 5 features shaking, temperature control to 65 °C, CO_2/O_2 gas control and dual injectors for kinetic assays and is controlled by integrated Agilent BioTek Gen5 microplate reader and imager software, which also automates image capture, analysis, and processing. The instrument was used to kinetically monitor 3D tumoroid activity over the incubation period.

Agilent BioTek BioSpa 8 automated incubator

The BioSpa 8 automated incubator links Agilent BioTek readers or imagers together with Agilent BioTek washers and dispensers for full workflow automation of up to eight microplates. Temperature, CO_2/O_2 and humidity levels are controlled and monitored through the Agilent BioTek BioSpa software to maintain an ideal environment for cell cultures during all experimental stages. Test plates were incubated in the BioSpa to maintain proper atmospheric conditions for a period of seven days and automatically transferred to the Cytation 5 every twelve hours for brightfield and fluorescence imaging.

Agilent BioTek MultiFlo FX multimode dispenser

The MultiFlo FX is a modular, upgradable reagent dispenser that can have as many as two peri-pump (8 tube dispensers), two syringe pump dispensers, and a strip washer. The syringe and washer manifolds can be configured for plate densities from 6- to 384-well.

Methods

Cell preparation and tumoroid formation

Prepared U-87 and fibroblast cells were each harvested and combined in a final concentration of 2.5×10^4 cells/mL for each cell type in complete medium. After dispensing 100 µL of cell suspension into appropriate microplate wells, the microplate was incubated at 37 °C/5% CO_2 for 48 hours to allow cells to aggregate into tumoroids. This process was repeated using LN-229 cells stained with CellTracker Deep Red dye and fibroblast cells at the same concentrations and volumes.

Invasion matrix preparation

Upon completion of tumoroid formation, 70 µL of complete medium was robotically removed from each well, and the tumoroid plate placed on ice in a refrigerator for five minutes to cool the cells. Matrigel matrix was then thawed on ice. 17-AAG was diluted to a 2x concentration of 20,000 nM in invasion media and used to create an eight-point titration from 20,000 nM to 0 nM using serial 1:4 dilutions. The inhibitor titrations were further diluted to a 1x concentration by combining with either invasion media or Matrigel matrix. With the plate still on ice, 70 µL of Matrigel matrix plus titrated compound were added to each well containing tumoroids, then overlaid with 100 µL invasion media containing titrated compound. The microplate was centrifuged at 300 × g for five minutes in a swinging bucket centrifuge that was previously set to 4 °C for tumoroid positioning, then transferred to a 37 °C/5% CO_2 incubator for one hour to initiate gel formation.

Tumor invasion assay performance

After gel formation was complete, the microplate was transferred to BioSpa 8, where the software was programmed such that the microplate was automatically transferred to Cytation 5 for brightfield and fluorescent imaging of the wells every twelve hours over the seven-day incubation period. Table 1 lists the settings used to perform automated image capture of each sample well.

Table 1. Automated 3D tumoroid invasion imaging parameters.

Imaging Parameters	
Brightfield Imaging Channel	Complete 3D invading structure
GFP Imaging Channel	U-87 Cells expressing GFP
RFP Imaging Channel	Fibroblasts expressing RFP
CY5 Imaging Channel	LN-229 Cells stained with CellTracker Deep Red dye
Objective	4x
Montage	3 Rows by 2 columns
Montage Overlap	Auto for stitching
Z-Stack	20 Slices
Z-Stack Step Size	53.8 µm (Default for 4x objective)

Image processing

Individual image tiles from each z-plane captured using the three by two montage were then stitched together (Table 2).

Table 2. Image stitching parameters.

Imaging Stitching Parameters	
Registration Channel	Brightfield
Fusion Method	Linear blend
Crop Stitched Image to Remove Black Rectangles on the Borders	Checked
Downsize Final Image	Checked (52.62%)

A single image projection was then created from the 20-slice stitched z-stack (Table 3). The focus stacking method was chosen, which automatically selects the most in focus pixel from each image in the stack for inclusion in the final projection. This allows the most accurate analysis to be carried out on each invading tumoroid at each time point.

Table 3. Image z-projection parameters.

Imaging Z-Projection Parameters	
Channel 1	Stitched[Brightfield]
Method	Focus stacking
Size of Maximum Filter	11 px
Z-Slices Included	1 to 20
Channels 2 to 4	Stitched[GFP], Stitched[RFP], Stitched[CY5]
Method (Channels 2 to 4)	Use settings of channel 1

Tumoroid invasion analysis

Primary mask cellular analysis criteria (Table 4) were applied using the brightfield channel to automatically place object masks around the entire invading structure in each final image. Secondary mask cellular analysis criteria (Table 5) were also applied to place an additional mask around noninvasive cells remaining within the original spherical tumoroid structure.

Table 4. Primary mask analysis parameters.

Primary Cellular Analysis Parameters	
Channel	ZProj[Stitched[Brightfield]]
Threshold	25,000
Background	Light
Split Touching Objects	Unchecked
Fill Holes in Masks	Checked
Minimum Object Size	300 µm
Maximum Object Size	2,000 µm
Include Primary Edge Objects	Checked
Analyze Entire Image	Checked
Advanced Detection Options	
Rolling Ball Diameter	2,000
Image Smoothing Strength	0
Evaluate Background On	5% of lowest pixels
Analysis Metric	
Metric of Interest	Object area

Table 5. Secondary mask analysis parameters.

Secondary Cellular Analysis Parameters	
Channel	ZProj[Stitched[Brightfield]]
Measure Within a Secondary Mask	Include primary mask
Reduce Primary Mask	1 µm
Threshold	12,000
Smooth	7
Fill Holes in the Mask	Unchecked
Analysis Metric	
Metric of Interest	Object Area_2[ZProj[Stitched[Brightfield]]]

Results and discussion

Raw image processing prior to cellular analysis

During the seven-day incubation period, uninhibited U-87/fibroblast tumoroids continued to increase in size, as well as invade into the protein matrix. To ensure that the entire invading structure, including invadopodia, was captured in the X- and Y-axes, regardless of size, multiple images were taken on a single z-plane in a montage format (Table 1). Figure 1 illustrates four of the six images that were captured containing portions of the invading structure.

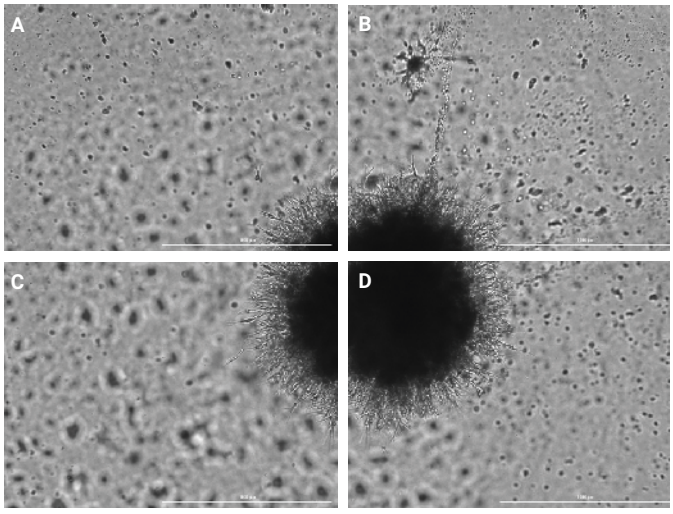

Figure 1. U-87/fibroblast 4x brightfield imaging showing (A to D) four image tiles containing the invading tumoroid of interest.

As invasion proceeds, proteins and cells invade on multiple planes within the Z-axis. Therefore, images were automatically taken across a range of z-heights so that all portions of the overall structure were in focus in the final z-projected images (Figures 2A to 2D).

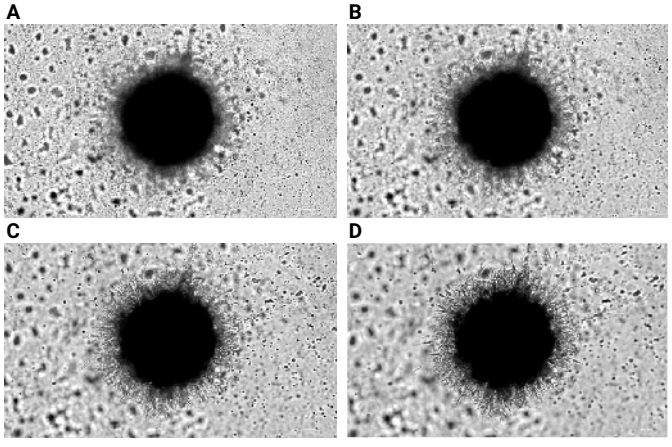

Figure 2. U-87/fibroblast 4x brightfield imaging showing (A to D) four of the twenty images captured at multiple z-planes as part of the z-stack and combined into the final z-projection.

Imaging of U-87/fibroblast individual co-cultured cell types

In addition to brightfield imaging, montage tiles and z-stacked layers were also captured using the GFP and RFP channels. Overlaying images tracks invasion of the entire structure (Figure 3).

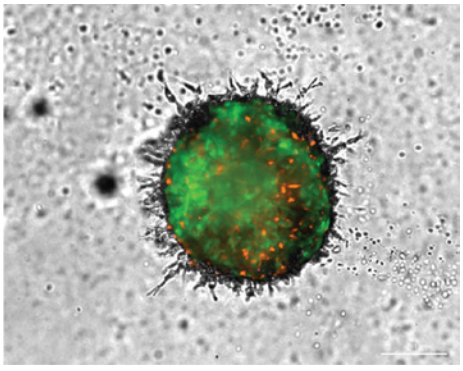

Figure 3. Brightfield and fluorescent overlaid z-projected image of U-87/fibroblast co-cultured cell model.

By viewing the fluorescent signal emitted by each co-cultured cell type, in comparison to the brightfield signal from the entire structure, individual cell migration can be observed. In the case of the U-87/fibroblast model, the brightfield image demonstrates extensive invadopodia extending out from the original propagating tumoroid (Figure 4A). From the GFP image in Figure 4B, it is evident that GFP-expressing U-87 cells follow invadopodia invasion into the matrix. This contrasts to the RFP image in Figure 4C confirming that RFP-expressing fibroblasts exhibit little to no migratory ability within this experimental model.

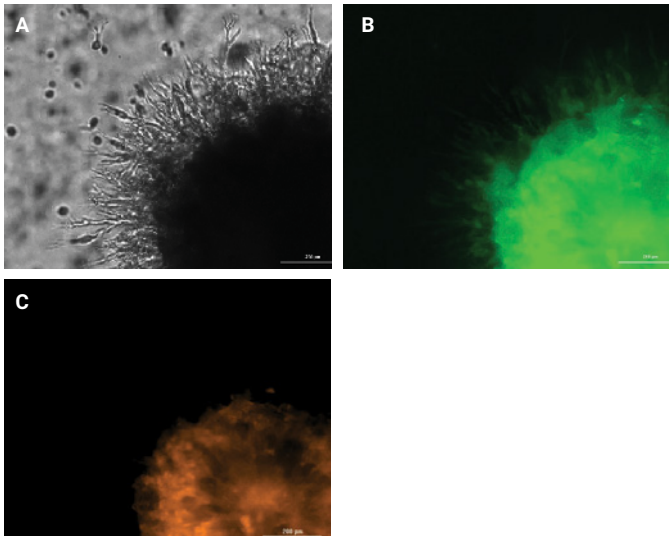

Figure 4. Confirmation of invasion by individual cell types. (A) Total tumoroid invasion via overlaid GFP, RFP, and brightfield channels. Individual cellular invasion by (B) GFP-expressing U-87 cells, or (C) RFP-expressing fibroblast cells. Digitally zoomed 4x images, 2 × 3 montage, 20-plane z-stack.

Kinetic image capture

Finally, z-projected images are captured kinetically every 12 hours to observe phenotypic changes in the U-87/fibroblast co-cultured tumoroids following treatment with varying concentrations of 17-AAG. Uninhibited tumoroids, as expected, demonstrate a highly invasive nature[4], exhibiting an increase in the size of the tumoroid body as well as a dramatic increase in invadopodia (Figure 5).

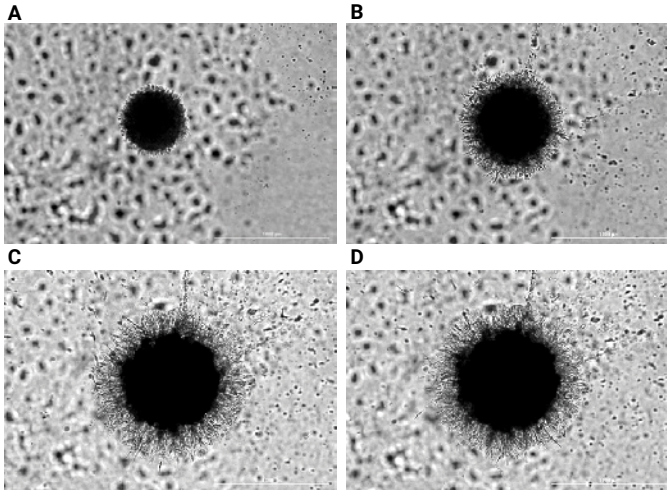

Figure 5. U-87/fibroblast tumoroid invasive potential over time, 4x brightfield images, 2 × 3 montage, 20-plane z-stack. (A) 0 hours; (B) 48 hours; (C) 120 hours; (D) 168 hours.

LN-229/Fibroblast tumoroid analysis

LN-229/fibroblast tumoroid imaging was also conducted in the same manner as that for the U-87/fibroblast tumoroids. This was done to compare differences in growth and invadopodia production between GBM cell types known to be highly invasive (U-87) and those with less invasive ability (LN-229).[5] Changes in the complete 3D structure were observed using the overlaid brightfield and fluorescent images (Figure 6A), while individual LN-229 or fibroblast invasion was monitored by signal captured with the individual CY5 or RFP channels, respectively (Figures 6B and 6C).

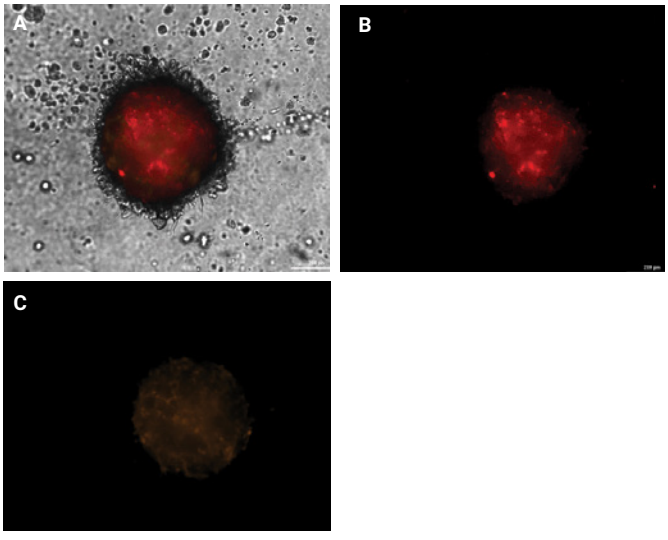

Figure 6. Imaging of LN-229/fibroblast co-cultured cell model. (A) Total tumoroid invasion via overlaid CY5, RFP, and brightfield channels. Individual cellular invasion by (B) CellTracker Deep Red stained LN-229 cells; or (C) RFP-expressing fibroblast cells. Digitally zoomed 4x images, 2 × 3 montage, 20-plane z-stack.

When comparing kinetic brightfield images from the two co-cultured cell types, it is evident that LN-229/fibroblast tumoroids propagate over time, as seen by the increase in spheroid size (Figure 7), but do not exhibit the invasive properties clearly demonstrated by U-87/fibroblast tumoroids over the same incubation period (Figure 5).

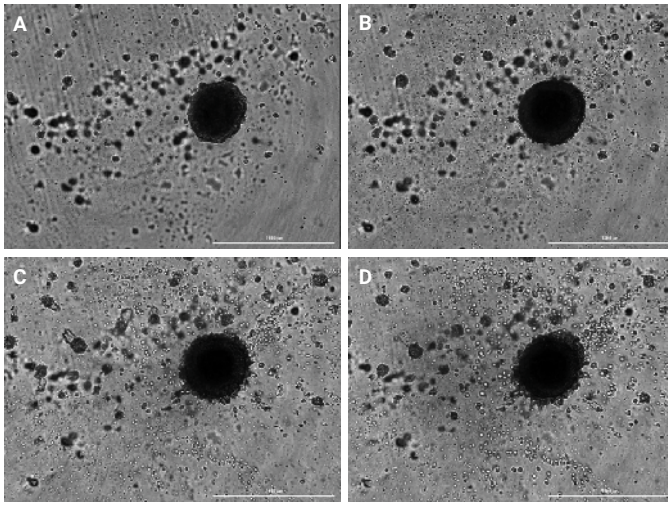

Figure 7. LN-229/fibroblast tumoroid invasive potential over time, 4x brightfield images, 2 × 3 montage, 20-plane z-stack. (A) 0 hours; (B) 48 hours; (C) 120 hours; (D) 168 hours.

Agilent BioTek Gen5 Image+-based cellular analysis of tumoroid invasion

In addition to qualitative assessments of tumoroid phenotypic changes, quantification of the extent of invasion was also carried out using the stitched, z-projected brightfield images. Two separate cellular analyses were performed following treatment with the 17-AAG titration. In the first, the primary cellular analysis capabilities available in Gen5 Image+, and the criteria listed in Table 4 used changes in brightfield signal within the image between cellular containing pixels and background to place detailed object masks around the complete invading 3D structure, despite the level of compound treatment (Figure 8).

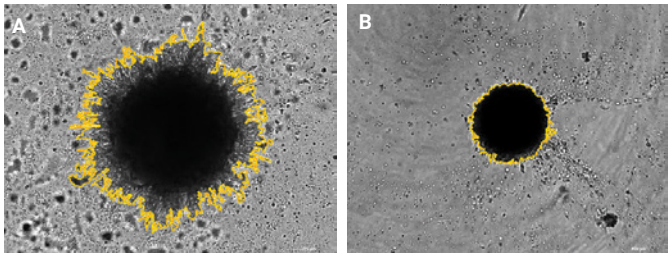

Figure 8. Invading tumoroid object masking. Zoomed 4x brightfield images of U-87/fibroblast tumoroids, 2 × 3 montage, 20-plane z-stack. (A) 0 µM 17-AAG treatment and (B) 10 µM 17-AAG treatment. Primary masks around cells and invadopodia.

The area covered by the entire tumoroid for each captured image over time was then calculated. Values from subsequent time points were then divided by the area value calculated at time 0 for the specific tumoroid to normalize results and account for variability in tumoroid size following cell dispensing and aggregation. Area ratios were then plotted (Y-axis) with regards to time (X-axis) (Figure 9).

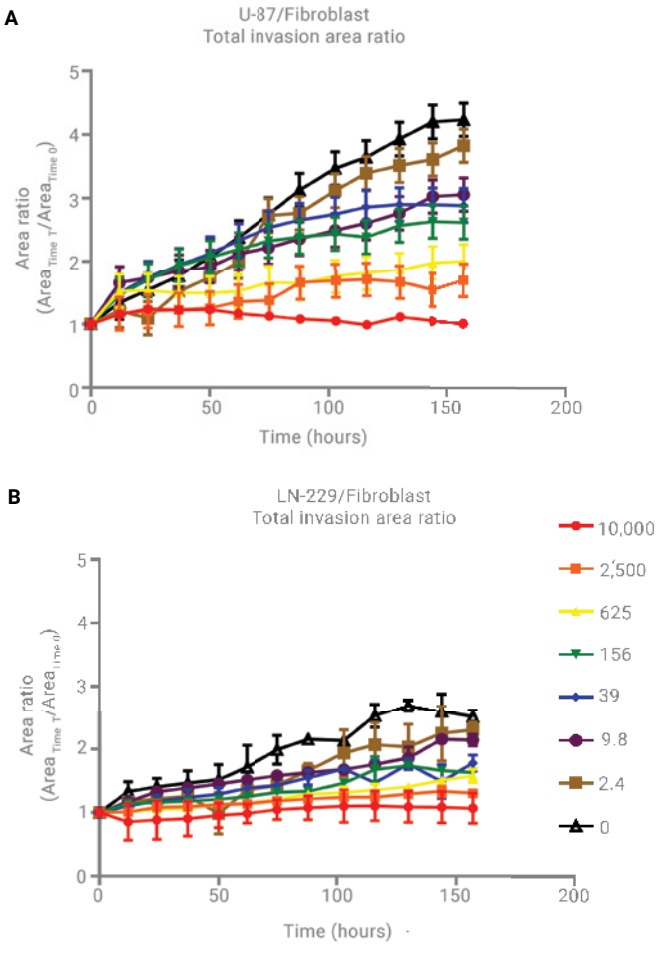

Figure 9. Kinetic total tumoroid area ratios. Area ratios plotted for (A) U-87/fibroblast tumoroids, or (B) LN-229/fibroblast tumoroids following 0 to 7-day treatments with 17-AAG concentrations ranging from 10,000 to 0 nM. Area ratio calculated by the following formula: ($Area_{time\ T}/Area_{time\ 0}$).

From the results seen in Figure 9, it is apparent that both U-87/fibroblast and LN-229/fibroblast tumoroids propagate within the Matrigel matrix when unimpeded over the seven-day incubation period. It can also be seen that the compound 17-AAG is able to limit, or even completely stop, tumoroid growth in a dose-dependent manner, as expected.[3] What is also clear from the total area ratio graphs is the increased rate of growth for the complete 3D structure exhibited by U-87/fibroblast tumoroids compared to those where LN-229 cells are co-cultured with fibroblasts. Increases in the area covered by the entire tumoroid are approximately 2x over time for tumoroids cultured with U-87 cells (ratio: 4.4) compared to those cultured with LN-229 cells (ratio: 2.4).

Agilent BioTek Gen5 Image Prime-based cellular analysis of tumoroid invasion

A second cellular analysis was also performed using the primary and secondary cellular analysis capabilities available in Gen5 Image Prime, and the criteria listed in Table 5, to measure the area solely covered by noninvading cells within the tumoroid. To determine the metastatic ability of 3D *in vitro* models, both uninhibited, or following treatment, it is important to distinguish between area covered by cells within the original tumoroid and that covered by invadopodia. As the more densely packed noninvasive, propagating cells appear darker compared to invadopodia in a brightfield image (Figure 10A), this additional change in signal within the original mask allows placement of a secondary mask to exclude the invading areas of each tumoroid and separate the area covered by the two portions of the entire 3D structure (Figure 10).

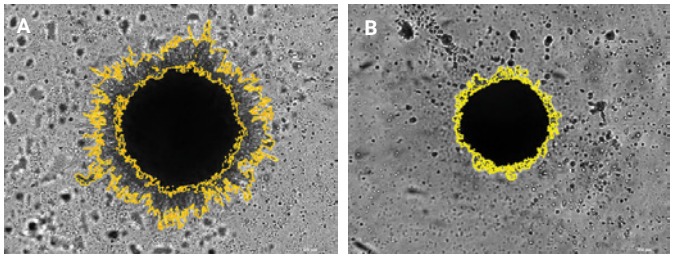

Figure 10. Invading and main tumoroid area object masking. Zoomed 4x brightfield 2 × 3 montage, 20-plane z-stack images of (A) uninhibited U-87/fibroblast tumoroids; or (B) uninhibited LN-229/fibroblast tumoroids. Exterior primary masks around cells and invadopodia, and interior secondary masks around noninvading cellular structure only.

By applying the secondary mask around noninvading portions of the tumoroid, differences in the invasive qualities of the two GBM cell types then becomes clear.

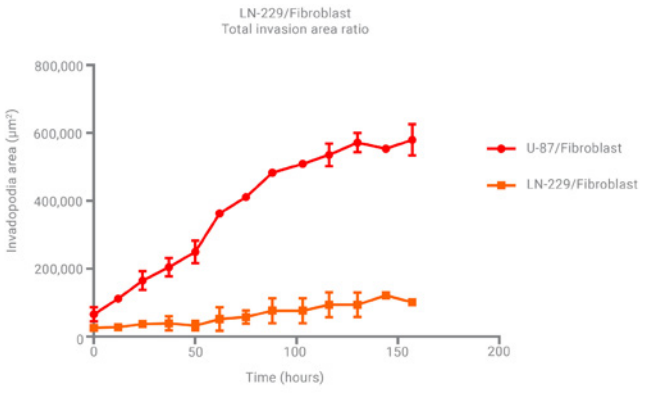

Figure 11. Kinetic uninhibited U-87 and LN-229 co-cultured tumoroid kinetic invadopodia areas. Calculated invadopodia area over time for nontreated U-87/fibroblast and LN-229/fibroblast tumoroids. Invadopodia area calculated by the following formula: (Total $Area_{time\ T}$ – Noninvading $Area_{time\ T}$).

The area covered by invadopodia for U-87/fibroblast tumoroids increases dramatically over the seven day incubation period. LN-229/fibroblast tumoroids, by comparison, show little increase in invadopodia over the same time (Figure 11). This dual analysis, therefore, has the potential to determine not only how rapidly tumoroid cells are propagating, but also the invasive nature of the cell model.

Conclusion

Application of advanced cellular imaging capabilities, such as taking multiple images on a single z-plane as well as in a z-stack, allows all portions of an invading 3D cellular tumoroid structure to be captured in focus. When stitched and projected to a final image, accurate analysis can then be performed. The ability to view entire tumoroids via brightfield imaging, as well as individual cell types through fluorescent imaging, also allows for determination of the invasive properties of each co-cultured cell type within the included cell model. Inclusion of label-free cellular analysis, carried out on brightfield images, can then quantify not only propagative qualities, but also the specific invasive nature of *in vitro* 3D cell models when uninhibited and in response to test molecules.

References

1. Furnari, F. B. *et al.* Growth Suppression of Glioma Cells by PTEN Requires a Functional Phosphatase Catalytic Domain. *Proc. Natl. Acad. Sci. USA* **1997**, *94(23)*, 12479–84.
2. McFall, T. B. Identification of HCMV UL97 in GBM Cell Lines and a Possible Role for Ganciclovir. Master's Dissertation, Northern Michigan University, Marquette, MI, **2014**.
3. Beckner, M. E. *et al.* Identification of ATP Citrate Lyase as a Positive Regulator of Glycolytic Function in Glioblastomas. *Int. J. Cancer.* **2010**, *126(10)*, 2282–95.
4. Formolo, C. A. *et al.* Secretome Signature of Invasive Glioblastoma Multiforme. *J. Proteome Res.* **2011**, *10(7)*, 3149–59.
5. Mallawaaratchy, D. M. *et al.* Membrane Proteome Analysis of Glioblastoma Cell Invasion. *J. Neuropathol. Exp. Neurol.* **2015**, *74(5)*, 425–41.

www.agilent.com/lifesciences/biotek

RA44412.5340972222

Printed in the USA, April 8, 2022
5994-3393EN

Agilent
Trusted Answers

Application Note

Agilent
Trusted Answers

A Novel Real-Time Co-Culture Assay Using xCelligence RTCA eSight for Immune Cell Invasion and Cytotoxicity

Authors

Jyothi T. Mony,
Alejandra Felix, Yama Abassi,
Brandon J. Lamarche,
Ryan Raver, and Xiaoyu Zhang
Agilent Technologies, Inc.

Introduction

Immune cells extravasate from blood vessels to infiltrate the tissues and perform effector functions that play a crucial role in tumor immune surveillance. These abilities are also harnessed by engineered cytotoxic natural killer (NKs) and Chimeric Antigen Receptor (CAR)-T cells used for cancer immunotherapy.

Although cellular immunotherapy has demonstrated effectiveness in hematological cancers, clinical responses in solid tumors need to be improved. The complex tumor microenvironment (TME) in solid tumors regulates lymphocyte recruitment and function. An important challenge faced by lymphocytes in solid tumors is to navigate the acellular space filled with structural scaffolding of the extracellular matrix (ECM) during migration/invasion. This ECM is heterogenous, and its components can modulate a wide array of cellular responses in both resident tumor cells and infiltrating lymphocytes.[1]

Traditionally, invasion, migration and cytotoxicity are evaluated in different endpoint assays using transwell assay systems to predict the in vivo function. The Boyden Chamber is a classical transwell arrangement that is widely used to evaluate migration and invasion.[2] It consists of a cylindrical cell culture insert with a porous membrane nested inside the well of a standard cell culture plate. Cell suspensions are added to the inner chamber of the insert and induced to migrate out through the pores of variable sizes (typically, 3 to 12 µm) using chemo-attractants in the outer chamber. The inner wells can be coated with ECM to evaluate invasion. The invaded/migrated cells are imaged and/or collected for quantification at predetermined time points. The Boyden Chamber can be modified for evaluating migration and cytotoxicity of effector cells in end-point assays.[3]

This application note describes a novel real-time co-culture assay using RTCA eSight for interrogating immune cell invasion and cytotoxicity that does not require the collection of embedded cells for end-point readouts (Figure 1). In this setup, the ECM layer is in direct contact with target tumor cells and can modulate response of both tumor targets and infiltrating lymphocytes, especially as the latter executes its cytotoxicity function. In the transwell-based approaches, cytotoxicity of the migrated immune cells is carried out in an outer chamber devoid of ECM.

The invasion and killing of target tumor cells by the NKs has been evaluated as proof of concept for the assay system. NKs are innate lymphocytes that kill infected, stressed, or transformed cells by identifying and distinguishing the "altered" cells from healthy cells using an array of activating and inhibiting receptors.[4] The NK92 cells were used as a model for studying invasion and cytotoxicity. The allogenic NKs derived from NK92 cell line are the first NK-based cellular immunotherapy to be granted the Investigational New Drug status by the US Food and Drug Administration.[5]

It is hypothesized that the Matrigel layer presents a challenge for the NK92 cells and increasing the distance for invasion would delay the killing of tumor cells. Also, NKs rely on proteases of the matrix-metalloproteinases (MMP) family to degrade various components in the ECM during invasion stage.

This application note demonstrates that the 96-well format of eSight can be easily used to systematically study the effects of different ECM constituents on tumor and immune cell interactions in the TME depending on user requirements.

Materials and methods

Cells

MCF7 human breast adenocarcinoma cell line (ATCC, part number HTB-22) was transduced with eLenti Red (Agilent Technologies, part number 8711011) at a multiplicity of infection of 1 and cultured in the presence of 2 µg/mL Puromycin (InvivoGen, part number ant-pr-1) for 14 days to select for MCF7-red cells stably expressing nuclear-localized red fluorescent protein (RFP). MCF7 and MCF7-red cells were cultured in EMEM media (ATCC, 30-2003) supplemented with 10% heat inactivated FBS (Sigma, part number 12106C-500ML) and 1% Pen/Strep (Hyclone, part number SV30010).

NK92 cells (Creative Bioarray, CSC-C0499) were grown in MyeloCult H5100 media (Stemcell Technologies, part number 05150) supplemented with 30 mL of horse serum (Gibco, part number 16050-122), 600 IU/mL of rhIL-2 (Stemcell Technologies, part number 78036) and 1% Pen/Strep (Hyclone, part number SV30010).

eGFP-NK92 cells (BPS Bioscience, part number 78399) were grown in X-VIVO 15 (Lonza Ltd, part number 04-418Q) supplemented with 5% human serum (Sigma, H4522), 500 IU/mL of rhIL-2 (Stemcell Technologies, part number 78036) and 0.5 µg/mL Puromycin.

ECM invasion and cytotoxicity assay

The ability of NK92 cells to invade the Matrigel and kill the MCF7-red target cells was evaluated by concurrent impedance and imaging readouts on an xCELLigence RTCA eSight (Agilent Technologies) as outlined in Figure 1. Background impedance signal was measured with 50 µL of EMEM media in the wells of E-plate VIEW microplate (Agilent Technologies, part number 0030060101030). MCF7-red target cells (30,000 in 100 µL) were added to the wells and the plate was placed at room temperature for 30 min to facilitate an even distribution at the bottom. The plate was returned to its cradle in the eSight to acquire data. Impedance was read every 15 minutes and images were taken every 60 minutes. Images from four fields of view were acquired in each well in brightfield, red, and green fluorescence channels. Exposure time was set at default in brightfield, 150 ms in red, and 300 ms in green channels. Matrigel (Corning, part number 356234, 354234) was thawed overnight at 4 °C, diluted with DMEM and supplemented with 10% FBS to a final total protein concentration of 6 mg/mL. After 24 hours the data collection was paused. Media in the wells were aspirated and varying volumes of Matrigel (50, 75, and 100 µL, data shown here) was layered over the MCF7-red cells and incubated for 30 minutes at room temperature, followed by 30 minutes at 37 °C/5% CO_2 for polymerization of the Matrigel. Impedance and imaging data were collected for an hour during which the NK92 cells were suspended in EMEM media and the cell numbers were adjusted to achieve E:T of 3:1 in 100 µL. NK92 cell suspension (100 µL) was layered over the Matrigel and the total volume in all wells was adjusted to 200 µL. The plate was loaded back into the eSight cradle and data acquisition was resumed. Percent cytolysis was calculated from normalized cell impedance readings using the formula [(1 – (treated/untreated) × 100].

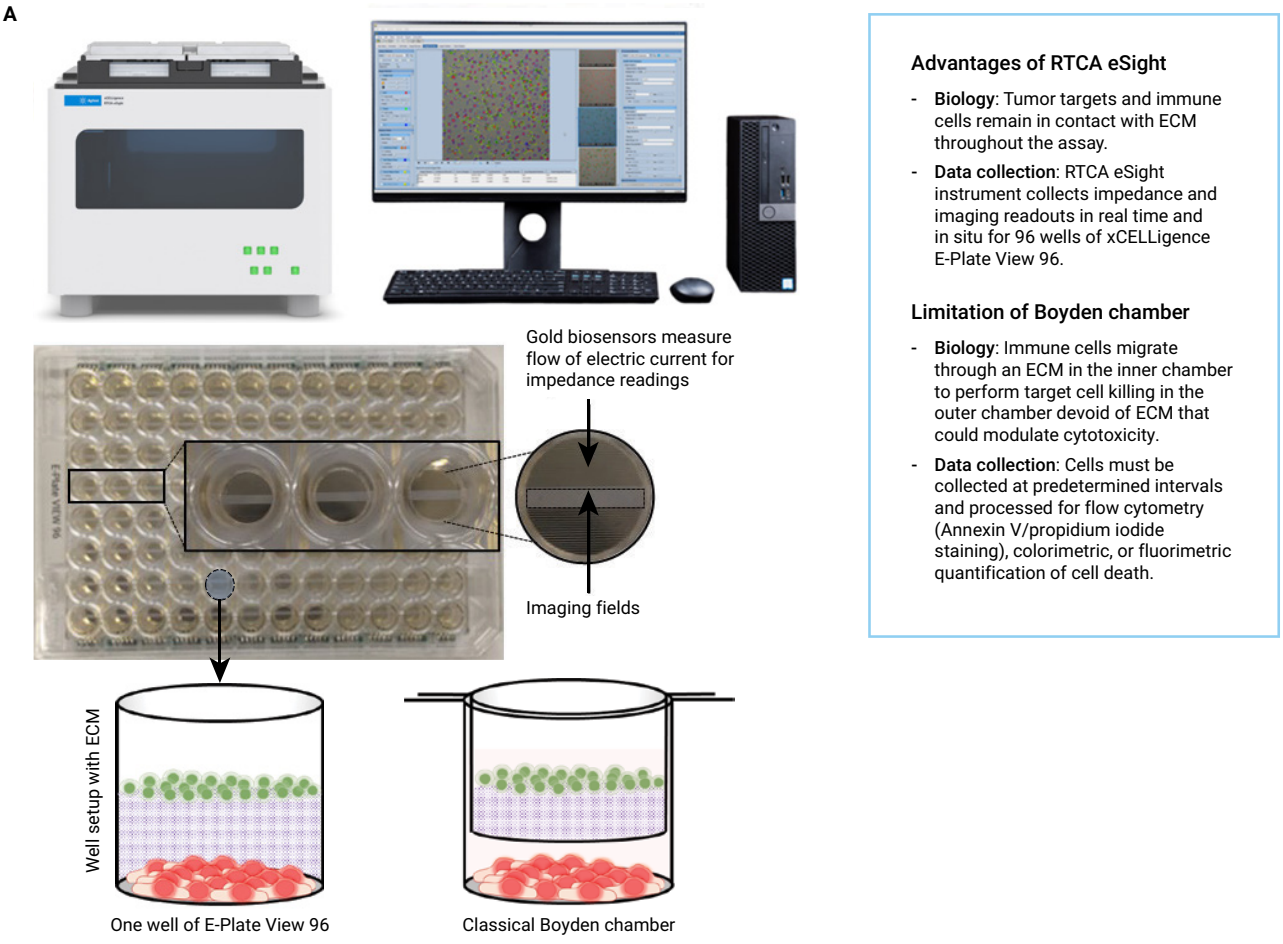

Figure 1. Invasion-cytotoxicity assay setup. (A) The RTCA eSight instrument, E-plate View 96 and comparison of the setup in one of the 96 wells with a Boyden chamber. Advantages of this setup and limitations in data collection of the classical approaches are outlined in the box. (B) Outline of the steps in the assay.

MMP inhibition and kinetics of NK invasion

Ilomastat (GM6001, Selleck Chemicals, part number S7157), a broad spectrum MMP inhibitor, was dissolved in the Matrigel and media at a final concentration of 2 and 10 µM to assess the role of MMP-dependent NK92 invasion. Percent cytolysis was calculated from normalized cell impedance readings and red object count data using the formula [(1 – (NK92 + MMPi/MMPi treated) × 100].

Results and discussion

Target cell killing is delayed with increasing invasion distance for NK cells

Impedance increases with time and stabilizes as the MCF7-red target cells adhere and proliferate to reach confluence (Figure 2A). The addition of Matrigel (50 µL) modulates the impedance signature of MCF7 cells and importantly, delays the cytolysis by NK92 cells added at 24 hours. The drop in impedance due to cytolysis is further delayed with increasing volumes of Matrigel (Figure 2B, representative data for 50, 75 and 100 µL). The KT60 (Figure 2C, time to achieve 60% killing with respect to controls) was 67, 76, and 89 hours, respectively.

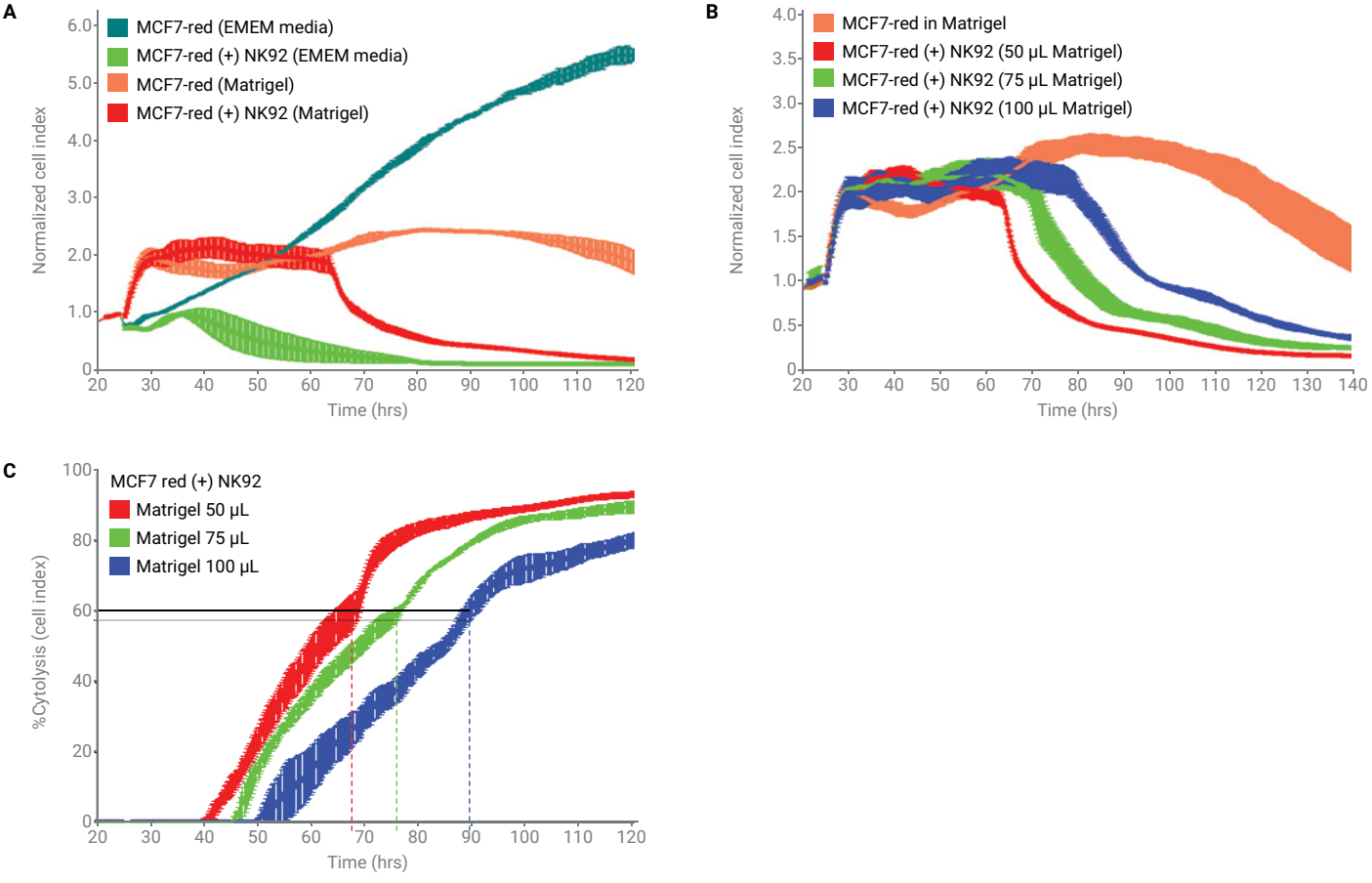

Figure 2. Cytotoxicity of NK92 is delayed with increasing invasion distance. (A) The addition of NK92 at 24 hours (E:T =3:1) results in a drop in impedance (CI) due to cytolysis of targets and it is delayed in Matrigel. (B) Cytolysis is further delayed in increasing volumes of Matrigel. (C) Percent cytolysis was calculated with reference to untreated MCF7 growing in Matrigel.

MMP inhibition delays target cell killing by NK cells

As cytolysis was delayed with increasing invasion distance for the NKs, it is hypothesized that MMPs would play an important role in lymphocyte invasion. Consistent with the function of MMPs in invasion, percent cytolysis computed from normalized impedance readings (Figure 3A) and live cell imaging (red fluorescence, Figure 3B) confirmed both delayed and reduced target cell killing by GFP-NK92 cells in the presence of Ilomastat (2 and 10 µM). Image analysis concurs with impedance measurements, confirming the kinetics of cell killing.

Image analysis corroborates delayed invasion and killing with increasing invasion distance

Representative images of MCF7 clusters reveal increased clumping and cell death in response to GFP-NK92 (Figure 3C). Although there is increased tumor cell death, only a few GFP-NK92 were detected in the imaging fields. Interestingly, highly active NK cells were detected that made multiple contacts with different MCF7 red targets in clusters suggesting serial killing activity.

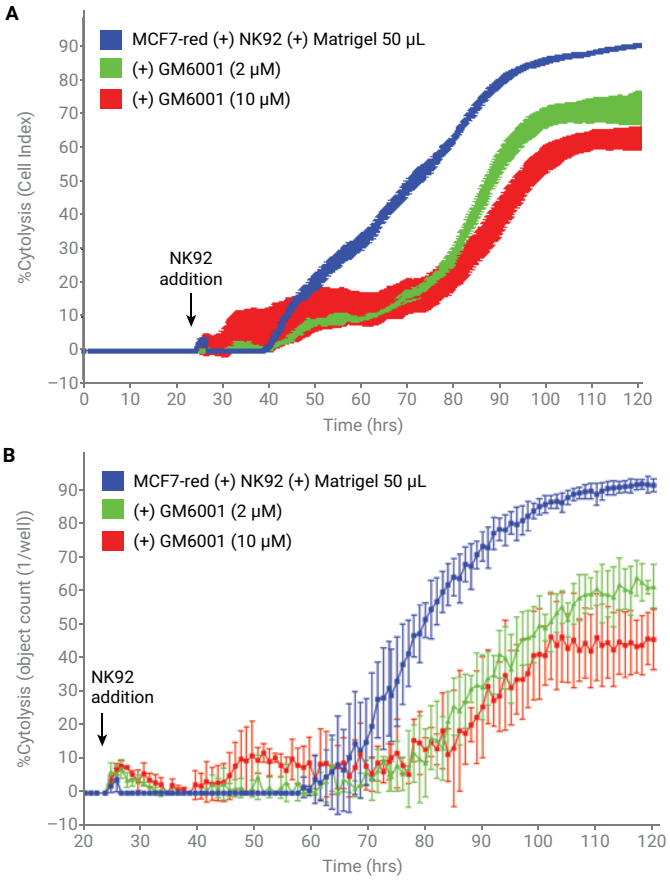

Figure 3. MMPs play an important role in invasion, and its inhibition results in delayed cytotoxicity. (A) Cytolysis is reduced GFP-NK92 at 24 hours (E:T = 3:1) results in a drop in impedance (CI) due to the killing of target cells. (B) Live cell imaging confirms the reduced loss of target cells (red fluorescence) in the visual fields in the presence of MMP inhibitor (2 µM and 10 µM).

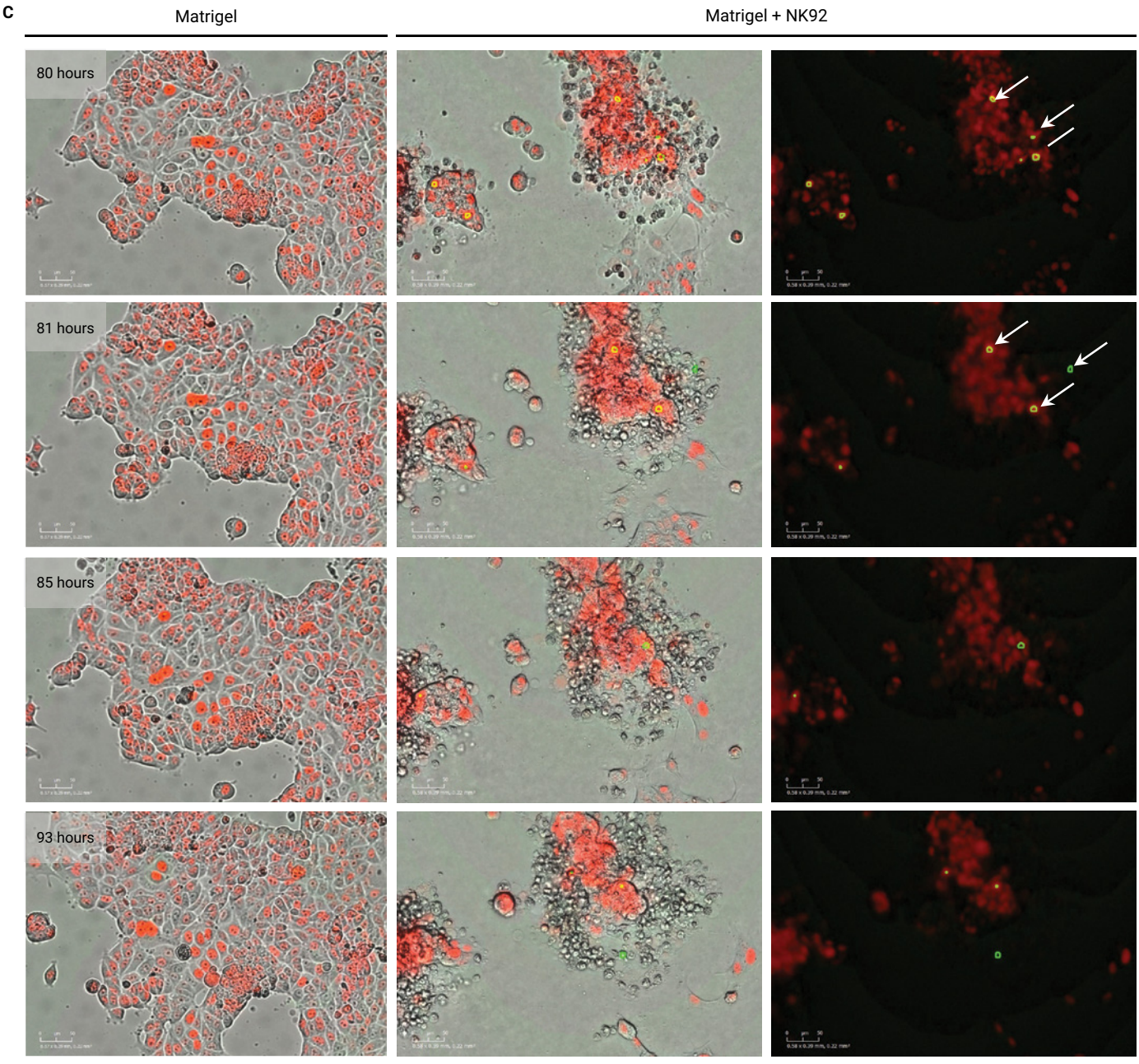

Figure 3C. Representative images for clustering of MCF7 and progressive loss red fluorescence associated with cytotoxicity. A few green GFP-NK92 cells (yellow outline) make multiple contacts with MCF7-red target cells in the clusters, resulting in cell death over the course of the assay.

Conclusion

Recapitulating the features of the tumor microenvironment in solid tumors could play a pivotal part in formulating and refining the strategies for cellular immunotherapy. The dysregulation of ECM in tumor microenvironment of solid tumors has been widely investigated for its ability to modulate diverse cellular responses. In this regard, there is a need for efficient in vitro assays that evaluate the responses of tumor and immune cells in the presence of ECM.

The ability of NKs and other immune cells to invade the extracellular space to reach the target cells could depend on the ability to degrade ECM.[6] Various constituents of ECM can regulate the function of NK cells.[7] In this application note, the ability of NK92 cells to invade a Matrigel layer and kill the target cells has been evaluated. The cytotoxicity outcome measured by loss in impedance and live cell imaging serves as a surrogate for the migratory/invasion potential of the NK92 cells. As a proof of concept, it was established that this assay format allows simultaneous evaluation of invasion and cytotoxicity in the presence of an ECM by demonstrating that the killing of target cells can be delayed by varying the invasion distance through the Matrigel.

NKs can express multiple MMPs and transmigration assays have shown that NK92 invasion in Matrigel is reduced in the presence of MMP inhibitor GM6001.[6] Typically, studies evaluate invasion/migration potential and cytotoxicity functions separately in complex workflows as is the case with the study that evaluated the effect of MMP inhibitor. Alternatively, some studies have evaluated both migration and cytotoxicity using complex cumbersome experimental setups.[8] Live cell imaging and real-time impedance readouts have been used to demonstrate the contribution of MMPs in invasion-cytotoxicity assays with NK92. Consistent with the role of MMPs in facilitating invasion, the killing of target cells is delayed by the broad spectrum MMP inhibitor.

Although imaging and impedance data were consistent in the invasion-cytotoxicity assay, relying on imaging data can be challenging. Tumor cells respond differently to the Matrigel and as highlighted in the representative images the MCF7 target cells form irregular and messy clumps as they undergo cell death. Surprisingly, rather than finding a swarm of invading NK cells, only a few NK cells in and around the MCF clusters were detected. Nonetheless, images and videos were generated of highly active GFP-NK92 cells that made multiple contacts with different targets in the clusters, leading to cell death of the contacted targets during the course of the assay.

The novel real-time co-culture assay described in this application note demonstrates the utility of eSight for the simultaneous evaluation of invasion and cytotoxicity functions of lymphocytes that are critical for immunotherapy in solid tumors.

References

1. Pickup, M. W.; Mouw, J. K.; Weaver, V. M. The Extracellular Matrix Modulates the Hallmarks of Cancer. *EMBO Rep.* **2014**, *15*, 1243–53.
2. Falasca, M., Raimondi, C.; Maffucci, T. Boyden Chamber. *Methods in Molecular Biology* **2011**, 769, 87–95.
3. Schomer, N.; Boissel, L.; Klingemann, H. Combined Invasion and Cytotoxicity Assay Using Chemokine Secreting Target Cells. **2020**.
4. Morvan, M. G.; Lanier, L. L. NK Cells and Cancer: You Can Teach Innate Cells New Tricks. *Nat. Rev. Cancer* **2016**, *16*, 7–19.
5. Laskowski, T. J.; Biederstädt, A.; Rezvani, K. Natural Killer Cells in Antitumour Adoptive Cell Immunotherapy. *Nat. Rev. Cancer* **2022**. doi:10.1038/s41568-022-00491-0.
6. Edsparr, K.; *et al.* Human NK Cell Lines Migrate Differentially In Vitro Related to Matrix Interaction and MMP Expression. *Immunol. Cell Biol.* **2009**, 87, 489–495.
7. Bunting, M. D.; *et al.* Extracellular Matrix Proteins Regulate NK Cell Function in Peripheral Tissues. *Sci. Adv.* **2022**, *8*, eabk3327.
8. Olofsson, P. E.; *et al.* A Collagen-Based Microwell Migration Assay to Study NK-Target Cell Interactions. *Sci. Rep.* **2019**, *9*.

agilent.com/chem/eSight

Printed in the USA, November 29, 2023
5994-6888EN

Agilent
Trusted Answers

Application Note

Cancer Research

Agilent

Trusted Answers

High-Throughput Methods to Quantitatively Evaluate TGF-β Signaling in Epithelial-to-Mesenchymal Transition

Authors

Ernest Heimsath, PhD
Agilent Technologies, Inc.

Antony Wood, PhD
Cell Signaling Technology

Abstract

The epithelial-to-mesenchymal transition (EMT) is a cellular differentiation process whereby epithelial cells lose many epithelial features, while acquiring mesenchymal, fibroblast-like properties, leading to reduced cell–cell contacts and increased motility. While recognized as a fundamental process required for normal embryonic development, EMT is understood to be co-opted by malignant epithelial tumors to facilitate their metastatic spread. Central to stimulating EMT is the TGF-β superfamily of growth factor ligands, which elicit receptor-mediated responses in cells, primarily via TGF-β/SMAD signaling pathways. In these pathways, receptor-mediated SMAD (R-SMAD) proteins serve as the primary downstream effector molecules, the activities of which are regulated through receptor-mediated phosphorylation. The magnitude and duration of ligand-induced receptor activation influences the level of SMAD phosphorylation, which, in turn, influences the magnitude of downstream cellular response. This study describes high-throughput methods to quantitatively evaluate the biochemical and cellular responses to TGF-β/SMAD pathway activation in a cellular model of TGF-β-induced EMT. Effects of pathway activation are examined at different levels of biological complexity—biochemical, cellular, and multicellular—using two- and three-dimensional (spheroid) models. Collectively, these approaches enable a comprehensive evaluation of TGF-β/SMAD pathway activation that is amenable to high-throughput analysis platforms .

Introduction

EMT is a cellular differentiation process whereby epithelial cells lose epithelial features while acquiring mesenchymal, fibroblast-like properties, such as reduced intercellular adhesion and increased motility. EMT is a critical feature of normal embryonic development, but is also used by malignant epithelial tumors to spread beyond their origin.[1-3] Central to stimulating EMT is the TGF-β/SMAD signaling axis, for which R-SMAD proteins represent primary downstream effector molecules.[4-7] TGF-β ligand–receptor binding elicits the formation of heterotetrameric TGF-β type I/II receptor complexes, leading to site-specific phosphorylation events that elicit receptor kinase activation. The activated receptor complexes recruit R-SMADs, which are then activated through receptor-kinase-mediated phosphorylation.

There are two primary signaling axes within the TGF-β superfamily. TGF-β ligand–receptor interactions result in recruitment and activation of SMAD2 and/or SMAD3 proteins, whereas bone morphogenetic protein (BMP) ligand–receptor interactions lead to recruitment and activation of SMAD1, SMAD5, or SMAD9. In either case, phosphorylated R-SMADs form a ternary complex with SMAD4; this complex then translocates to the nucleus where it regulates the expression of target genes (Figure 1).

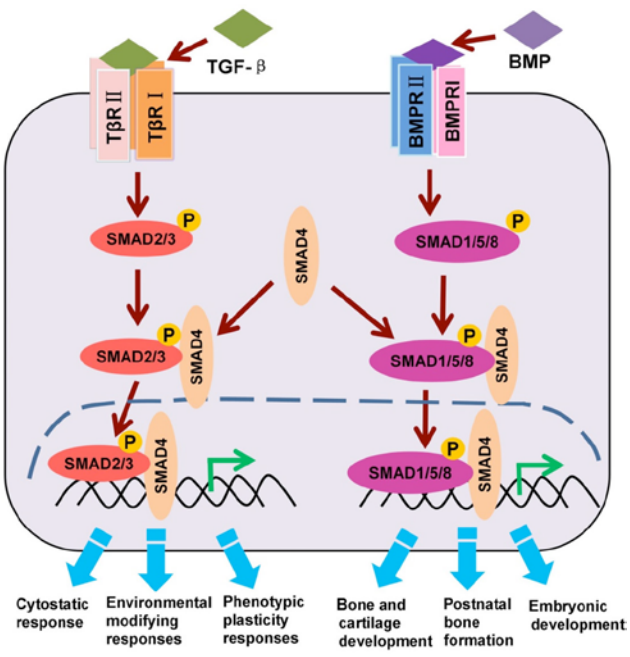

Figure 1. The canonical TGF-β/BMP/SMAD signaling pathway (adaptation).[7]

Activation of the TGF-β-SMAD2/3 pathway is known to upregulate the expression levels of numerous EMT-associated genes, including *HMGA2*, *ZEB1*, *Snai1*, and *Slug*, all of which have furthermore been associated with cancer metastasis.[1-3, 8-13]

The ability to investigate this pathway in detail, at multiple levels of biological complexity, is critical to gain a better understanding of the role of EMT in cancer. This application note demonstrates high-throughput methods—using the Agilent BioTek Cytation C10 confocal imaging reader and Agilent BioTek Gen5 microplate reader and software—to quantitatively evaluate the biochemical and cellular responses to TGF-β/SMAD pathway activation in a cellular model of TGF-β-induced EMT. The effects of pathway activation are examined at different levels of biological complexity—biochemical, cellular, and multicellular—using 2D and 3D (spheroid) models. Collectively, these approaches enable a comprehensive evaluation of TGF-β/SMAD pathway activation that is amenable to high-throughput analysis platforms.

Experimental

Materials

Cell lines

A549 lung epithelial carcinoma cells, part number CC-185, were purchased from ATCC (Manassas, VA, U.S.) and were cultured in Advanced DMEM (part number 12491; Gibco Thermo Fisher Scientific; Waltham, MA, U.S.) containing 10% FBS and 1x penicillin/streptomycin/glutamine.

Assay reagents

Human TGF-β1 recombinant protein (part number 75362) was from Cell Signaling Technology (“CST”, Danvers, MA, U.S.). Cell lysis buffer (10x) was from CST (part number 9803). PathScan Phospho-Smad2 (Ser465/467)/Smad3 (Ser423/425) Sandwich ELISA kit (part number 12001, CST) detects SMAD2 (Ser465/467) and/or SMAD3 (Ser423/425), only when phosphorylated at the indicated residues. PathScan Total Smad2/3 Sandwich ELISA kit (part number 12000, CST) detects SMAD2 and/or SMAD3 proteins irrespective of phosphorylation status. SMAD4 (D3R4N) XP Rabbit mAb (part number 46535, CST) detects total SMAD4 protein, and is validated for use in western blot, immunoprecipitation, immunocytochemistry, immunohistochemistry, flow cytometry, and chromatin immunoprecipitation. Antibodies targeting HMGA2 (D1A7) Rabbit mAb (part number 8179, CST), ZEB1 (E3G6Y) XP Rabbit mAb (part number 70512, CST), and Slug (C18G7) Rabbit mAb (part number 9585, CST) were used to evaluate TGF-β1-stimulated changes in the expression of EMT-associated target genes.

Fibronectin coating

Agilent 96-well imaging microplates (part number 204626-100) were treated with 10 µg/mL fibronectin (part number F1141; Sigma-Aldrich, Burlington, MA, U.S.) diluted in DPBS for 30 minutes, followed by three washes with DPBS prior to cell seeding.

Cell seeding and growth factor treatment

Cells seeded in culture plates, or spheroids cultured in round-bottom 96-well plates, were serum starved for 18 hours in basal culture medium (described previously) lacking FBS (A-DMEM) or BulletKit supplements (EBM).Cells were then treated for 60 minutes at 37 °C with human TGF-β1 recombinant protein, at the indicated concentrations. After treatment, cells were either fixed in 4% paraformaldehyde (PFA) for 10 minutes for immunostaining analysis, or used for lysate collection, using 1x cell lysis buffer supplemented with cOmplete, Mini Protease Inhibitor Cocktail (part number 1186153001; Roche Diagnostics GmbH, Mannheim, Germany).

Three-dimensional spheroid outgrowth assay

The 3D spheroid outgrowth assay was conducted by preforming 2000-cell A549 spheroids in a 96-well ultralow-attachment (ULA), round- bottom microplate (part number 650979; Greiner Bio-One, Monroe, NC, U.S.). Spheroids were then transferred (one spheroid per well) to an Agilent 96-well imaging microplate (part number 204626-100) containing 40 µL of pregelled type I collagen matrix (part number 254236; Corning, NY, U.S.). Once the spheroids settled on top of the matrix, the plate was returned to a tissue culture (TC) incubator and cultured for three days at 37 °C.

Sample preparation

For ELISA analyses, lysates from cells cultured in 12-well, TC-treated plates were collected, sonicated for 30 minutes at 4 °C, then centrifuged at 14,000 rpm for 10 minutes. Supernatants were collected and stored at –80 °C, and thawed as needed.

For 2D cellular assays, cells were collected after treatment and fixed with 4% PFA for 10 minutes, followed by three washes with DPBS containing 0.5 M glycine. Cells were permeabilized with 0.5% Triton X-100 for 5 minutes, then blocked for 30 minutes with 5% bovine serum albumin (BSA). Cells were then incubated overnight at 4 °C with the indicated antibodies, which were diluted in 5% BSA containing 0.1% Tween 20 (according to supplier recommendations).. After three washes with PBS + 0.1% Tween 20, cells were incubated with a CF633-conjugated goat anti-rabbit polyclonal antibody (part number 20131; Biotium, Fremont, CA, U.S.) diluted to 1:1000 in 5% BSA containing 0.1% Tween 20, 2 µM Hoechst 34580, and 1x Alexa Fluor 488-conjugated phalloidin (part number A12379; Thermo Fisher Scientific).

For the 3D EMT assay, samples in 96-well microplates were washed three times with DPBS before fixation in 4% PFA for 1 hour at room temperature, followed by three washes with DPBS containing 0.5 M glycine. Spheroids were then permeabilized with 0.5% Triton X-100 for 1 hour, followed by an overnight block with 5% BSA at 4 °C. Fixed, permeabilized spheroids were then incubated overnight at 4 °C in primary antibodies, which were diluted in 5% BSA + 0.1% Tween 20 (according to supplier recommendations), followed by hourly washes with immunowash buffer, concluding with a final overnight wash at 4 °C.

Samples were then incubated with secondary antibodies and counterstains which were diluted in 5% BSA + 0.1% Tween 20, followed by hourly washes with immunowash buffer with a final overnight wash at 4 °C.

Gen5 Imaging, image processing, and cellular analysis

Imaging and image processing

Using the Agilent BioTek Cytation C10 confocal imaging reader and a 20x 0.45 NA objective in widefield mode, a single Z-plane of adherent cell samples was imaged in three channels: GFP (AF488- conjugated phalloidin), CY5 (CF633-conjugated goat anti- rabbit secondary antibody, used to visualize phosphorylated SMAD2/3), and DAPI (Hoechst 34580), with the DAPI channel used to set Z-focus height using laser autofocus. With the same three channels, multichannel, 2 x 2 montage Z-stacks spheroids were imaged in confocal mode (60 µm disk using a 20x 0.4 NA objective. Following montage stitching, multichannel Z-stacks underwent a background reduction transformation step before generating a maximum intensity project.

Cellular analysis

Primary masks of nuclei were established using Hoechst 34580 signal (DAPI channel; yellow outlines in Figures 3 and 4), and integrated phosphorylated SMAD2/3 or SMAD4 nuclear signals of individual nuclei were quantified using the CY5 channel as a secondary mask. The reported phosphorylated SMAD2/3 signal was derived by first adjusting for the nuclear area using the following custom metric formula: [area-corrected Integral signal] = (Integrated CY5 signal) / (nuclear area). The area-corrected integral phosphorylated SMAD2/3 signal measured at each TGF-β1 concentration was converted to, and reported as, fold change of the signal response relative to vehicle control using the following custom data reduction step: [nuclear P-SMAD2/3 fold change] = (area-corrected integrated P-SMAD2/3 signal) / (mean area-corrected integrated P-SMAD2/3 signal of

vehicle control). To quantify the number of cells (nuclei) that migrated away from the core spheroid (Figure 4D and E), a primary mask identifying the core spheroid was established using the GFP channel (phalloidin stain). Cells outside of the core spheroid were then defined by identifying nuclei using the DAPI channel as a secondary mask, where the primary mask zone is excluded. A ring width for the secondary mask zone was set to 600 µm to ensure all migrated cells were accounted for.

Results and discussion

Biochemical quantification of TGF-β1-induced SMAD2/3 phosphorylation using PathScan Sandwich ELISA kits coupled with the Cytation C10

ELISA is a powerful and sensitive assay that enables quantitative analysis of biochemical events in biological fluids, including cell lysates. PathScan Sandwich ELISA kits from CST employ a horseradish peroxidase (HRP)-conjugated secondary antibody that provides a colorimetric readout measured by absorbance at 450 nm. Phosphorylated SMAD2/3 values were normalized against total SMAD2/3 protein values to control for protein loading.

Using the plate-reader function of the Cytation C10, we demonstrate dose-dependent TGF-β1-induced SMAD2/3 phosphorylation in lysates from A549 lung carcinoma cells with a calculated EC_{50} value of 0.286 ng/mL (Figure 2).

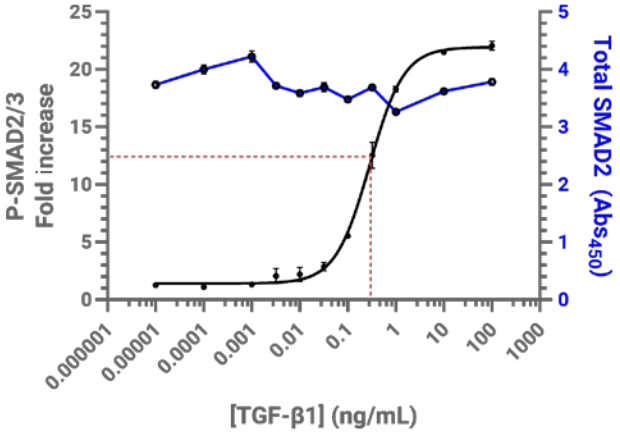

Figure 2. Dose-dependent SMAD2/3 phosphorylation in response to TGF-β1. The PathScan Sandwich ELISA kit quantifies TGF-β1-dependent SMAD2/3 phosphorylation in A549 cells. The phosphorylated SMAD2/3 values (pSMAD2/3, black) are reported as fold change above no treatment control, which were normalized for total SMAD2 (blue values).

Quantitative cellular analysis of SMAD phosphorylation and translocation using phospho-specific SMAD antibodies and fluorescence widefield imaging on the Cytation C10

Immunofluorescent image analysis in 2D-cultured cells can provide cellular and subcellular (spatial) insights into signal transduction pathway activity. The Cytation C10 confocal imaging reader enables quantitative analysis of immunostaining data in a high-throughput format.

Treatment of A549 cells with TGF-β1 (100 ng/mL) resulted in a detectable increase in nuclear-localized phosphorylated SMAD2/3 compared with vehicle-treated controls (Figure 3A and B). Using a high-throughput, 96-well format for analysis, a dose–response curve was plotted with a calculated EC_{50} for A549 cells treated with TGF-β1 of 0.037 ng/mL (Figure 3D). Similarly, dose-dependent increases in the nuclear expression of EMT-associated transcription factors HMGA2, ZEB1, and Slug were observed in response to TGF-β1 treatment, with EC_{50} values of 14.6, 2.8, and 6.2 ng/mL, respectively (Figure 3D). Inhibition of the TGF-β signaling axis via pretreatment with the TGF-β receptor inhibitor SB431542 (before TGF-β1 treatment) resulted in reduced SMAD2/3 phosphorylation and nuclear translocation (Figure 3C), and a corresponding dose-dependent reduction in the expression of TGF-β1-induced EMT markers (Figure 3E) relative to that observed in cells treated with TGF-β1 alone, further confirming a direct role for the TGF-β pathway in regulating the expression of EMT-associated genes.

Quantifying phosphorylated SMAD2/3 and SMAD4 nuclear translocation in a 3D spheroid outgrowth assay

Acute, 1-hour treatment of A549 spheroids with TGF-β1 (100 ng/mL) resulted in a four-fold increase in nuclear phosphorylated SMAD2/3 (Figure 4A to C). To examine this response in a more complex (multicellular) context, we evaluated the cellular responses to sustained TGF-β1 treatment in a spheroid outgrowth assay. Preformed A549 spheroids were seeded (one spheroid per well) in a 96-well microplate precoated with collagen matrix and cultured for 3 to 4 days in the presence or absence of TGF-β1 (100 ng/mL).

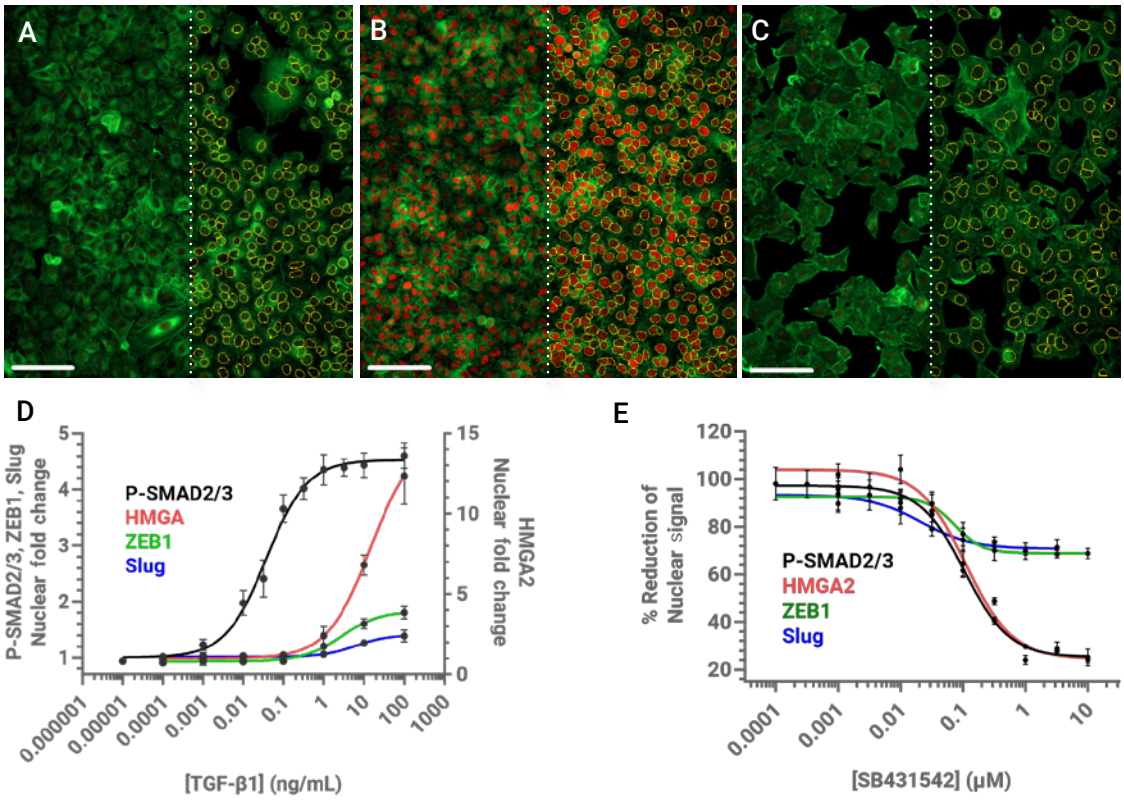

Figure 3. TGF-β1-mediated SMAD phosphorylation and spatial translocation can be quantified in A549 cells. Following a serum starvation period, A549 cells were treated for one hour with (A) vehicle control, (B) 100 ng/mL TGF-β1, or (C) 100 ng/mL TGF-β1 + 10 ng/mL of the TGF-β1 inhibitor SB431542. Cells were then fixed and immunostained for phosphorylated SMAD2/3 or the EMT markers HMGA2, ZEB1, and Slug, and counterstained with Hoechst 34580 and AF488-phalloidin (scale bar = 100 μm). (D) High-throughput imaging in a 96-well plate using nuclear phosphorylated SMAD2/3, HMGA2, ZEB1, or Slug signal as a readout established a respective dose-dependent response to TGF-β1. (E) TGF-β1 inhibition by SB431542 is dose dependent for phosphorylated SMAD2/3, HMGA2, ZEB1, and Slug. The right halves of A, B, and C illustrate the nuclear masking methods used to quantify phosphorylated SMAD2/3 signal, as described in the "Experimental" section.

Being a 3D, multicellular model, spheroids present technical challenges in sample preparation, immunostaining, and image analysis. SMAD4 (D3R4N) XP Rabbit mAb was selected as the immunostaining reagent, due to its validation and approval for use in complex biological samples (e.g., FFPE). Spheroids were imaged using the confocal imaging mode of the Cytation C10, which enables optical resolution of Z-planes in a 3D biological sample. After immunostaining, spheroids were counterstained with the Hoechst 34580 and CF633-conjugated phalloidin, and a maximum-intensity projection was generated and analyzed, which consisted of a stitched 3 x 3 montage comprised of a 101-slice Z-stack (2 μm step size) spanning 200 μm (Figure 4D to F).

In contrast to vehicle-treated controls, spheroids cultured in the presence of TGF-β1 exhibited dramatic out-migration of cells from the initial (core) spheroid mass, consistent with the increased migratory capacity of cells undergoing EMT (Figure 4F). The extent of cell extrusion from the spheroid mass was furthermore positively correlated with increased nuclear SMAD4 signal (Figure 4G to I), clearly visible in cells outside of the core spheroid (Figure 4H). These observations confirm activation of the TGF-β pathway activation in TGF-β1-treated spheroids exhibiting phenotypic changes consistent with EMT.

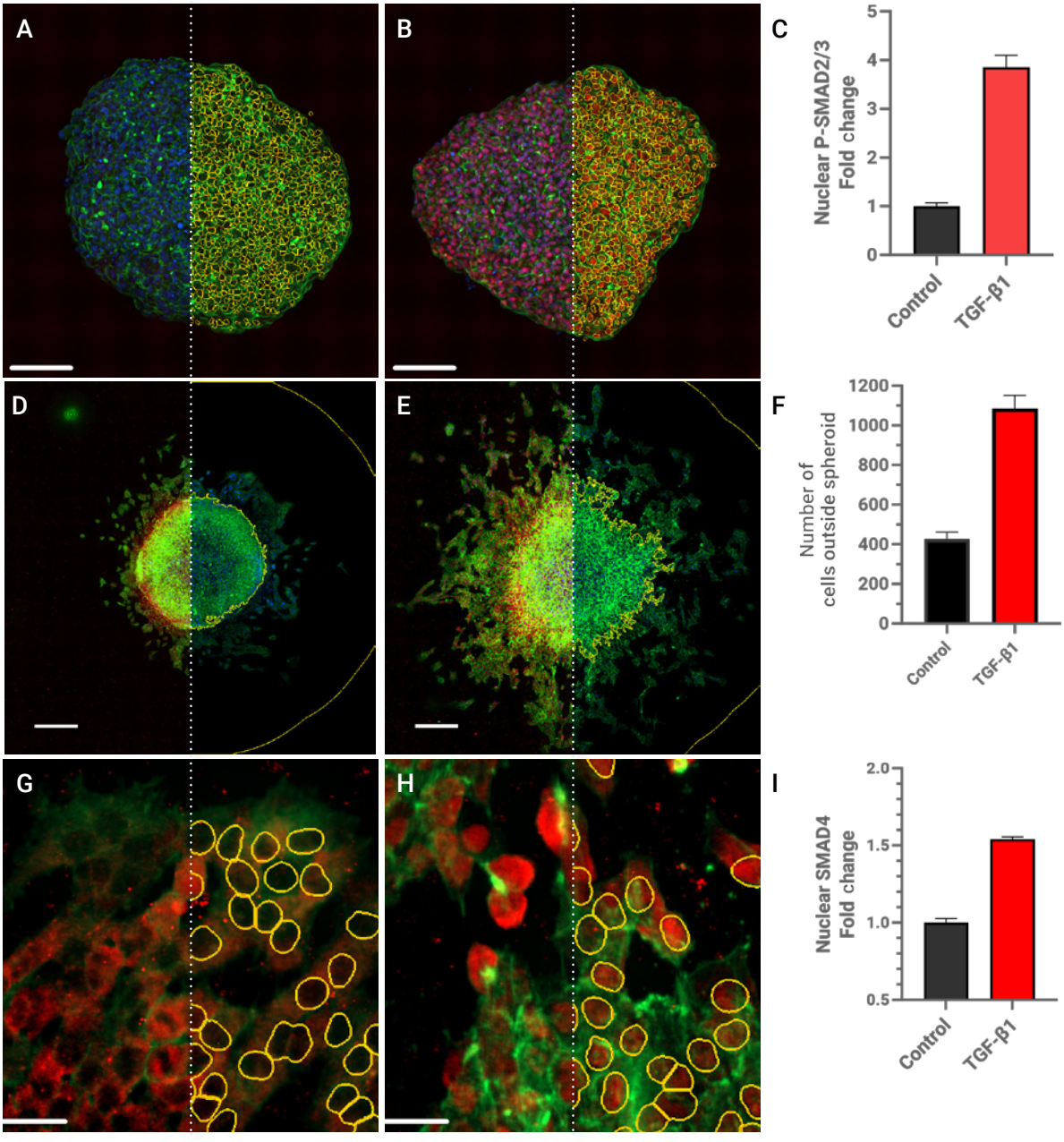

Figure 4. Phosphorylated SMAD2/3 and SMAD4 nuclear translocation can be quantified in a 3D spheroid outgrowth model. (A-C) A maximum projection of an A549 spheroid cultured in suspension, treated with (A) vehicle, or (B) TGF-β1, immunostained for phosphorylated SMAD2/3 (red), and counterstained with phalloidin (green) and Hoechst 34580 (blue). (C) Quantification of nuclear phosphorylated SMAD2/3 using DAPI signal as a primary mask. Scale bar = 100 µm. (D to F) A maximum projection from a 3 x 3 montage Z-stack of an A549 spheroid demonstrates increased out-migration of cells from the core spheroid mass in the presence of (E) 100 ng/mL TGF-β1 compared to (D) vehicle-treated controls. Scale bar = 100 µm. (F) Quantitative analysis of spheroid cell out-migration in response to sustained treatment with TGF- β1 (100 ng/mL). (G-I) Insets indicated in panels D and E. Increased nuclear SMAD4 observed after sustained treatment with (G) 100 ng/mL TGF-β1 versus (H) control; (I) quantification of nuclear SMAD4 signal in spheroid cells in response to sustained treatment with TGF- β1 (100 ng/mL). Scale bar = 50 µm. The right halves of A, B, D, E, G, and H illustrate the nuclear masking methods used to quantify nuclear SMAD signal, as described in the "Experimental" section.

Conclusion

Rigorously validated antibody reagents from Cell Signaling Technology, combined with the multifunctional capabilities of the Agilent BioTek Cytation C10 confocal imaging reader and the Agilent BioTek Gen5 microplate reader and imager software, together enable high-throughput, quantitative analysis of TGF-β pathway activation in 2D and 3D cellular models.

References

1. Aigner, K. *et al.* The Transcription Factor ZEB1 (δEF1) Promotes Tumour Cell Differentiation by Repressing Master Regulators of Epithelial Polarity. *Oncogene*. **2007**. 26, 6979-88. DOI: 10.1038/sj.onc.1210508
2. Peinado, H., Olmeda, D., and Cano, A. Snail, Zeb and bHLH Factors in Tumour Progression: An Alliance Against the Epithelial Phenotype? *Nature Reviews. Cancer.* **2007**. 7, 415-28. DOI: 10.1038/nrc2131
3. Moreno-Bueno, G., Portillo, F., and Cano, A. Transcriptional Regulation of Cell Polarity in EMT and Cancer. *Oncogene.* **2008**. 27, 6958-69. DOI: 10.1038/onc.2008.346
4. Derynck, R. and Zhang, Y. E. Smad-Dependent and Smad-Independent Pathways in TGF-β Family Signalling. *Nature.* **2003** Oct 9; *425*(6958):577-84. DOI: 10.1038/nature02006
5. Tzavlaki, K. and Moustakas, A. TGF-β Signaling *Biomolecules*. **2020** Mar 23; *10*(3):487. DOI: 10.3390/biom10030487
6. Bragdon, B., Moseychuk, O., Saldanha, S., King, D., Julian, J., and Nohe, A. Bone Morphogenetic Proteins: A Critical Review *Cell Signal.* **2011** Apr; *23*(4):609-20. DOI: 10.1016/j.cellsig.2010.10.003
7. Xie, F., Zhang, Z., Van Dam, H. Zhang, L., and Zhou, F. Regulation of TGF-β Superfamily Signaling by SMAD Mono-Ubiquitination *Cells.* **2014** Oct 15; *3*(4):981-93. DOI: 10.3390/cells3040981
8. Fusco, A. and Fedele, M. Roles of HMGA Proteins in Cancer *Nature Reviews. Cancer* **2007**. 7, 899-910. DOI: 10.1038/nrc2271
9. Rawlinson, N.J., West, W. W., Nelson, M., and Bridge, J. A. *Cancer Genetics and Cytogenetics* **2007**. 181, 119-24. DOI: 10.1016/j.cancergencyto.2007.11.008
10. Wei, J.J., Jingjing, W., Chunyan, L., Anjana, Y., Peng, L., Pacita, K., and Jinsong, L. HMGA2: A Potential Biomarker Complement to P53 for Detection of Early-Stage High-Grade Papillary Serous Carcinoma in Fallopian Tubes *The American Journal of Surgical Pathology* **2010**. 34, 18-26. DOI: https://doi.org/10.1097/PAS.0b013e3181be5d72
11. Mahajan, A., Liu, Z., Gellert, L., Zou, X., Yang, G., Lee, P., Yang, X., and Wei, J-J. HMGA2: A Biomarker Significantly Overexpressed in High-Grade Ovarian Serous Carcinoma *Modern Pathology* **2010**. 23, 673-81. DOI: 10.1038/modpathol.2010.49
12. Barrallo-Gimeno, A. and Nieto, M.A. The Snail Genes as Inducers of Cell Movement and Survival: Implications in Development and Cancer *Development* **2005**. 132, 3151-61. DOI: 10.1038/modpathol.2010.49
13. Castro Alves, C., Rosivatz, E., Schott, C., Hollweck, R., Becker, I., Sarbia, M., Carneiro, F., and Becker, K-F. Slug Is Overexpressed in Gastric Carcinomas and May Act Synergistically with SIP1 and Snail in the Down-Regulation of E-Cadherin *The Journal of Pathology* **2007**. 211:507-15. DOI: 10.1002/path.2138
14. Mouillesseaux, K. P. *et al.* Notch Regulates BMP Responsiveness and Lateral Branching in Vessel Networks via SMAD6 *Nature Communications*. **2016** Nov 11; 7, 13247. DOI: 10.1038/ncomms13247

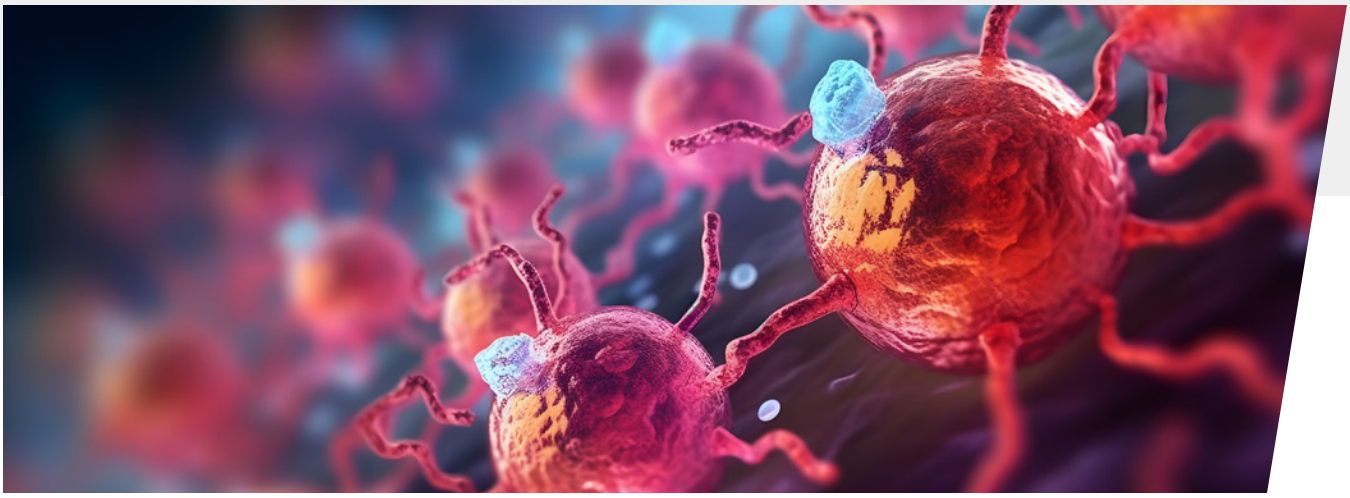

Chapter 5 : Metabolic Reprogramming to Enhance Immune Cell Activity

Strategies and new tools for optimizing immune cell fitness and antitumor activity

Optimizing immune cell metabolic fitness

Metabolism is a critical component of oncogenesis. Unlike normal cells, cancer cells generate energy mainly by increased aerobic glycolysis in the cytosol. In general, solid tumors are poorly vascularized with blood vessels, and some cells will experience hypoxia, nutrient deprivation, and acidosis. To counteract this, these tumor cells will shift to rely on alternative metabolites or methods for acquiring nutrients. This activity, in turn, can condition the microenvironment in their favor.

T cells can undergo metabolic reprogramming to adapt to these changing circumstances for long-term, cell-mediated antitumor immunity. Metabolic reprogramming during activation—the shift from oxidative phosphorylation to glycolysis—plays an essential role in the transition to an active state, where there is a massive spike in proliferation, migration, and differentiation into effector T cells. Nutrient competition, however, can lead to T cell exhaustion, characterized by a gradual loss of activity and changes in the expression and function of critical transcription factors.

There is a strong impact of metabolic modulation on T cells. Determining the metabolic signatures of T cell therapies can play a crucial role in defining T cell persistence and antitumor function. Moreover, modulation or reprogramming of the metabolic pathways of T cells can be used as a strategy to improve their antitumor efficacy[14]. CAR-T cells that acquire an effector phenotype with high metabolic activity during in vitro expansion have been reported to display poor persistence and antitumor activity in vivo. However, CAR-T cells that show low-to-medium metabolic activity during in vitro expansion and high spare respiratory capacity confer good antitumor immunity, characterized by enhanced proliferation capabilities, higher rates of tumor cell killing, and cytokine production[15]. These disparities between in vitro activities and in vivo efficacies emphasize the need for multiple assay approaches in order to fully characterize antitumor immunity.

Chapter 5 :
Metabolic Reprogramming to Enhance Immune Cell Activity

Related Solutions

Measure oxygen consumption rate (OCR), proton efflux rate (PER) or extracellular acidification rate (ECAR), as well as ATP production rates of live cells using **Agilent Seahorse XF technologies**.

The **Agilent Seahorse XF T cell metabolic profiling kit** allows for robust and accurate measurements of both glycolytic and mitochondrial activities in T and NK cell populations, providing a complete picture of cell energy metabolism.

The **Agilent Seahorse XF Hu T cell activation assay kit** measures human (Hu) T cell activation response within several minutes of stimulation using Seahorse XF Analyzers.

Application Note

Cell Analysis

Agilent

Trusted Answers

Assessing T Cell Bioenergetic Poise and Spare Respiratory Capacity Using Extracellular Flux Analysis

Authors

Jessica Walls and
Natalia Romero
Agilent Technologies, Inc.

Abstract

The Agilent Seahorse XF T Cell Metabolic Profiling kit is a robust solution for the complete assessment of T cell metabolism in real time. Metabolism has emerged as a key driver of T cell fate and function. Indeed, it has been demonstrated that metabolic reprogramming of T cells can be used as a strategy to improve the antitumor efficacy of adoptive T cell therapies. The XF T Cell Metabolic Profiling kit allows the simultaneous measurement of glycolytic and mitochondrial activity in T cell populations combined with the measurement of mitochondrial respiratory capacity. These parameters have been linked with optimal function and improved persistence of T cell therapies. Previously, measurement of mitochondrial respiratory capacity using FCCP required concentration optimization between cell types, differentiation stage, donor and healthy or disease state. The XF T Cell Metabolic Profiling kit uses an improved uncoupler (BAM15) for more consistent and accurate measurements of T cell bioenergetic capacity with less concentration optimization required than FCCP. In addition, this application note highlights the use of the kit in assessing the impact of the medium composition during T cell expansion following the XF T Cell Persistence Assay workflow. This workflow allows for evaluation of glycolysis and mitochondrial activity and capacity simultaneously, providing a comprehensive metabolic profile of T cells that can be incorporated into monitoring and improving the design and development of T cell therapies.

Introduction

The development of cell-mediated immunotherapies has revolutionized cancer research as well as the study of the immune system. One of the most promising types of cell therapies involves the genetic engineering of novel chimeric antigen receptor (CAR) T cells to target cancer cells. There is strong evidence suggesting that metabolic properties of T cells – that is, how T cells sustain bioenergetic demands – play an essential role in regulating their antitumor function and dictating the effectiveness of T cell-based immunotherapies.[1]

T cells undergo a series of changes in their metabolic phenotype during the activation and differentiation into effector and memory cells, which are critical to maintaining T cell function.[2] Naïve T cells are in a quiescent state, with low metabolic demands sustained mainly by mitochondrial respiration. Antigen stimulation induces the exit of the quiescent state, a rapid increase in nutrient uptake, increased anabolic metabolism, and reprogramming of mitochondrial metabolism. These metabolic changes are critical to support rapid T cell proliferation and differentiation to produce cytokines or molecules that trigger cytotoxicity. After successfully clearing the antigenic stimulus, remaining differentiated memory T cells revert to a more quiescent phenotype supported primarily by mitochondrial activity and high spare respiratory capacity (SRC). Under the conditions of chronic stimulation or in a metabolically restricted environment, T cells can become metabolically dysfunctional – a state known as T cell exhaustion – where T cells exhibit decreased mitochondrial bioenergetic capacity and effector function (Figure 1).

Due to the strong impact of metabolic modulation in T cell fate and function, determining the metabolic signatures of CAR-T and other adoptive T cell therapies can play a crucial role in defining T cell persistence and antitumor function. Moreover, modulation or reprogramming of the metabolic pathways of T cells can be used as a strategy to improve the antitumor efficiency of T cells.

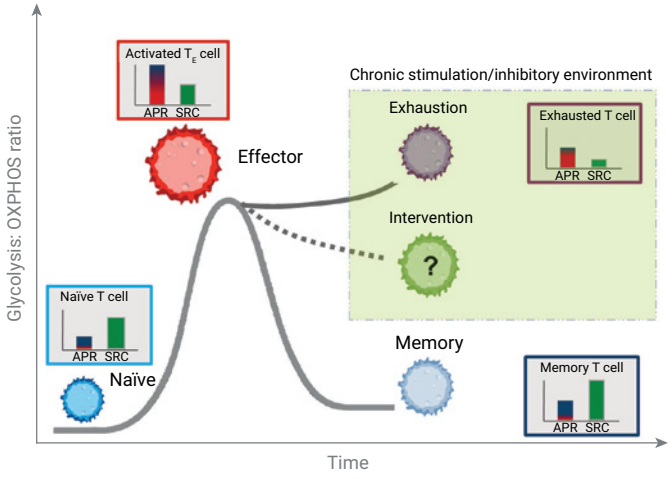

Figure 1. The fundamentals of T cell energy metabolism with measurements of T cell metabolic phenotypes, illustrating a relationship between glycolysis/OXPHOS ratio and cell fate, fitness, and function. Under chronic stimulation or in the presence of an inhibitory environment such as the tumor microenvironment, T cells can develop into an exhausted phenotype with impaired mitochondrial function.

The complete characterization of both glycolytic and mitochondrial bioenergetic pathways in T cells at different stages of T cell lifespan, as well as information about metabolic adaptations to different cellular environments or stress signals, are critical outputs to optimize T cell therapies and improve the antitumor potency of immunotherapy products. Designed to simultaneously interrogate glycolytic and mitochondrial function in live cells, Agilent Seahorse XF technology is one of the leading platforms used to study immune cell metabolism and is a key contributor to the current understanding of immunometabolism and the recognition of the fundamental role of the metabolic changes that occur during T cell activation and differentiation.[3,4]

This application note presents the new Agilent Seahorse XF T Cell Metabolic Profiling Kit, designed to enable the simultaneous acquisition of robust measurements of glycolytic and mitochondrial activity in T cell populations combined with mitochondrial respiratory capacity. These measurements provide complete characterization of the T cell metabolic profile from a single assay and can be used to correlate with increased or decreased antitumor function of T cell therapy products. Obtaining these measurements can be especially valuable during the therapy development processes targeted at improving T cell persistence or avoid metabolic exhaustion postactivation in the tumor microenvironment.

Performance review of mitochondrial uncoupler used in T cells

The study of mitochondrial function in T cells using the Agilent Seahorse XF Cell Mito Stress Test combined with Agilent Seahorse XF analyzers has provided the foundational knowledge about T cell energy metabolism and its role in directing T cell fate and function.[3,4] The Agilent Seahorse XF Cell Mito Stress Test Kit combines a series of reagents that allow a complete characterization of mitochondrial function. In particular, sequential injections of an ATP synthase inhibitor (oligomycin), a mitochondrial uncoupler (carbonyl cyanide *p*-(trifluoromethoxy)phenylhydrazone, FCCP) and a mitochondrial inhibitor (mixture of rotenone and antimycin A (rot/AA)) allow calculation in intact cells of the oxygen consumption rate coupled to mitochondrial ATP production (ATP-linked respiration), the uncoupled maximal respiration as well as the SRC, i.e, the difference between basal respiration and maximal respiratory capacity. These parameters have been widely used to characterize the mitochondrial function of different T cell populations and to describe processes that improve antitumor potency of T cells.[5-7] However, despite the wide adoption of this assay in the immunometabolism field, its use in T cells presents some challenges, primarily due to the use of the protonophore uncoupler FCCP.

There are several reasons that the use of FCCP with T cells (and potentially other immune cells) is not ideal. First, the optimal concentration of FCCP varies depending on many factors, including immune cell type, differentiation stage, donor, and disease state. If its concentration is not titrated or optimized for each individual experiment, it can lead to underestimation of maximal respiratory capacity. Second, in naïve T cells and some other differentiated T cells, the oxygen consumption rate (OCR) after FCCP exposure is not stable, resulting in high variation in the measurements, and potentially under-reporting the maximal respiratory capacity.

In addition, the use of FCCP in the XF Cell Mito Stress Test limits the ability of the assay to provide quantitative measurements of the glycolytic activity which is the glycolytic ATP (glycoATP) production rate. Calculation of glycoATP production rate using Seahorse XF ECAR (extracellular acidification rate) measurements requires correction from CO_2 contribution which is estimated using basal OCR measurements and OCR after addition of rot/AA.[8] However, when FCCP is used before rot/AA in the assay, it can result in underestimation of CO_2 contribution and impacts quantification of glycolytic activity. This is especially important in cells that are highly oxidative, i.e., cells that rely primarily on mitochondrial oxidative phosphorylation (OXPHOS) for energy, where CO_2 contribution to ECAR is not negligible.

Simultaneous assessment of mitochondrial ATP (mitoATP) production rate and glycoATP production rates allows characterizing basal cellular energetic demand (i.e., total cellular ATP production rate) and basal metabolic poise (i.e., the ratio between glycoATP and mitoATP production rates). These are critical parameters for determining T cell fate and function. Yet, they are not provided by the XF Cell Mito Stress Test, resulting in an incomplete characterization of T cell bioenergetics.

Development of the new Agilent Seahorse XF T Cell Metabolic Profiling Kit

To enable the simultaneous acquisition of accurate, consistent, and quantitative bioenergetic measurements for both glycolytic and mitochondrial activity in T cell populations, the Agilent Seahorse XF T Cell Metabolic Profiling Kit was developed. This kit allows accurate measurements of the maximal respiratory capacity in T cells by using the uncoupler BAM15 ((2-fluorophenyl){6-[(2-fluorophenyl)amino] (1,2,5-oxadiazolo[3,4-e]pyrazin-5-yl)}amine). BAM15 is a novel uncoupler reported to have similar potency as FCCP but with less cytotoxicity and lower affinity for the plasma membrane, resulting in a broader effective range.[9]

As shown in Figures 2A to 2C (red lines), when naïve T cells are tested with XF Cell Mito Stress Test Kit, the rate of change in O_2 level during the three minutes of the instrument measurement after FCCP injection is not constant or linear, resulting in variable OCR calculations and underestimation of maximal respiration (Figures 2D to 2F, red lines). In addition, there could be a significant overestimation of OCR after rot/AA injection, as indicated by the comparison of the kinetic traces obtained with FCCP injection or with vehicle injection (Figure 2D, red or blue trace). However, when the uncoupler BAM15 is used instead of FCCP, a stable increase in OCR is obtained after BAM15 injection (Figures 2A to 2C, green lines), resulting in a more accurate and precise determination of maximal respiration (Figures 2D to 2F, green lines).

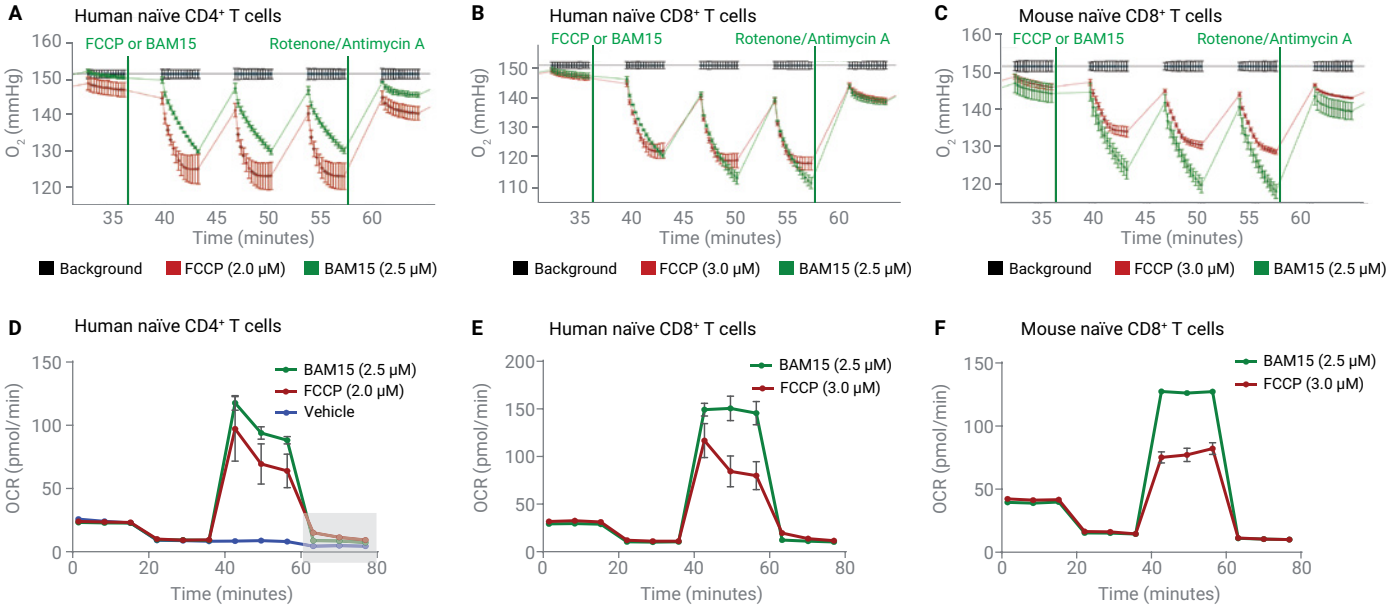

Figure 2. Comparison of Oxygen consumption measurements using uncoupler FCCP and BAM15. Human and mouse naïve T cells were seeded at 2×10^5 and 1.5×10^5 cells/well, respectively, in Seahorse XF RPMI assay medium, pH 7.4 supplemented with 10 mM glucose, 2 mM glutamine, and 1 mM pyruvate. Changes in extracellular oxygen level in naïve human CD4+ (A), naïve human CD8+ (B), and spleen-derived mouse CD8+ T cells (C) after addition of optimal concentrations of the uncouplers FCCP (red lines) or BAM15 (green lines). Oxygen consumption rate (OCR) obtained from the XF Cell Mito Stress Test (red lines) or T Cell Metabolic Profiling Kit assay (green lines) in naïve human CD4+ (D), naïve human CD8+ (E), and spleen-derived mouse CD8+ T cells (F). Blue line in 2D corresponds to the condition where assay medium was injected instead of uncoupler.

These preliminary tests were followed with additional experiments using human naïve CD4⁺, human naïve CD8⁺, human PBMC, and spleen-derived mouse CD8⁺ T cells from at least three different donors per cell type. In all the cases, side-by-side titrations using FCCP or BAM15 were performed. Higher maximal respiration and lower standard deviations were consistently obtained with BAM15 as the uncoupler, when compared to those obtained at the optimal FCCP concentrations (Figures 3A to 3C). Titration experiments also demonstrated that the range of optimal BAM15 concentration is wider than the optimal FCCP range, indicating minimal need to optimize uncoupler concentration for each sample when BAM15 is used (Figures 3A and 3B, middle bar graphs).

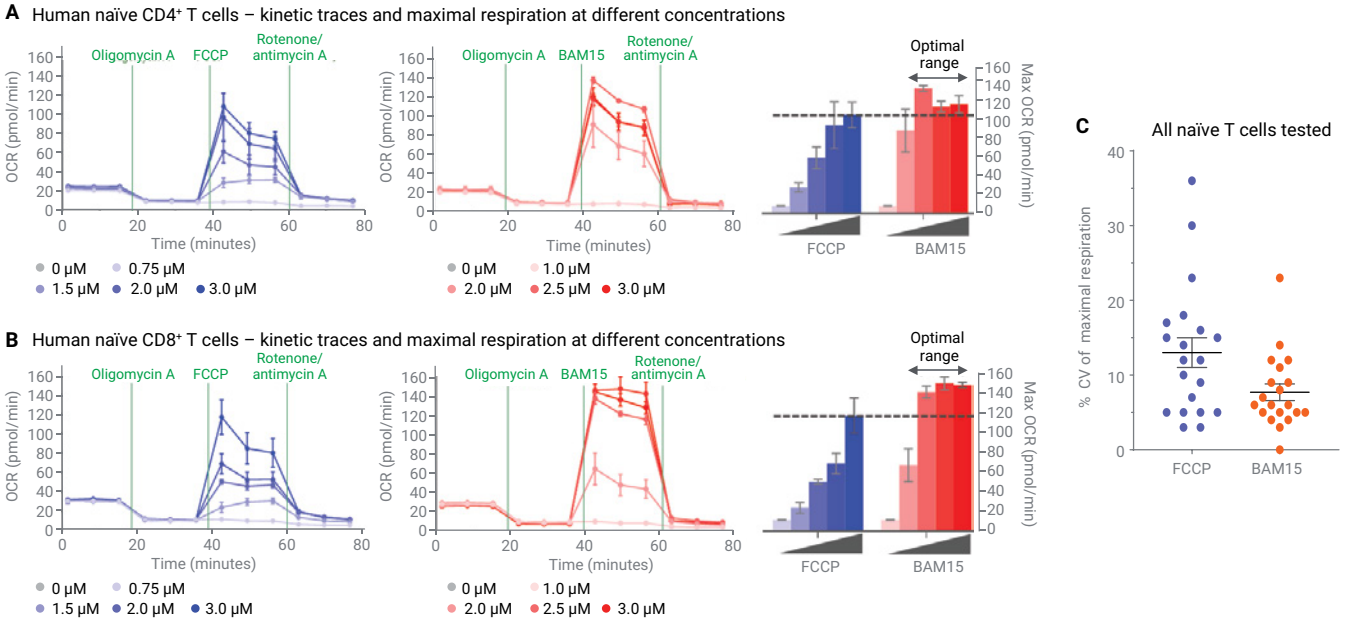

Figure 3. Comparison of maximal respiration measurements from FCCP and BAM15 titration experiments using human naïve CD4⁺ T cells (A) and CD8⁺ T cells (B). Bar graphs in the middle represents the maximal respiration obtained at different uncoupler concentration. (C) % CV of maximal respiration obtained for the panel of naïve T cells tested when optimal concentrations of FCCP or 2.5 µM BAM15 were used.

The glycoATP production rates calculated from using the XF T Cell Metabolic Profiling Kit (with BAM15 uncoupler) were also compared with those obtained in parallel experiments using the Agilent Seahorse XF Real-Time ATP Rate Assay Kit. The results show that there are no significant differences in the basal glycoATP production rates obtained from these two kits or assays (Figure 4).

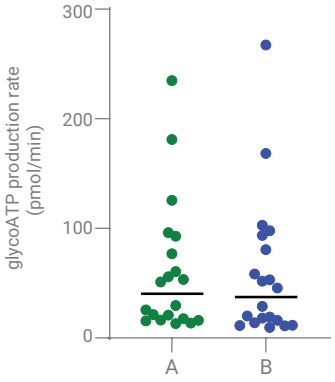

Figure 4. Comparison of basal glycoATP production rates in naïve T cells, calculated using the Agilent Seahorse XF Real Time ATP Rate Assay Kit (B) or the XF T Cell Metabolic Profiling Kit (A) with BAM15 injected between oligomycin and rot/AA injections.

Finally, a broad panel of T cells was selected to further evaluate the XF T Cell Metabolic Profiling Kit, from humans to mice and including different donors and differentiation states. Titration experiments were performed and maximal OCR values obtained at optimal FCCP concentration were compared with the values obtained at a single concentration of BAM15 (2.5 µM) for the T cell panel (Figure 5). In all the cases, the maximal OCR obtained with 2.5 µM BAM15 was at least 90% of the maximal OCR obtained at the optimal FCCP concentration within the same cell type. Maximal OCR obtained with 2.5 µM BAM15 was, on average, 20% higher than the value obtained with the optimal FCCP concentration, demonstrating that the BAM15 reagent from the kit can be used at a fixed concentration of 2.5 µM for all T cell types or requires minimal optimization.

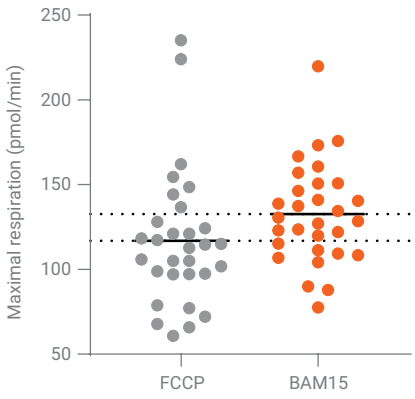

Figure 5. Comparison of maximal respiration obtained at optimal FCCP concentration or 2.5 µM BAM15 from a broad panel of T Cells, including human PBMC, naïve CD4$^+$, naïve CD8$^+$, activated CD4$^+$, activated CD8$^+$, effector CD8$^+$, memory CD8$^+$, and mouse naïve and activated CD8$^+$ T cells (n = 3 per cell type).

Application of XF T Cell Metabolic Profiling Kit in optimizing persistence for T cell therapy products

One critical attribute to consider when evaluating CAR-T and other adoptive T cell therapies is the metabolic signature of the cells, since it plays a crucial role in defining T cell persistence and antitumor function. Indeed, CAR-T cells that acquire an effector phenotype with high metabolic activity during *in vitro* expansion have been reported to display poor persistence and antitumor activity *in vivo*. However, CAR-T cells that show low-to-medium metabolic activity during *in vitro* expansion and high spare respiratory capacity confer good antitumor immunity, characterized by enhanced proliferation capabilities, higher rates of tumor cell killing, and cytokine production.[10] Several publications indicate that expansion conditions during manufacturing could produce T cell products with an undesired metabolic phenotype that results in reduced *in vivo* potency. These publications also point out that metabolic conditioning of T cells during expansion can induce metabolic reprogramming that results in extended *in vivo* persistence and improved antitumor function.[5,11,12]

Designed to assist T cell therapy development, the XF T Cell Metabolic Profiling Kit delivers a complete picture of T cell metabolic profile from a single assay which includes total basal energetic demand, basal metabolic poise, and spare respiratory capacity – all parameters were previously used to describe T cell metabolic states with increased or reduced persistence.[10] Therefore, it is ideally suited for assessing and optimizing T cell expansion conditions that result in the desired metabolic phenotype for increased T cell persistence.

Here, the XF T Cell Metabolic Profiling Kit was used to evaluated how cell culture medium composition (RPMI containing 10 mM glucose + 10% FBS or ImmunoCult XF Medium (STEMCELL Technologies)), as well as the addition of different interleukins (IL-2 or IL-15), can impact metabolic profile of T cell products. Previous studies indicated that cells expanded in IL-15 present a less differentiated phenotype than cells cultured in IL-2.[13] In this study, pan T cells were activated from different healthy human donors with magnetic beads conjugated with CD3/CD28 antibodies. After three days, the magnetic beads were removed, and cells expanded in the indicated medium conditions (Figure 6). Cells were maintained in culture at a cell density of 1 × 10^6 cells/mL, with medium refreshed and volume adjusted every three days. At day 7, 14, and 22, samples were removed and analyzed using the XF T Cell Persistence assay supported by the XF T Cell Metabolic Profiling Kit following the recommended assay conditions.[14]

First, SRC in the course of cell expansion was compared. As shown in Figure 6A, at day 7 a difference in the SRC of cells expanded in IL-15 or IL-2 is observed, independent of the cell culture media used during expansion. The increased SRC of cells expanded in IL-15 is accentuated at day 22, particularly in the cells cultured in the optimized ImmunoCult XF medium (Figure 6C). Increased SRC is characteristic of memory-like phenotype and has been previously associated with increased persistence.

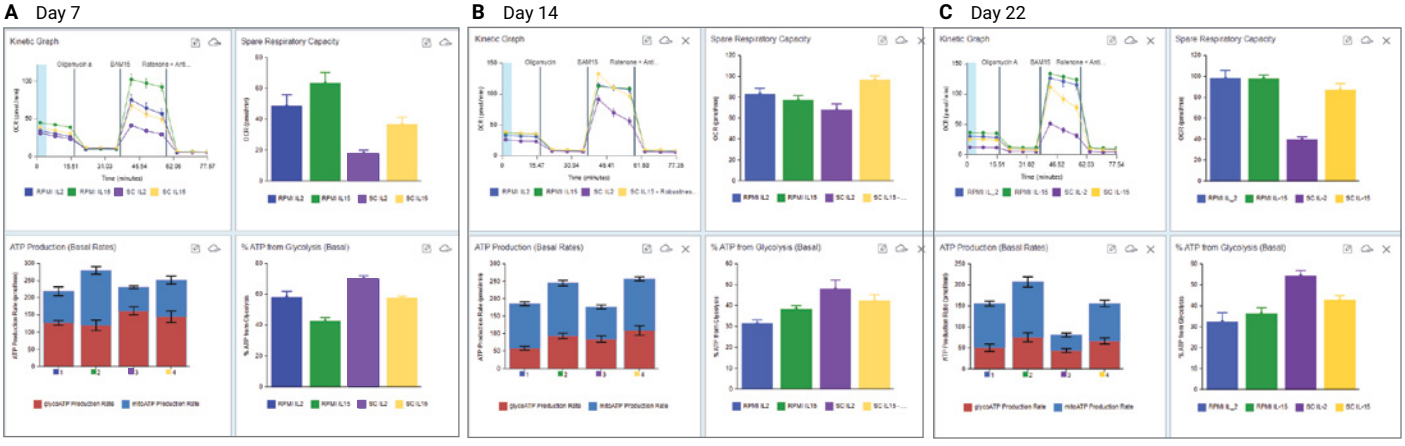

Figure 6. Impact of cell expansion condition on T cell metabolic measurements. Human peripheral blood pan T cells were activated with Dynabeads Human Activator CD3/CD28 in ImmunoCult XF T Cell Expansion Medium and cultured at 37 °C in a 5% CO_2 incubator. Two days after activation, Dynabeads were removed and cells were split in 4 groups and resuspended at 1 × 10^6 cells/mL in the following 4 medium conditions: Blue – RPMI supplemented with 2 mM glutamine, 10% FBS and IL-2 (300 U/mL); Green – RPMI supplemented with 2 mM glutamine, 10% FBS and IL-15 (10 ng/mL); Purple – ImmunoCult XF Medium supplemented with IL-2 (300 U/mL); Yellow – ImmunoCult XF Medium supplemented with IL-15 (10 ng/mL). Samples were taken and analyzed at day 7, day 14, and day 22 post activation. Data reported for each day include OCR kinetic traces (top left), SRC (top right), ATP production rates (bottom left), and percent of ATP from glycolysis (bottom right).

The next step was examining the additional outputs enabled by this assay for better characterizing and improving expansion conditions, which are the basal ATP production rates from glycolysis and mitochondria (Figure 6, lower two graphs in each panel). Cells expanded in ImmunoCult XF medium containing IL-15 have a more oxidative metabolic poise (lower % ATP from glycolysis) compared to that containing IL-2 (Figure 6, lower right graph in each panel, yellow versus purple bars). In addition, cells expanded and differentiated in RPMI medium present higher metabolic demand (higher total basal ATP production rate) than cells expanded and differentiated in ImmunoCult XF medium, regardless which interleukin was used (Figure 6, lower left graph in each panel). Increased metabolic demand is associated with effector T cell phenotype. In fact, when the expression of the CCR7-A and CD45RO-A surface markers was analyzed using the Agilent NovoCyte Advanteon flow cytometer, it was observed that cells expanded in ImmunoCult XF medium maintained a higher ratio of CCR7-A$^+$/CD45RO-A$^+$ central memory population compared to cells expanded in RPMI that were enriched in effector memory phenotype (Figure 7).

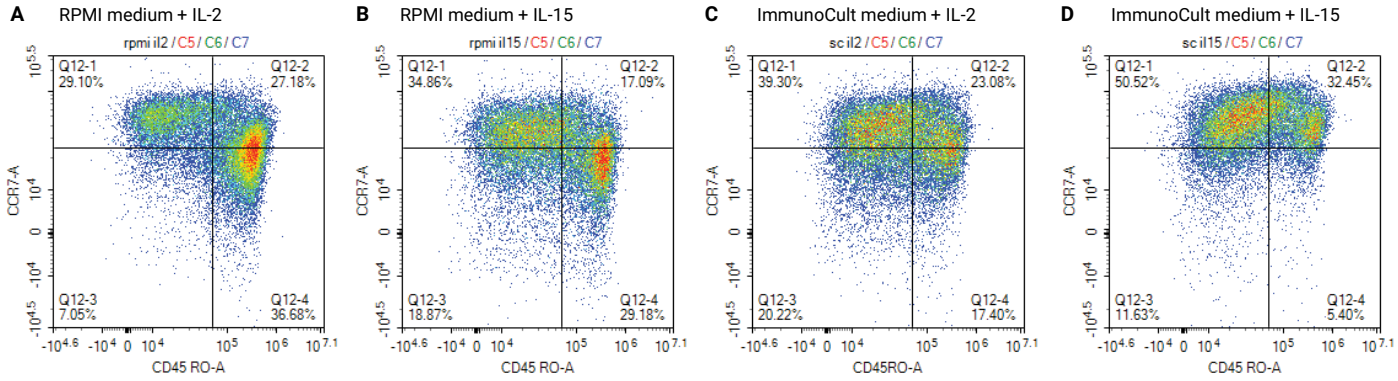

Figure 7. Flow cytometry analysis of the cell surface markers CCR7-A and CD45RO-A with day 22 samples expanded in different medium conditions as indicated in the graphs. RPMI medium is also supplemented with 2 mM glutamine and 10% FBS.

Conclusion

This document presents an optimized assay for the complete characterization of the metabolic profile of T cells. The assay combines the use of the XF analyzer with the XF T Cell Metabolic Profile Kit, providing an optimized uncoupler that allows for robust measurements of maximal respiration and spare respiratory capacity in T cells and minimal uncoupler concentration optimization. In addition, this assay allows users to obtain quantitative information about glycolytic activity in the same cell sample, together with a unique measurement of basal cell bioenergetic demand.

To improve the ability to develop and predict T cell therapy efficiency, it is required to use a combination of tools and orthogonal assays that provide a comprehensive data set to characterize CAR-T cell therapeutic products. It is clear that metabolic characterization of T cells is one of the critical attributes that need to be analyzed to improve the persistence and antitumor potency of T cell products. The XF T Cell Persistence Assay delivers a multiparametric outputs that provide a complete characterization of T cell metabolic profile from the same sample and can be incorporated as a routine assay to optimize the design and manufacture of T cell-derived therapeutics.

References

1. Chang C. H.; Pearce, E. L. *Nature Immunology* **2016**, *17*, 364–368. https://dx.doi.org/10.1038%2Fni.3415.
2. Sukumar *et al. Current Opinion in Immunology* **2017**, *46*, 14–22. https://doi.org/10.1016/j.coi.2017.03.011.
3. Wei *et al. Frontiers in Immunology* **2021**, *12*, 717014. https://doi.org/10.3389/fimmu.2021.717014.
4. Voss *et al. Nature Reviews Immunology* **2021**, *21*, 637–652. https://doi.org/10.1038/s41577-021-00529-8.
5. Geiger *et al. Cell* **2016**, *167*, 829–842. http://dx.doi.org/10.1016/j.cell.2016.09.031.
6. Kawalekar *et al. Immunity* **2016**, *44*, 380–390. http://dx.doi.org/10.1016/j.immuni.2016.01.021.
7. Scharping *et al. Immunity* **2016**, *45*, 374–388 http://dx.doi.org/10.1016/j.immuni.2016.07.009.
8. Natalia, R. Quantifying Cellular ATP Production Rate Using Agilent Seahorse XF Technology. *Agilent Technologies white paper*, publication number 5991-9309EN.
9. Kenwood *et al. Molecular Metabolism* **2014**, *3*, 114–123. http://dx.doi.org/10.1016/j.molmet.2013.11.005.
10. Rostamian *et al. Cancer Letters* **2021**, *500*, 107–118. https://doi.org/10.1016/j.canlet.2020.12.004.
11. Hermans *et al. PNAS* **2020**, *117(11)*, 6047–6055. https://www.pnas.org/cgi/doi/10.1073/pnas.1920413117.
12. Geltink *et al. Nature Metabolism* **2020**, *2*, 703–716. https://doi.org/10.1038/s42255-020-0256-z.
13. Alizadeh *et al. Cancer Inmunol. Res.* **2019**, *7(5)*, 759–772. https://doi.org/10.1158/2326-6066.CIR-18-0466.
14. Agilent Seahorse XF T Cell Metabolic Profiling Kit User Guide. *Agilent Technologies*, publication number 5994-3493EN.

www.agilent.com/chem/xfpro

RA44573.6858796296

Printed in the USA, March 15, 2022
5994-4494EN

Agilent
Trusted Answers

Technical Overview

Agilent
Trusted Answers

Metabolic Preconditioning Improves Engineered T Cell Fitness and Function

Using real-time cell potency and bioenergetic assays to optimize critical process parameters for manufacturing of engineered T cells

Authors

Rashmi R. Pillai,
Caryn Gonsalves,
Natalia Romero, Xiaoyu Zhang,
Yama A. Abassi, and
Brandon J. Lamarche
Agilent Technologies, Inc.

Introduction

Adoptive transfer of Chimeric antigen receptor (CAR) T cell-based therapies has shown promising results in multiple cancers. Decisive features needed to achieve improved clinical outcomes in CAR/engineered T cell receptor (TCR) T cell-based therapy are clonal stability, persistence, and metabolic fitness. A recently published, decade-long follow-up study by Melenhorst *et al.* on chronic lymphocytic leukemia (CLL) remission demonstrates this fact.[1] Optimal CAR/TCR T cell metabolic fitness enables their extravasation to the tumor[2] physical remodeling of the extracellular, matrix in the TME[3], avoidance of suppressive signaling[4,5], coping with nutrient depletion[6], tolerance of hypoxia[7], and overcoming oxidative stress[8] in addition to execution of cytolytic activity, particularly in the context of solid tumors. Augmented T cell phenotypes are, in turn, associated with increased mitochondrial capacity, ATP production, and spare respiratory capacity (SRC).[9] Several studies have aimed at improving CAR T cell metabolic fitness using CAR engineering approaches or by introduction of supplemental genes that enhance mitochondrial respiration.[10]

Beyond introduction of genetic modifications, growing evidence demonstrates that simple preconditioning protocols can also improve T cell fitness/function by enhancing mitochondrial bioenergetic capacity. Preincubating TCR/CAR T cells *in vitro* under reduced glucose[12] or elevated arginine[13] conditions improves potency and ability to clear tumors in xenograft-bearing mice. Indeed, preconditioning in either low glucose or high arginine alters bioenergetics (glycolysis and oxidative phosphorylation), which affects differentiation, persistence, tumor infiltration, and resistance to exhaustion.[13] Collectively, these preconditioning results highlight the diverse means by which T cell fitness/function can be enhanced. Because preconditioning is both inexpensive and technically facile, it is likely to become integral to CAR/TCR T cell manufacturing in the future.

This study presents a comprehensive, robust, real-time workflow using the xCELLigence eSight, where T cell potency as measured by immune cell killing is combined with biogenetics and persistence parameters. This workflow provides two independent perspectives from the same experiment that can replace several time-consuming assays performed in series during cell therapy process development.

As proof of concept, this study used eSight to examine the impact of preconditioning in elevated concentrations of arginine on the killing efficacy of MART-1-specific TCR T cells. In parallel, the Seahorse XF Pro Analyzer was used to assess T cell metabolic fitness. Supplementing the growth medium with 6 mM arginine increased killing efficacy dramatically (more than 5-fold). Concurrent Seahorse XF assays demonstrated that these high arginine-stimulated gains in killing efficacy were also associated with an increase in maximal and basal oxygen consumption rates (OCR) and SRC of the T cells.

Materials and methods

Please refer to the application note Metabolic Preconditioning Improves Engineered T Cell Fitness and Function for information about methods and materials.

Results and discussion

Preliminary validation of TCR activity and specificity

Before interrogating the impact of varying preconditioning parameters, it is important to validate the function and specificity of the transduced receptor. Towards this end, E-Plate wells were seeded with 8,000 Mel-624.38 melanoma target cells. After allowing cells to adhere and proliferate for 24 hours, a T cell cytotoxicity assay was performed using an E:T ratio of 5:1. Addition of mock transduced T cells had minimal impact on the growth and proliferation of Mel-624.38 target cells over the 75-hour window (black trace in Figure 1A). In contrast, MART-1 TCR T cells led to an immediate and sustained decrease in impedance, consistent with target cell death (aqua trace in Figure 1A). The killing observed in this study was expected considering the previously characterized activity of the DMF5 receptor[11], and the fact that Mel-624.38 cells express HLA-A*02:01, which is required for displaying the MART-127-35 peptide that DMF5 recognizes (Figure 1A). When the same assay is repeated with Mel-624.28 cells, which express significantly less HLA-A*02:01 and therefore present less MART-127-35 peptide on their surface, no killing is observed (Figure 1B). This conclusion is corroborated by the real-time imaging time course shown in Figures 1C and 1D. Specifically, this data set demonstrates that when seeding 8,000 melanoma target cells, using an E:T of 5 yields robust killing within a reasonable time frame.

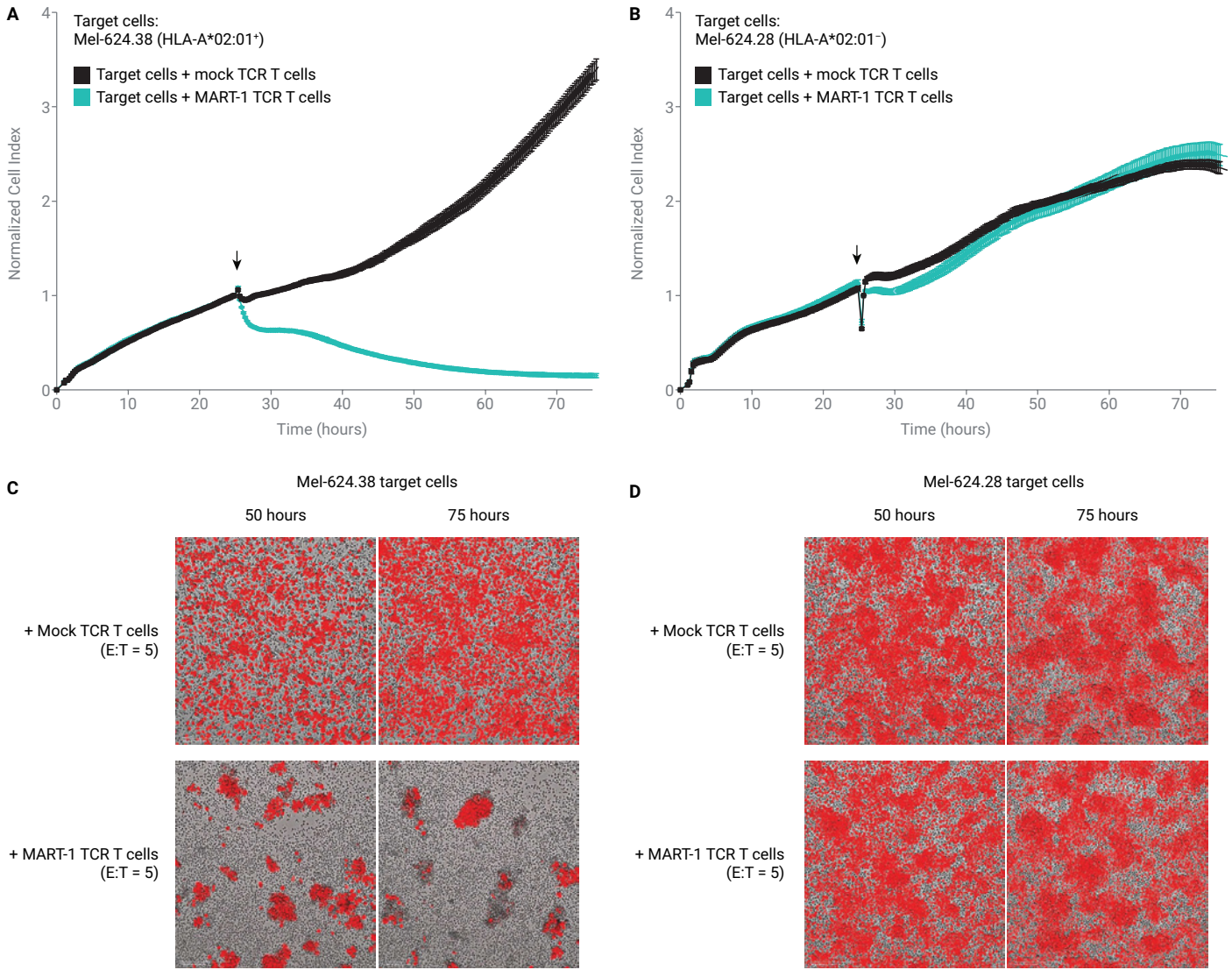

Figure 1. Preliminary validation of DMF5 TCR activity and specificity. (A,B) Using impedance to track MART-1 TCR T cell-mediated killing of Mel-624.38 (A) and Mel-624.28 (B) target cells that display the MART-1 peptide on their surface. The black arrow at 24 hours denotes the time when T cells were added. (C,D) Composite brightfield + red fluorescence photos corroborate killing kinetics observed in impedance traces.

Arginine preconditioning enhances T cell cytotoxicity and mitochondrial respiration

It is well established that differentiation of T cell fitness and function are intimately linked to their metabolism. Preconditioning TCR T cells *in vitro* in an elevated concentration of arginine shifted bioenergetics (increasing oxidative phosphorylation), and was associated with increased killing efficacy once T cells were transfused into tumor bearing mice.[10] Unfortunately, screening a broad array of T cell preconditioning parameters using mouse xenograft models is both costly and time-consuming. For this reason, an *in vitro* assay to evaluate the functional impact of diverse preconditioning parameters would be advantageous. As a demonstration of eSight's ability to address these types of questions, the killing efficacy of MART-1 TCR T cells was evaluated after being preconditioned in three different concentrations of arginine. A Seahorse assay was performed simultaneously to asses the relationship between cytoxicity and bioenergetics under different conditions.

After transduction, T cells were metabolically preconditioned for 7 days in RPMI supplemented with 6 mM arginine, and base RPMI media. The killing assay was set up at an E:T ratio of 5:1, to demonstrate the eSight's capability to distinguish differences in potency using impedance curves (Figure 2A). All killing assays were performed at a 5:1 E:T ratio. While preconditioning, MART-1 TCR T cells in RPMI supplemented with 6 mM arginine stimulated killing efficacy substantially (Figure 2A). Geiger and coworkers demonstrated that high arginine stimulated gains for *in vivo* killing efficacy were coupled with a shift towards use of oxidative phosphorylation as the ATP source.[10] To confirm whether this is also true for MART-1 TCR T cells, the XF Cell Mito Stress Test was performed in the XF Analyzer in parallel with the eSight cytotoxicity assays. To perform this assay, MART-1 TCR transduced 6 mM arginine preconditioned T cells, RPMI T cells, and non-transduced T cells were used. The result shows that spare respiratory capacity (SRC) and maximal respiration of arginine preconditioned T cells was significantly higher than RPMI-preconditioned T cells (Figures 2B and 2C), a parameter previously correlated with increased T cell persistence.[13]

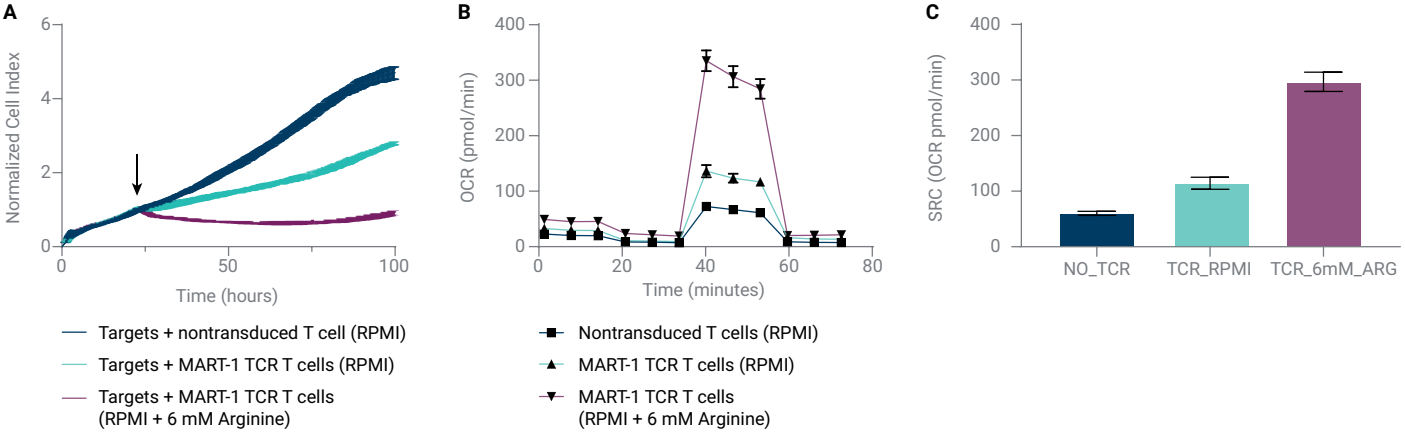

Figure 2. (A) Impedance traces for Mel-624.38 target cell cytotoxicity assay with MART-1 TCR T cells preconditioned for 7 days in RPMI medium supplemented with an additional 0- and 6-mM arginine. The E:T ratio was 5. Black arrow denotes time of T cell addition (24 hours). (B) Kinetic trace of OCR in basal conditions and after injection of oligomycin, uncoupler, and rotenone/antimycin A. (C) SRC of non-transduced, expanded in RPMI, or preconditioned in 6 mM arginine for 7 days.

Discussion

The maximal therapeutic efficacy of T cells depends on cell potency and bioenergetics status. This study shows a unique workflow that combines two Agilent T cell analysis platforms, eSight and XF Seahorse Analyzers, to provide a comprehensive picture of T cell potency and metabolic fitness. This study demonstrates eSight's ability to screen in real time for T cells with high potency after preconditioning with 6 mM arginine. If one wishes to evaluate the impact preconditioning has on T cell killing capacity, the eSight assay shown here can do so efficiently. Using real-time XF Seahorse measurements in parallel, the metabolic fitness of these potent arginine preconditioned T cells was associated with increased oxidative phosphorylation (Figures 2B and 2C). T cell persistence and memory phenotypes have previously been associated with higher SRC.[15,16] SRC provides valuable information about the bioenergetics of a T cell, which can be correlated with T cell potency using the Agilent XA eSight. The combination of these two techniques supplies valuable information about the critical parameters of T cell function relevant to cell therapy. The data from both eSight and XF Seahorse assays provide a comprehensive view of potency and metabolic fitness that can enable testing critical process parameters during CAR T cell manufacturing.

As the field of engineered T cell therapy continues to evolve, it seems increasingly clear that maximal therapeutic efficacy will be achieved not simply by transducing T cells with a single receptor, but by making multifaceted adjustments to their phenotype before transfusion. While supplementing TCR/CAR T cells with additional genes (for cytokines, metabolic enzymes, etc.) holds great promise, it is evident from past publications and this study that substantial gains in fitness can be achieved simply by changing the composition of the growth medium. Thus, it would seem that a huge array of preconditioning parameters have yet to be examined. Combining two or more preconditioning parameters previously proven to be beneficial will likely bring additive or even synergistic gains.

By eliminating the need for tedious, less informative endpoint analyses, the eSight real-time killing assay significantly lowers the barrier to systematically evaluate different preconditioning protocols.

References

1. Melenhorst, J. J. *et al.* Decade-Long Leukaemia Remissions with Persistence of CD4+ CAR T Cells. *Nature* **2022**, *602*, 503–509.
2. Finlay, D. K. *et al.* PDKI Regulation of mTOR and Hypoxia-Inducible Factor 1 Integrate Metabolism and Migration of CDS+ T Cells. *J. Exp. Med.* **2012**, *209(13)*, 2441–2453.
3. Caruana, I. *et al.* Heparanase Promotes Tumor Infiltration and Antitumor Activity of CAR-Redirected T Lymphocytes. *Nat. Med.* **2015**, *27*, 524–529.
4. Cherkassky, L. *et al.* Human CAR T Cells with Cellintrinsic PD-1 Checkpoint Blockade Resist Tumormediated Inhibition. *J. Clin. Invest.* **2016**, *126*, 3130–3144.
5. Newick, K. *et al.* Augmentation of CAR T-Cell Trafficking and Antitumor Efficacy by Blocking Protein Kinase A Localization. *Cancer Immunol. Res.* **2016**, *4*, 541–551.
6. Fultang, L. *et al.* Metabolic Engineering Against the Arginine Microenvironment Enhances CAR-T Cell Proliferation and Therapeutic Activity. *Blood* **2020**, *136*, 1155–1160.
7. Veliça, P. *et al.* Modified Hypoxia-Inducible Factor Expression in CDS + T Cells Increases Antitumor Efficacy, *Cancer Immunol Res.* **2021** Apr, *9(4)*, 401–414.
8. Ando, T. *et al.* Transduction with the Antioxidant Enzyme Catalase Protects Human T Cells Against Oxidative Stress. *J. Immunol.* **2008**, *181*, 8382–8390.
9. Rangel Rivera, G. O. *et al.* Fundamentals of T Cell Metabolism and Strategies to Enhance Cancer Immunotherapy. *Front. Immunol.* **2021**, *12*, 645242.
10. Pellegrino, M. *et al.* Manipulating the Metabolism to Improve the Efficacy of CART-Cell Immunotherapy. *Cells* **2020**, *10(1)*, 14.
11. Riley, T. P. *et al.* T Cell Receptor Cross-Reactivity Expanded by Dramatic Peptide-MHC Adaptability. *Nature Chem. Biol.* **2018**, *14*, 934–942.
12. Zhang, M. *et al.* Optimization of Metabolism to Improve Efficacy During CAR-T Cell Manufacturing. *J. Translat. Med.* **2021**, vol. 19.
13. Geiger, R. *et al.* L-Arginine Modulates T Cell Metabolism and Enhances Survival and Anti-Tumor Activity. *Cell* **2016**, *167*, 829–842.
14. Gadsbøll, A.-S. Ø. *et al.* Pathogenic CDS+ Epidermis-Resident Memory T Cells Displace Dendritic Epidermal T Cells in Allergic Dermatitis. *J. Invest. Dermatol*. **2020**, *140(4)*, 806–815.
15. Flores-Santibáñez, F. *et al.* In Vitro-Generated Tc17 Cells Present a Memory Phenotype and Serve as a Reservoir of Tc1 Cells In Vivo. *Front. Immunol.* **2018**, *9*, 209.

www.agilent.com/chem/eSight

RA44848.6690277778

Printed in the USA, January 8, 2024
5994-5852EN

Agilent
Trusted Answers

References

1. Rohaan, M. W.; Wilgenhof, S.; Haanen, J. B. A. G. Adoptive cellular therapies: the current landscape. *Virchows Arch*. **2019**, *474*, 449–461. **https://doi.org/10.1007/s00428-018-2484-0** (2-26-2024 (SprinkerLink))
2. Rafiq, S.; Hackett, C. S.; Brentjens, R. J. Engineering strategies to overcome the current roadblocks in CAR T cell therapy. *Nat Rev Clin Oncol.* **2020**, *17*, 147–167. **https://doi.org/10.1038/s41571-019-0297-y** (2-25-2024 (Nature))
3. Stadtmauer, E. A.; Faitg, T. H.; Lowther, D. E.; Badros, A. Z.; Chagin, K.; Dengel, K.; Lyengar, M.; Melchiori, L.; Navenot, J. M.; Norry, E.; Trivedi, T.; Wang, R.; Binder, G. K.; Amado, R.; Rapoport, A. P. Long-term safety and activity of NY-ESO-1 SPEAR T cells after autologous stem cell transplant for myeloma. *Blood Adv.* **2019**, *3 (13),* **2022**-2034. **https://doi.org/10.1182/bloodadvances.2019000194** (2-26-2024 (ASH Publications))
4. Irvine, D. J.; Purbhoo, M. A.; Krogsgaard, M.; Davis, M. M. Direct observation of ligand recognition by T cells. *Nature*. 2002, *419 (6909)*, 845-9. **https://doi.org/10.1038/nature01076** (2-25-2024 (Nature))
5. Pan, K.; Farrukh, H.; Reddy Chittepu, V.C.S.; Xu, H.; Pan C.; Zhu, Z. CAR race to cancer immunotherapy: from CAR T, CAR NK to CAR macrophage therapy. *J. Exp. Clin. Cancer Research* **2022**, *41 (119),* **https://doi.org/10.1186/s13046-022-02327-z** (2-24-2024 (BMC Springer Nature))
6. Li, X.; Dai, H.; Wang, H.; Han, W. Exploring innate immunity in cancer immunotherapy: opportunities and challenges. *Cell & Mol. Immunol.* **2021**, 18 1607-1609. **https://doi.org/10.1038/s41423-021-00679-8** (2-25-2024 (PubMed Central))
7. Liu, Q.; Li, J.; Zheng, H.; Yang, S.; Hua, Y.; Huang, N.; Kleeff, J.; Liao, Q.; Wu, W. Adoptive cellular immunotherapy for solid neoplasms beyond CAR-T *Mol. Cancer* **2023**, 22(28) **https://doi.org/10.1186/s12943-023-01735-9**
8. Nagarsheth, N. B.; Norberg, S. M.; Sinkoe, A.L.; Adhikary, S.; Meyer, T. J.; Lack, J. B.; Warner, A. C.; Schweitzer, C.; Doran, S. L.; Korrapati, S.; Stevanović, S.; Trimble, C. L.; Kanakry, J. A.; Bagheri, M. H.; Ferraro, E.; Astrow, S. H.; Bot, A.; Faquin, W. C.; Stroncek, D.; Gkitsas, N.; Highfill, S.; Hinrichs, C. S. TCR-engineered T cells targeting E7 for patients with metastatic HPV-associated epithelial cancers. *Nat Med.* **2021**, *27 (3)*, 419-425. **https://doi.org/10.1038/s41591-020-01225-1** (2-25-2024 (PubMed Central))
9. Sadelain, M.; Rivière, I.; Riddell, S. Therapeutic T cell engineering. *Nature*. **2017**, 545 (7655), 423-431. **https://doi.org/10.1038/nature22395** (2-25-2024 (PubMed Central))
10. Finck, A. V.; Blanchard, T.; Roselle, C. P.; Golinelli, G.; June, C. H. Engineered cellular immunotherapies in cancer and beyond. *Nat Med.* **2022**, *28 (4)*, 678-689. **https://doi.org/10.1038/s41591-022-01765-8** (2-25-2024 (PubMed Central)
11. Kiesgen, S.; Messinger, J. C.; Chintala, N. K.; Tano, Z.; Adusumilli, P. S. Comparative analysis of assays to measure CAR T-cell-mediated cytotoxicity. *Nat Protoc.* **2021**, 16, 1331–1342. **https://doi.org/10.1038/s41596-020-00467-0**
12. *National Cancer Institute: CAR T Cells: Engineering Patients' Immune Cells to Treat Their Cancers.* **https://www.cancer.gov/about-cancer/treatment/research/car-t-cells** (2-25-2024)
13. Kirtane, K.; Elmariah, H.; Chung, C.H.; Abate-Daga, D. Adoptive cellular therapy in solid tumor malignancies: review of the literature and challenges ahead. *Journal for ImmunoTherapy of Cancer.* **2021**, 9. **https://doi.org/10.1136/jitc-2021-002723** (2-25-2024 (BMJ Journals))
14. Dabi, Y. T.; Andualem, H.; Degechisa, S. T.; Gizaw, S. T. Targeting Metabolic Reprogramming of T-Cells for Enhanced Anti-Tumor Response. *Biologics*. **2022**, *16*, 35-45. **https://doi.org/10.2147/BTT.S365490** (2-25-2024 (PubMed Central))
15. Rostamian, H.; Fallah-Mehrjardi, K.; Khakpoo-Koosheh, M.; Pawelek, J.M.; Hadjati, J.; Brown, C.E.; Mirzaei, H.R. A Metabolic Switch to Memory CAR T cells: Implications for Cancer Treatment. *Cancer Letters* **2021**, 500, 197-118. **https://doi.org/10.1016/j.canlet.2020.12.004** (2-26-2024 (ScienceDirect))

Agilent

For more information about the products in this eBook visit

www.agilent.com/cell/cell-therapeutics

RA45373.6374189815

April 2024

5994-7421EN